NASA CONTRACTOR REPORT

NASA CR - 61040

NASA CR - 61040

APOLLO LOGISTIC SUPPORT SYSTEMS MOLAB STUDIES

INTERIM REPORT ON MISSION COMMAND AND CONTROL

Prepared under contract No. NAS8-11096 by

Arch W. Meagher and Robert J. Bonham

NORTHROP SPACE LABORATORIES
Space Systems Section
6025 Technology Drive
Huntsville, Alabama

For

NASA - GEORGE C. MARSHALL SPACE FLIGHT CENTER
Huntsville, Alabama

January 8, 1965

CR-61040

Task Order N-46
January 8, 1965

APOLLO LOGISTIC SUPPORT SYSTEMS

MOLAB STUDIES

INTERIM REPORT ON

MISSION COMMAND AND CONTROL

By

Arch W. Meagher
Robert J. Bonham

Prepared by Northrop Space Laboratories under
Contract NAS 8-11096

For

R-ASTR-A
ASTRIONICS LABORATORY

NASA-GEORGE C. MARSHALL SPACE FLIGHT CENTER

PREFACE

This Technical Report was prepared by the Northrop Space Laboratories (NSL), Huntsville, Department, for the George C. Marshall Space Flight Center under authorization of Task Order N-46, Contract NAS8-11096.

The NASA Technical Representative was Mr. John F. Pavlick of the MSFC Astrionics Laboratory (R-ASTR-A).

The work completed was a twenty-four man week effort ending on December 23, 1964.

The data presented herein include equations of motion, computer programs, and analysis of a four-wheeled LSV in the pitch and roll planes where such an analysis pertains to the stability of the suspension and steering systems. Also included are equations of motion and computer diagrams for a six-wheeled LSV and a general block diagram which will serve as a basis for studying the control of LSV's.

This is an interim report.

TABLE OF CONTENTS

LIST OF ILLUSTRATIONS

LIST OF ILLUSTRATIONS (Cont.)

LIST OF ILLUSTRATIONS (Cont.)

LIST OF TABLES

SUMMARY

The Mission Command and Control Task Order for which this report is written covers an analysis continued from the previous LSV task order. Areas to be covered are:

(1) Vehicle Stability (Suspension systems and vehicle design limits)

(2) Vehicle Steering

(3) Control Systems (Beginning definition of control systems characteristics)

This is an interim report to cover the work done up until the time the task time limit was extended.

As a basis for this task, the NASA Technical Representative furnished parametric data for two LSV's. One was a four-wheel vehicle and the other was a six-wheel, two-module, spring-coupled, articulated vehicle. With the exception of using specified constants and data, this task was performed similarly to previous tasks in this area by examining, first the pitch plane performance for selected perturbations and then the steering (Roll Plane performance). This portion of the task for the four-wheel vehicle has been completed and the results, along with the equations of motion and computer diagrams used, are shown in the text of the report. Equations of motion and computer diagrams for completing the stability studies for the six wheel vehicle also are shown in the text of the report. Only study of Ackerman steering has been outlined for either vehicles.

As a preliminary approach to the control systems study, a block diagram is included in this report. It is intended as a first attempt in defining the basic control problem and its expansion in the final report will include transfer functions and studies of the major systems and their components.

1.0 INTRODUCTION

This report is presented in three parts. Part I contains the equations of motion, the mathematical model and the results of pitch and roll plane studies for a four wheel Lunar Surface Vehicle (LSV). Part II contains the pitch and roll plane equations of motion for studying a six wheel articulated LSV. In both cases a particular vehicle with specified parameters is studied. Part III contains a preliminary block-diagram study of the LSV command and control systems. In the latter case the final report will be expanded to include transfer functions and individual system component analysis.

The purpose of the Part I and Part II studies is to establish the lunar surface stability of a given design and specified parameters. While it is impractical to study completely the stability and performance of the LSV, it is the intent to establish critical stability areas and to indicate limits in areas that may need further study.

The purpose of Part III of this report is to present a preliminary approach to controls problem studies for the LSV. The complete controls problem is intricate, depending on numerous time delays, power regulation, surface conditions and types of equipment used. No attempt will be made to determine the equipment types used---just to establish in a general way the critical areas of operation and the functional feasibility of some equipment.

PART 1

FOUR WHEEL VEHICLE

2.1 ROLL PLANE ANALYSIS

2.1.1 PROCEDURE

The four-wheel vehicle was studied in the roll plane for two conditions--Ackerman steering effects and the effects of having the vehicle traverse obstacles while in an Ackerman turn. The mathematical model used for studying the vehicle is shown in Figure 1A and the equations of motion used are shown in Figures 1B and 1C. Since the perturbations used in the roll plane were impulse-type distrubances, the effects of the pitch plane coupling are included in the simulation. In these studies each of the wheels (on one side of the vehicle) struck an obstacle sequentially and the length of time elapsed between the striking of the front and rear wheels was correlated with the vehicle speed. The forcing function for traversing obstacles was simulated with a half-sine wave. A ramp was used for the forcing function where Ackerman steering was simulated. The derivation of this forcing function is developed in Figure B4 of Appendix B. Finally, the simulation of the LSV's operating on a slope (in the roll plane) was accomplished through the use of a fixed moment added to the quation (6) of Figure 1B. The development of the use of this moment is shown in Figure B3 of Appendix B. This simulation is applicable as long as less than three of the four vehicle wheels are off of the Lunar surface.

The inclusions of the IC in the equations of motion (Figure 1B) will be explained in Section 2.2.1.

The analog computer schematic used for the roll plane studies is shown in (Figure B1) Appendix B, and the data are shown in Figure B2. The forcing functions for obstacle traverse were applied at the terrain-level position (Z_{of}, Z_{or}, etc.) for all roll plane simulations. The forcing functions were set to zero when the vehicle wheel was off of the Lunar surface.

2.1.2 RESULTS

2.1.2.1 Ackerman Steering

The results of the Ackerman steering studies are shown in Figure 5. These studies were made with the vehicle on level terrain or slopes, as indicated, with the yaw angle increasing negatively and the roll angle increasing negatively. That is, the vehicle was turned up the slope (or to the right) while traveling forward (See Figure 1). No surface obstacles were simulated in obtaining the results of Figure 5.

Since the analog computer simulation assumed no skid condition for any of the tests, approximate skid lines using the soil coefficient of friction and the moments created by the vehicle roll and yaw have been

calculated and added to the computer results. The skid point curves mean that the soil coefficient of friction had to be as great as that shown on the skid curve for a particular roll angle and wheel angle condition at that point--or skidding occurred. When skidding occurred both the vehicle yaw and roll angles were reduced.

Figures 5A, 5B, 5C, and 5D will show that the vehicle is stable for the range of speeds (16.72 Km/hr is beyond the stated LSV design range), maximum wheel angles, and roll angle slopes indicated for the LSV. At the higher speeds, slopes and wheel angles the safety margin seems small.

Angular accelerations (maximum) that occurred during the tests are shown on Figure 5E. Time history traces of other parameters performances are on file with R-ASTR-A Marshall Space Flight Center.

2.1.2.2 Obstacle Traverse While in an Ackerman Turn

The conditions for testing the ability of the LSV to negotiate an obstacle while making an Ackerman turn were the same as those described in Section 2.2.2.1, except in this case the wheel angle had already reached its maximum before the simulation (addition of perturbations) was started. This means that the ramp of equation (Figure 1B) 6 was set at the maximum value initially for a represented turning radius. The perturbations were added to the simulation by disturbing the wheels on the inside (up-hill) of the turn in a timed sequence related to the vehicle speed. The results of these studies are shown in Figure 6. The maximum roll angle of all the curves (ordinates) include the terrain slope.

The results indicate that for all slopes (including level terrain) the vehicle is unstable while making an Ackerman turn with a wheel of 24^{o} and vehicle speeds of above 8Km/hr. As can be seen in Figures 6B, 6C, 6D, 6E, and 6F, the vehicle was also either unstable or marginally stable (roll angles greater than 40^{o}) for smaller wheel angles. This situation would be eased somewhat if the vehicle had skidded. However, in studying the "worst case" it should be remembered that there may be cases where the vehicle cannot skid on level terrain or on slopes.

2.2 PITCH PLANE ANALYSIS

2.2.1 PROCEDURE

Where care is exercised in the choice of perturbations the stability characteristics of a rather complicated vehicle can be studied in a relatively simple manner. This was the approach used in studying the four wheel vehicle shown in Figure 1.

In studies to determine responses in the pitch plane step functions were used. This simulates a Lunar ledge which is struck first by the two front wheels and then, after a time delay (determined by the vehicle's speed), by the rear wheels. Since tire indentation and reverse thrust was neglected--or not completely known--a quarter-sine wave function was used on the computer to simulate the step function. Such a function takes into consideration the tire indentation and reverse thrust present when the vehicle strikes a sharp edged object. The frequency of the quarter-sine wave is a function of the speed of the vehicle.

Pitch plane studies were made to determine resonance responses. In this case the forcing function was a continuous sine wave. The resonant response was determined by taking frequency increments and noting the amplitudes and amplitude build-up for a particular amplitude and frequency input. The speed of the vehicle was correlated with the frequencies used by use of the vehicle wheel-base. In order to compare the vehicle pitch plane response to studies of other vehicles the modified step function described above was applied to all four vehicle wheels simultaneously. By varying the bump height of the obstacle traversed, the nonlinear vehicular response to different speeds and bump heights is shown.

Figures 1D, 1E, and 1F show the mathematical models and the equations of motion for the pitch plane studies. As is indicated, the vehicle was studied both for level terrain and for the condition where the vehicle was going down slopes of 10, 20 and 30 degrees. A body axis system was used for the latter study. Note an initial condition (IC) indicated in the equations. This is used since the rear wheels of this vehicle are physically attached to levers that extend to the rear of the main body. By the inclusion of the IC in the equations the vehicle was made to settle (with no perturbations) so that the rear wheel levers and the main body were parallel to level terrain.

The analog computer model used for the pitch plane studies is shown in Figure A1 of Appendix A, and the data are shown in Figure A2. The forcing functions were applied at the terrain level position (Z_{of}, Z_{or}, etc.) for all pitch plane simulations. The forcing function became zero when the vehicle wheel was off of the Lunar surface.

2.2.2 RESULTS

2.2.2.1 Resonance Analysis

Resonance analysis results of the four-wheel (using data of Appendix A) vehicle are shown in Figure 2. Since forcing function amplitude was low for this simulation, the vehicle did not leave the Lunar surface. Under this operating condition the vehicle resonance occurs between six and eight kilometers per hour. It should be noted that this is within the specified operating range of the vehicle and may cause difficulties with the LSV stability.

2.2.2.2 Forcing Functions Applied Simultaneously to All Wheels

Figure 3 shows the nonlinear vehicle response to different heights of obstacles traversed. The nonlinearity varies both with obstacle height and with the speed of the vehicle. This is primarily caused by the discontinuity of the forcing function when the LSV leaves the Lunar surface.

Figure 3A shows the peak displacement (ratioed to the height of the obstacle traversed) of the vehicle center of gravity. The data are self-explanatory and indicate the difficulty in keeping the LSV on the Lunar surface while it traverses surface obstacles. Both the displacement and the acceleration compare favorably with those of other vehicles previously studied. This is particularly true of the damping. In all cases the perturbations caused overshoot, but in all cases the oscillations of the distrubance always settled in six to eight seconds. For this and most of the studies on this vehicle a small amount of damping was inserted in the tires. It had very little effect, however, when compared to results obtained under the same conditions-but with no tire damping. The time history traces of parameters such as wheel displacement, acceleration, etc., are on file at the Marshall Space Flight Center, R-ASTR-A.

2.2.2.3 Sequential Bumps

When the vehicle traversed an object, such as a ledge, first the front wheels struck and later, depending on the length of the wheel base and the vehicle speed, the rear wheels struck the same ledge. The results of the four wheel LSV's traversing this type of obstacle is shown in Figure 4. During these studies the height of the obstacles traversed were changed and the speed of the vehicle was changed. Figures 4A, 4B, 4C, and 4D show the resulting maximum displacement of the LSV center of gravity of under the test conditions. In most cases two curves are shown for each condition--the maximum CG displacement caused from the front wheel's striking and the maximum CG displacement from

the rear wheel's striking. The inclusion of two curves for a test condition indicates that the vehicle had started to settle from the front wheel perturbation when the rear wheels struck. One dashed curve for a test condition indicates that the peak of the CG displacement had not been reached when the rear wheel struck. The somewhat perculiar shapes of the curves are attributed both to the long wheel base and the method of attaching the rear wheels (on a lever) to the main vehicle body. Attention is called to the difference in the general curve shapes for the 8.36 Km/hr conditions. This could be caused from the resonance described earlier. Further examination would be required to make certain. A comparison between Figure 3A and Figure 4A will demonstrate the effects of the high moment of inertia and the long wheel base given for this vehicle. Effects of slopes on the vehicle's operation can be seen by comparing Figure 4A with Figures 4B, 4C and 4D.

CG accelerations under the test conditions are shown in Figures 4E and 4F. Comparison of the upper curve of Figure 4E with those of Figure 3B will again point out the advantages of a high moment of inertia and a long wheelbase. Also the effects on the CG acceleration for the 8.36 Km/hr test condition are unique. The result of the rear wheel's striking is shown by the dash-line curve. Accelerations to the CG from the rear wheels' striking at other speeds were either less than those caused by the front wheels or they were identical to those of the front wheels, and are not shown.

Care should be taken in interpreting the curves of Figures 4G, 4H, 4I, 4J, 4K, and 4L. On Figure 1 the coordinate system is shown with right-hand rotation and the Z axis as positive up. This makes the pitch angle positive in clockwise rotation. Since the curves of the above figures result from operations on the level terrain or down a slope the curves maked "minimum" are counterclockwise (front of the vehicle displaced upward) variations of the vehicle's pitch angle. When an obstacle was struck with the vehicle going down a slope, the initial variation reduced the pitch angle. The test conditions were set with the vehicle traveling down a grade because it was felt that this represented a "worst case" condition and that the vehicle was more likely to pitch over during such tests. Even though the vehicle did not pitch over, it did near the critical point for high obstacles at the two higher test speeds, leaving some doubt as to its stability under these conditions for the 30^{o} slope. Positive pitch angles of 45^{o} were reached. The critical angle is just above 50^{o}.

The random surface traverse represents the LSV's CG while it is driven over an irregular Lunar surface. For the low amplitudes of the forcing function there is an indication that irregular surface perturbations will cause the LSV to reacha nearly constant frequency of oscillation at a nearly constant amplitude. This, of course, would be changed by large spike-type irregularly-spaced obstacles, but this theory should hold as long as the LSV does not leave the Lunar surface. Figures 4M and 4N show the time history traces of the CG displacements for the tests that were run, along with the forcing functions that were used. Figures 4O

and 4P show that the average CG displacement for random surface bumps is approximately two-thirds the average height of the bumps. It should be noted that for this test condition, the LSV did not leave the Lunar surface.

2.3 CONCLUSIONS AND RECOMMENDATIONS

While this vehicle was tested using only one set of parameters, the values of suspension and tire constants appear to be well chosen. For instance, in previous studies (Task Order N-22 ; Reference 1) it was demonstrated by parametric studies of suspension systems that:

(1) Stiff suspension springs and tire (spring) constants will cause a greater CG displacement than soft springs while an LSV is traversing an obstacle with a given height. Softer springs, on the other hand, allow more ringing after an obstacle is struck. Initial vehicle settling also is greater for softer springs.

(2) Greater damping will reduce settling times, but, in the case of the LSV, will cause greater initial CG displacement (at higher vehicle speeds) when an obstacle is traversed.

The choice of constants is, therefore, a compromise.

Table I shows a comparison of the results found for a 6500 pound vehicle (Reference 1), tested under several conditions, and the 4-wheel vehicle of this report. The results are shown for each vehicle traversing a 0.31 meter obstacle at 8.36 Km/hr. Step functions were used for all cases.

In the case of this vehicle, the suspension and tire constants allow an initial vehicle settling of nearly 0.9 feet. This appears to be reasonable since the vehicle bottoms (in these tests) only for 0.62 meter obstacles at slow speeds. The suspension damping gave a performance similar to that of a damping factor (ζ) of 0.5 to 0.6. This appears to be within range since in control systems the most common damping factor generally chosen is 0.7.

Some difficulty with this vehicle was noted on higher slopes. The difficulty is not peculiar to this design or suspension system. The difficulty presents itself through the effects of the low Lunar gravity. The margin of safety from turnover is low when the vehicle makes turns up slopes or makes Ackerman turns with the full 24^{o} wheel on level terrain --particularly at the higher recommended speeds. The margin of safety is also low when the vehicle strikes large objects while going down slopes. Pitch angle for the latter conditions reached 45^{o} while overturn occurred at approximately 50^{o}.

This type of task does not call for recommendations, and no recommendations are made.

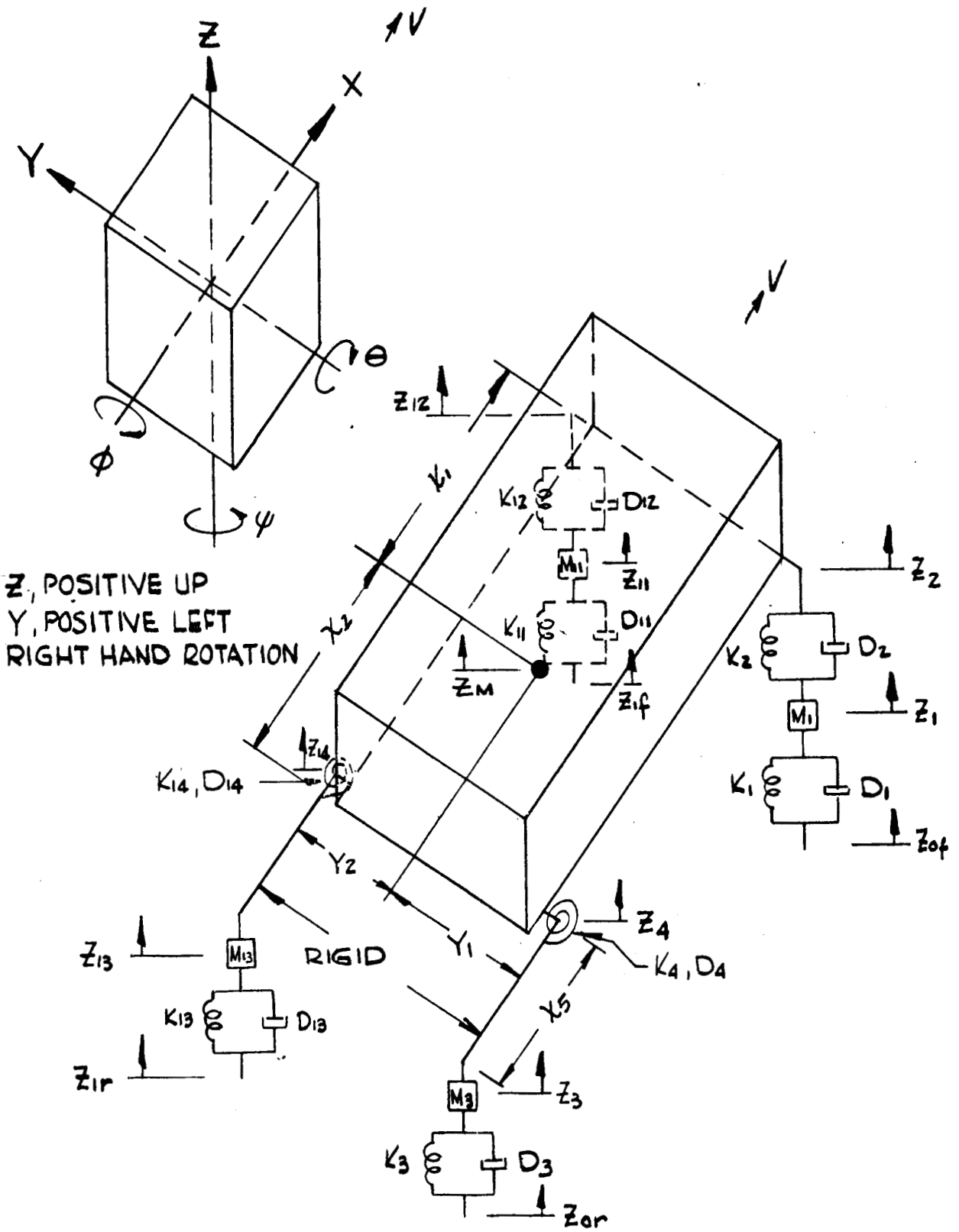

FIGURE 1A. 4 WHEEL LSV - MATHEMATICAL MODEL

ROLL PLANE:

(1) $\ddot{Z}_1 M_1 = K_1 (Z_{of} - Z_1) + D_1 (\dot{Z}_{of} - \dot{Z}_1) - K_2 (Z_1 - Z_2) - D_2 (\dot{Z}_1 - \dot{Z}_2) - g M_1$

(2) $\ddot{Z}_{11} M_{11} = K_{11} (Z_{1f} - Z_{11}) + D_{11} (\dot{Z}_{of} - \dot{Z}_{11}) - K_{12} (Z_{11} - Z_{12}) - D_{12} (\dot{Z}_{11} - \dot{Z}_{12}) - g M_{11}$

(3) $\ddot{Z}_M M_M = K_2 (Z_1 - Z_2) + D_2 (\dot{Z}_1 - \dot{Z}_2) + K_{12} (Z_{11} - Z_{12}) + D_{12} (\dot{Z}_{11} - \dot{Z}_{12}) + K_4 [Z_3 + IC - (Z_4 - X_5 \theta_M)] + D_4 [\dot{Z}_{13} - (\dot{Z}_{14} - X_5 \dot{\theta}_M) - g M_M$

(4) $\ddot{Z}_3 M_3 = K_3 (Z_{or} - Z_3) + D_3 (\dot{Z}_{or} - \dot{Z}_3) - K_4 [Z_3 + I_c - (Z_4 - X_5 \theta_M)] - D_4 [\dot{Z}_3 - (\dot{Z}_4 - X_5 \dot{\theta}_M)] - g M_3$

(5) $\ddot{Z}_{13} M_{13} = K_{13} (Z_{1r} - Z_{13}) + D_{13} (\dot{Z}_{1r} - \dot{Z}_{13}) - K_{14} [Z_{13} + I_c - (Z_{14} - X_5 \theta_M)] - D_{14} [\dot{Z}_{13} - (\dot{Z}_{14} - X_5 \dot{\theta}_M)] - g M_{13}$

(6) $\ddot{\phi}_M I_{xM} = Y_2 [K_{13} (Z_{1r} - Z_{13}) + D_{13} (\dot{Z}_{1r} - \dot{Z}_{13}) + K_{11} (Z_{1f} - Z_{11}) + D_{11} (\dot{Z}_{1f} - \dot{Z}_{11})] - Y_1 [K_3 (Z_{or} - Z_3) + D_3 (\dot{Z}_{or} - \dot{Z}_3) + K_1 (Z_{of} - Z_1) + D_1 (\dot{Z}_{of} - \dot{Z}_1)] - M_o$

(7) $\ddot{\theta}_M I_{YM} = (X_2 + X_5) [K_3 (Z_{or} - Z_3) + D_3 (\dot{Z}_{or} - \dot{Z}_3) + K_{13} (Z_{1r} - Z_{13}) + D_{13} (\dot{Z}_{1r} - \dot{Z}_{13})] X_1 [K_1 (Z_{of} - Z_1) + D_1 (\dot{Z}_{of} - \dot{Z}_1) + K_{11} (Z_{1f} - Z_{11}) + D_{11} (\dot{Z}_{1f} - \dot{Z}_{11})]$

(8) $\ddot{Z}_4 = \ddot{Z}_M + X_2 \ddot{\theta}_M - Y_1 \ddot{\phi}_M$

$\dot{Z}_4 = \dot{Z}_M + X_2 \dot{\theta}_M - Y_1 \dot{\phi}_M$

$Z_4 = Z_M + X_2 \theta_M - Y_1 \phi_M$

FIGURE 1B. 4 WHEEL LSV - ROLL PLANE EQUATIONS

$$(9)\quad \ddot{Z}_{14} = \ddot{Z}_M + X_2 \ddot{\Theta}_M + Y_2 \ddot{\Phi}_M$$
$$\dot{Z}_{14} = \dot{Z}_M + X_2 \dot{\Theta}_M + Y_2 \dot{\Phi}_M$$
$$Z_{14} = Z_M + X_2 \Theta_M + Y_2 \Phi_M$$

$$(10)\quad \ddot{Z}_2 = \ddot{Z}_M - X_1 \ddot{\Theta}_M - Y_1 \ddot{\Phi}_M$$
$$\dot{Z}_2 = \dot{Z}_M - X_1 \dot{\Theta}_M - Y_1 \dot{\Phi}_M$$
$$Z_2 = Z_M - X_1 \Theta_M - Y_1 \Phi_M$$

$$(11)\quad \ddot{Z}_{12} = \ddot{Z}_M - X_1 \ddot{\Theta}_M + Y_2 \ddot{\Phi}_M$$
$$\dot{Z}_{12} = \dot{Z}_M - X_1 \dot{\Theta}_M + Y_2 \dot{\Phi}_M$$
$$Z_{12} = Z_M - X_1 \Theta_M + Y_2 \Phi_M$$

FIGURE 1C. 4 WHEEL LSV - ROLL PLANE EQUATIONS

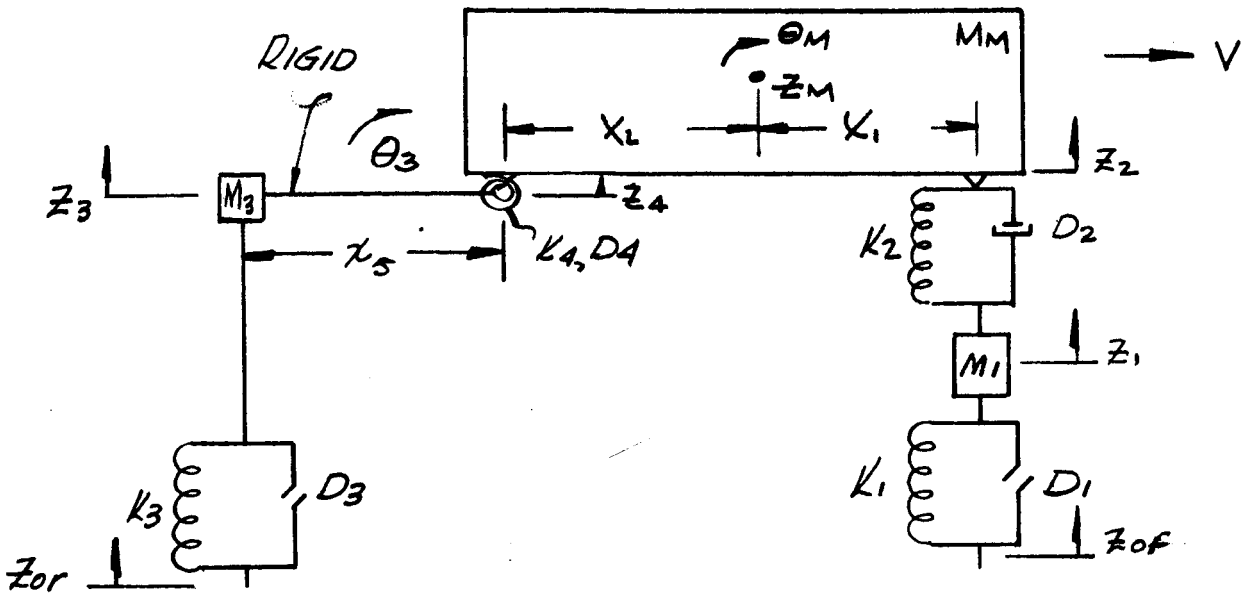

FIGURE 1D. 4 WHEEL LSV - MATHEMATICAL MODEL, PITCH PLANE, LEVEL TERRAIN

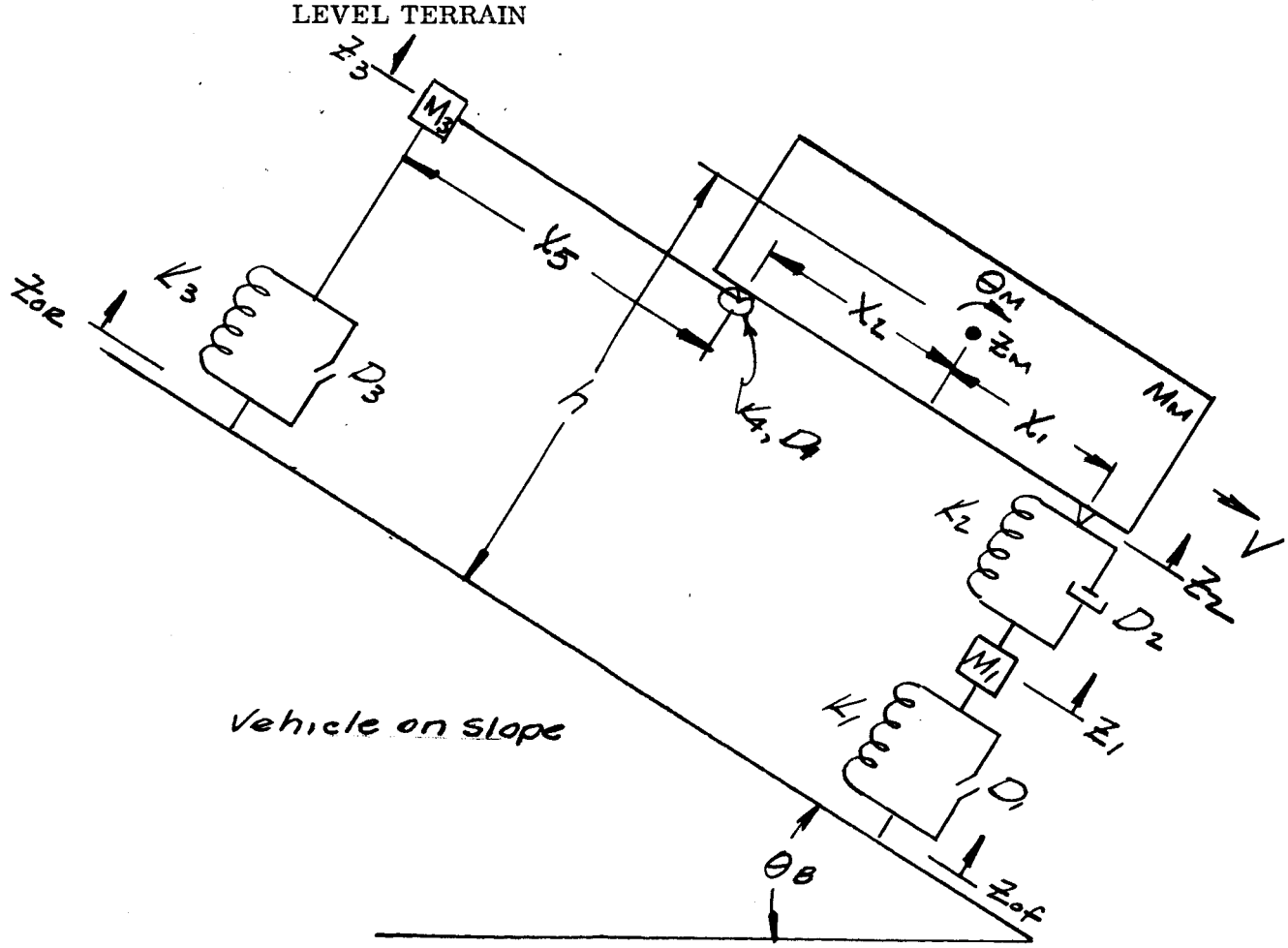

FIGURE 1E. 4 WHEEL LSV - MATHEMATICAL MODEL, PITCH PLANE, VEHICLE ON SLOPE

FOR FIGID,1E: (Body Axis for Figure 1E)

$$(1)\ \ddot{z}_1 M_1 = K_1(z_{of} - z_1) + D_1(\dot{z}_{of} - \dot{z}_1) - K_2(z_1 - z_2) - D_2(\dot{z}_1 - \dot{z}_2) - g M_1 \cos(\theta_B)$$

$$(2)\ \ddot{z}_M M_M = K_2(z_1 - z_2) + D_2(\dot{z}_1 - \dot{z}_2) + K_3(z_{or} - z_3) + D_3(\dot{z}_{or} - \dot{z}_3) - \ddot{z}_3 M_3 - g M_M \cos(\theta_B)$$

$$(3)\ \ddot{\theta}_M I_{YM} = \left[K_3(z_{or} - z_3) + D_3(\dot{z}_{or} - \dot{z}_3) - \ddot{z}_3 M_3\right]\left[(X_2 + X_5) + h \sin\theta_B\right] - \left[K_2(z_1 - z_2) + D_2(\dot{z}_1 - \dot{z}_2)\right]\left[K_1 - h \sin\theta_B\right]$$

$$(4)\ \ddot{\theta}_3 I_{YM_{3+B}} = X_5\left[K_3(z_{or} - z_3) + D_3(\dot{z}_{or} - \dot{z}_3)\right] - K_4(\theta_3 + IC - \theta_M) - D_4(\dot{\theta}_3 - \dot{\theta}_M)$$

$$(5)\ \ddot{z}_4 = \ddot{z}_M + X_2\ddot{\theta}_M$$
$$\dot{z}_4 = \dot{z}_M + X_2\dot{\theta}_M$$
$$z_4 = z_M + X_2\theta_M$$

$$(6)\ \ddot{z}_2 = \ddot{z}_M - X_1\ddot{\theta}_M$$
$$\dot{z}_2 = \dot{z}_M - X_1\dot{\theta}_M$$
$$z_2 = z_M - X_1\theta_M$$

$$(7)\ \ddot{z}_3 = \ddot{z}_4 + X_5\ddot{\theta}_3$$
$$\dot{z}_3 = \dot{z}_4 + X_5\dot{\theta}_3$$
$$z_3 = z_4 + X_5(\theta_3 + .117)$$

I.C.

FIGURE 1F. 4 WHEEL LSV - PITCH PLANE EQUATIONS

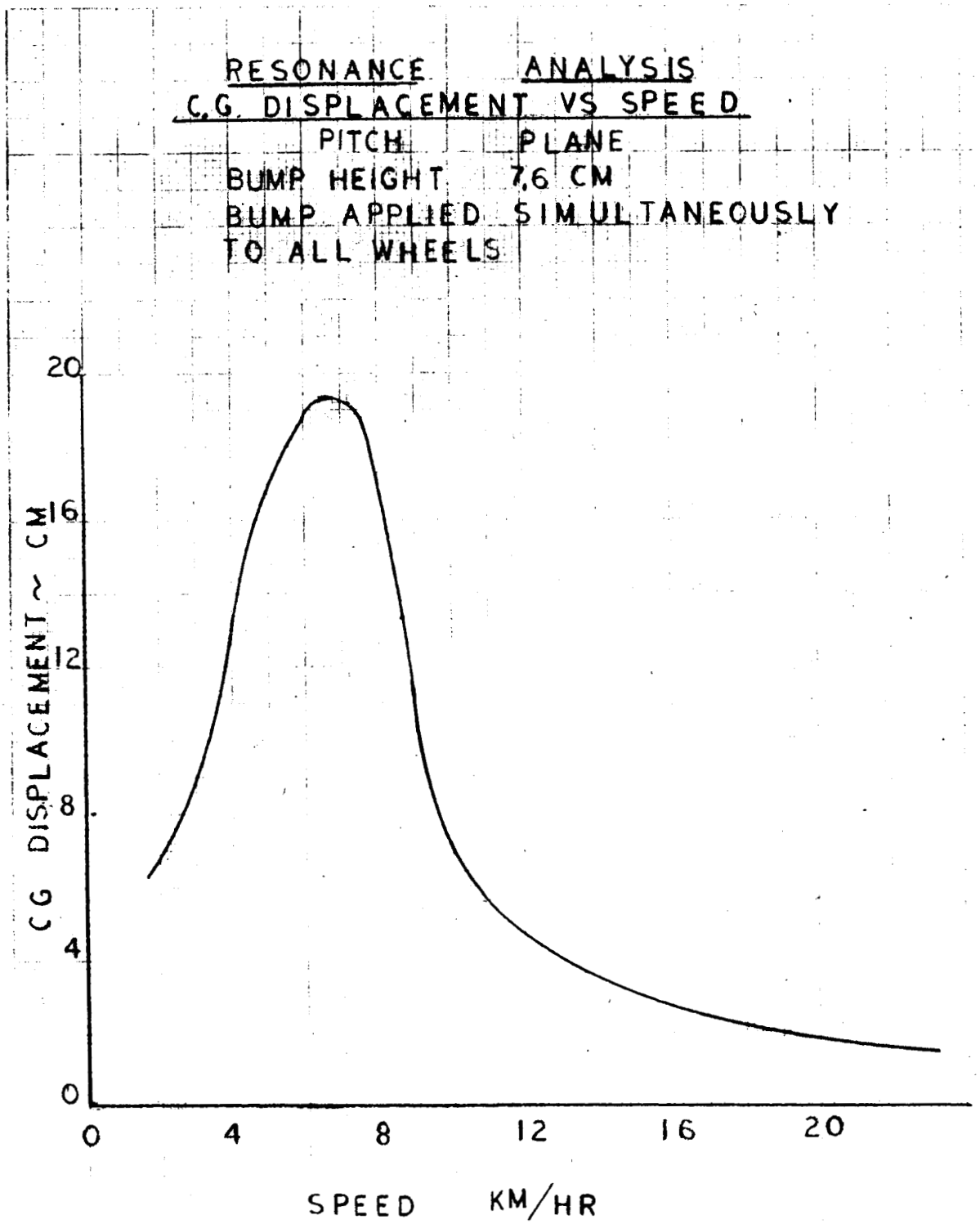

FIGURE 2. CG DISPLACEMENT VERSUS SPEED

PITCH PLANE ANALYSIS

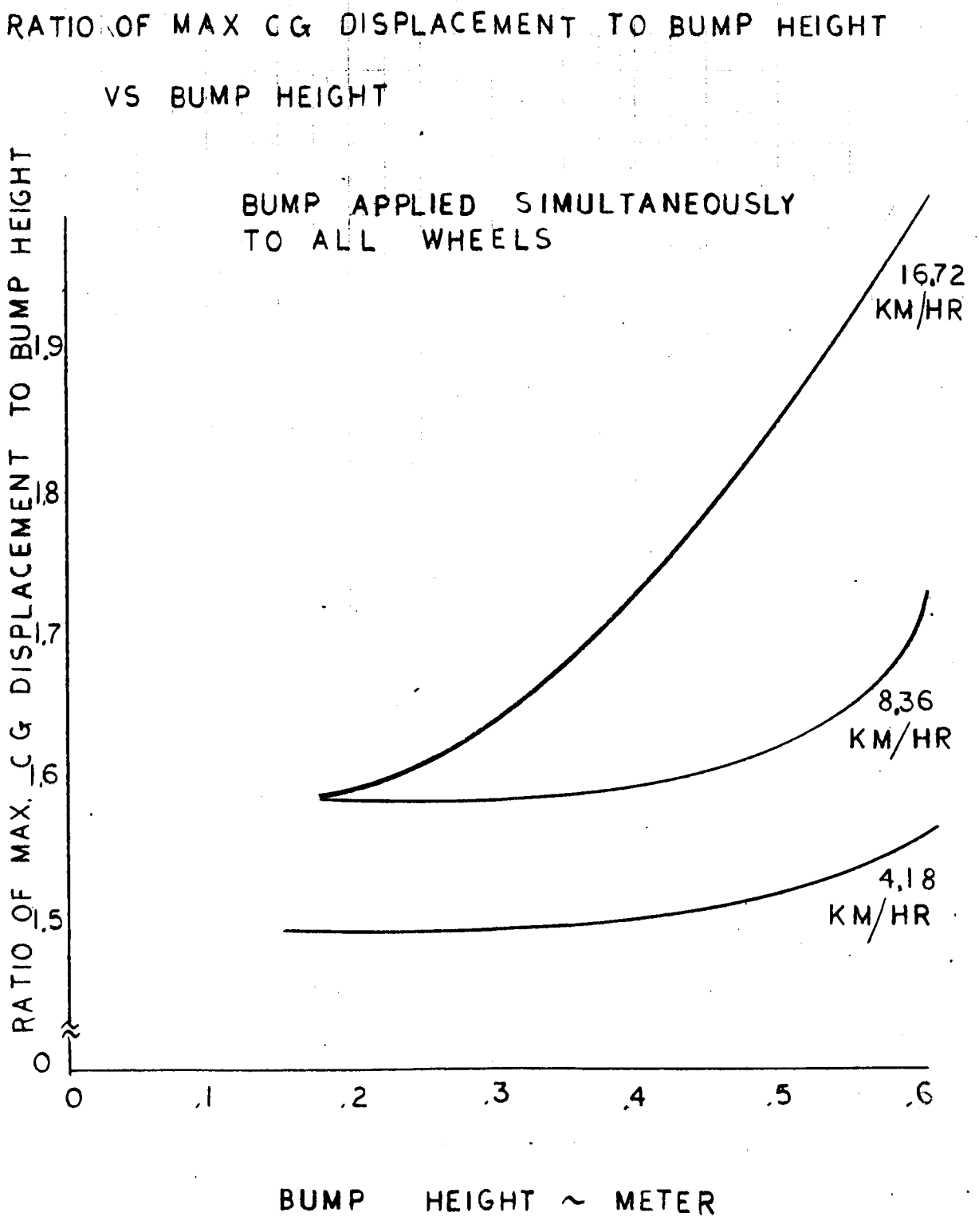

FIGURE 3A. RATIO CG DISPLACEMENT TO BUMP HEIGHT VERSUS BUMP HEIGHT

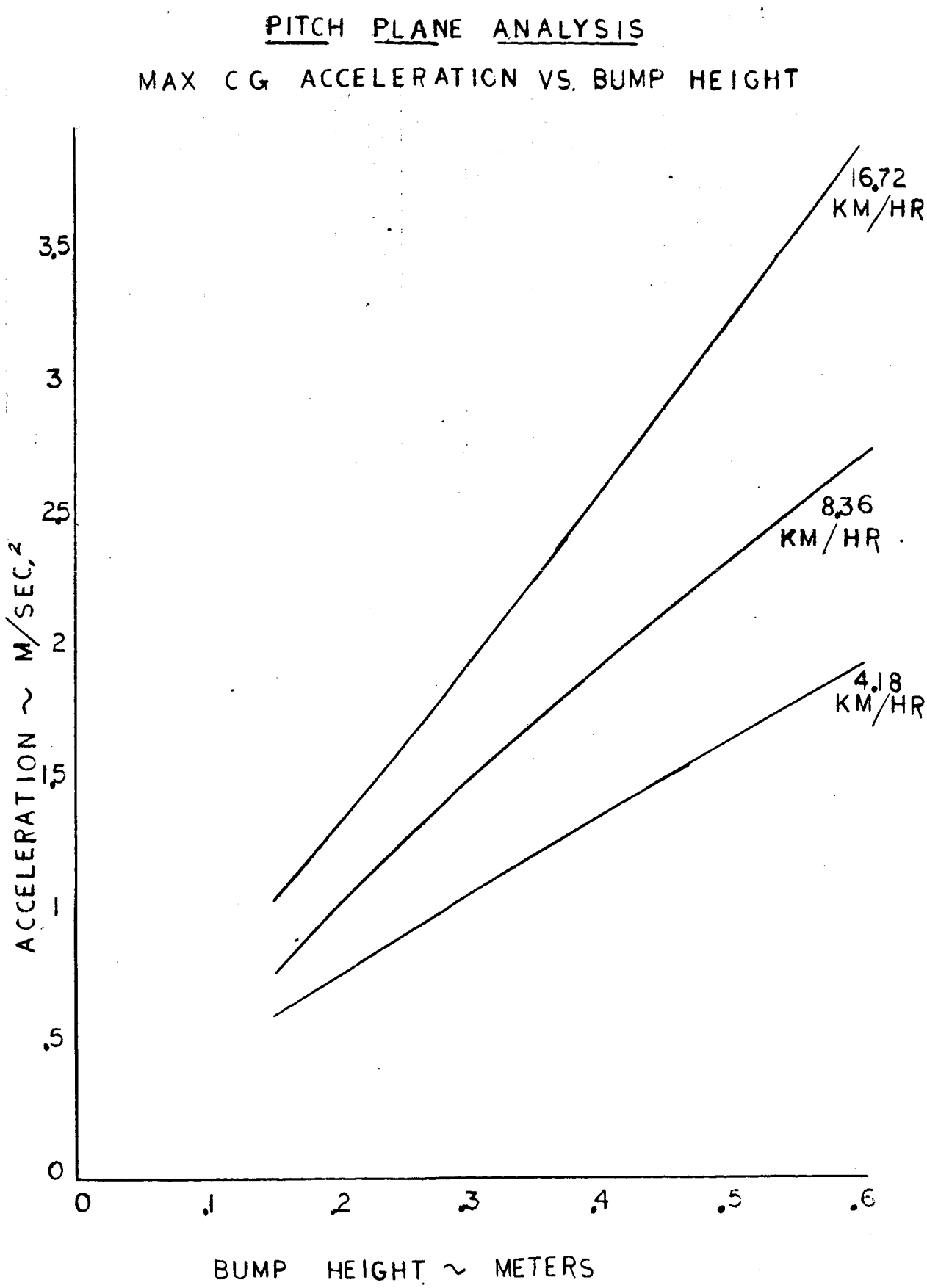

FIGURE 3B. MAXIMUM CG ACCELERATION VERSUS BUMP HEIGHT

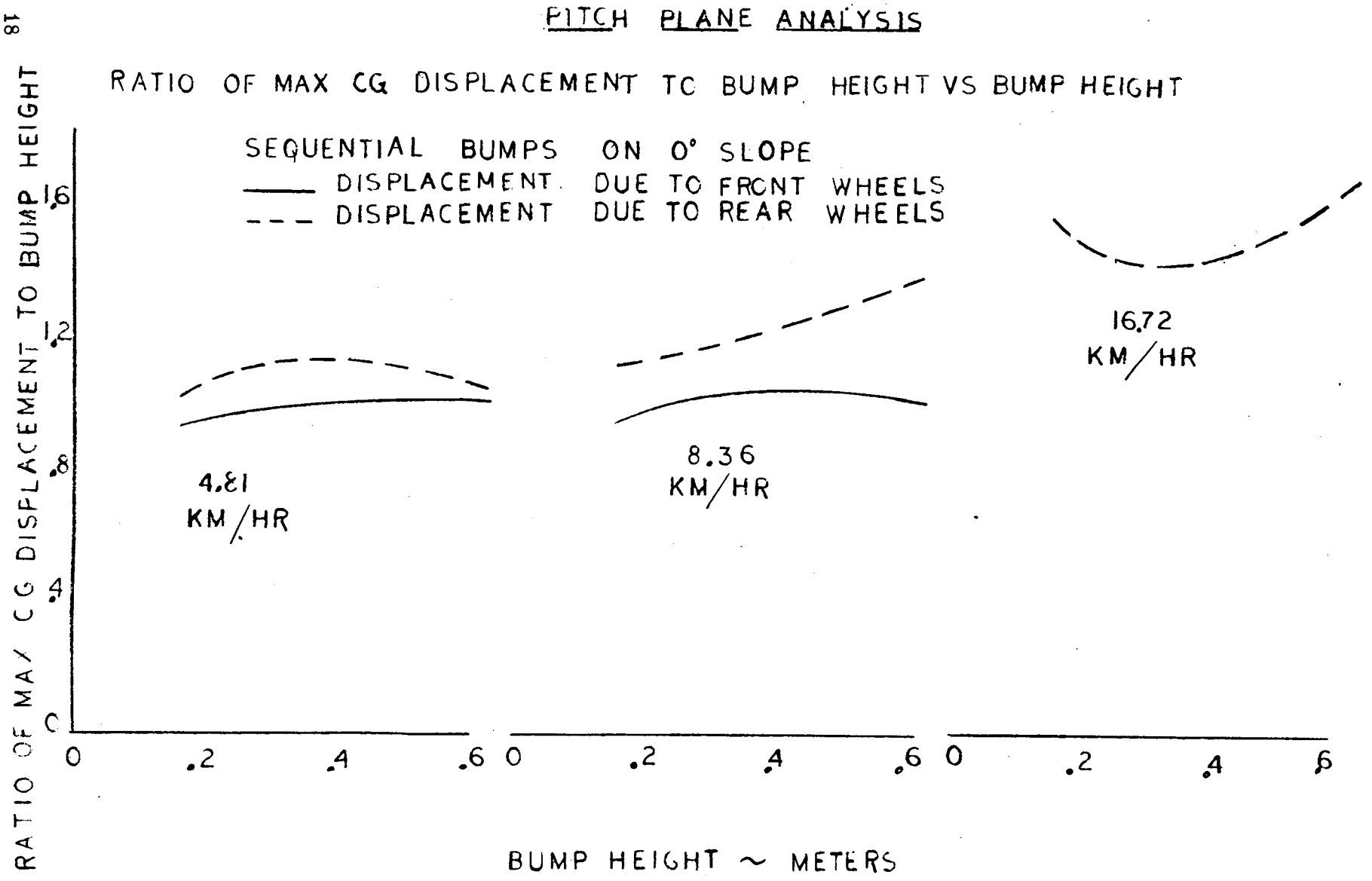

FIGURE 4A. MAXIMUM RATIO CG DISPLACEMENT TO BUMP HEIGHT VERSUS BUMP HEIGHT

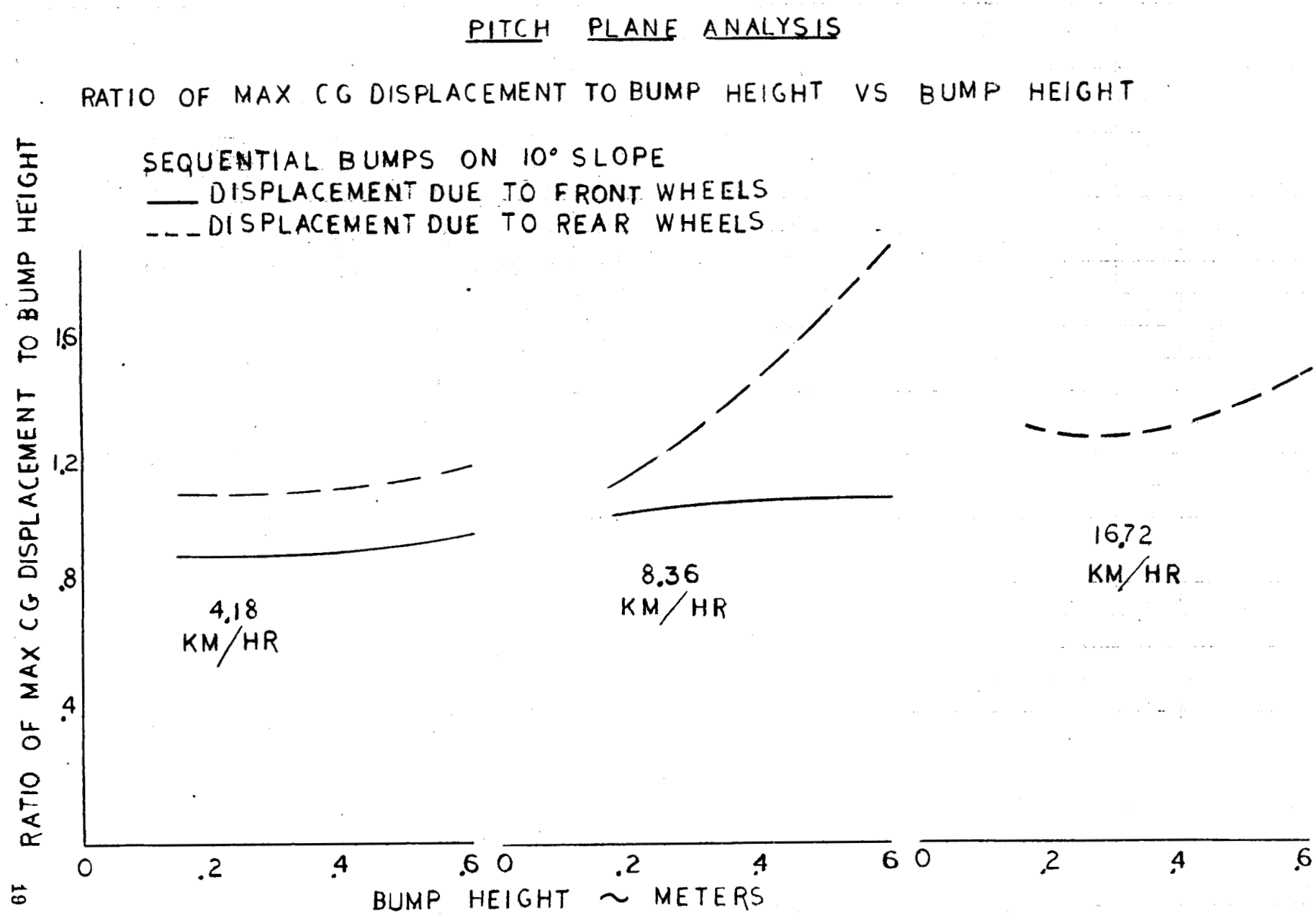

FIGURE 4B. MAXIMUM RATIO CG DISPLACEMENT TO BUMP HEIGHT VERSUS BUMP HEIGHT

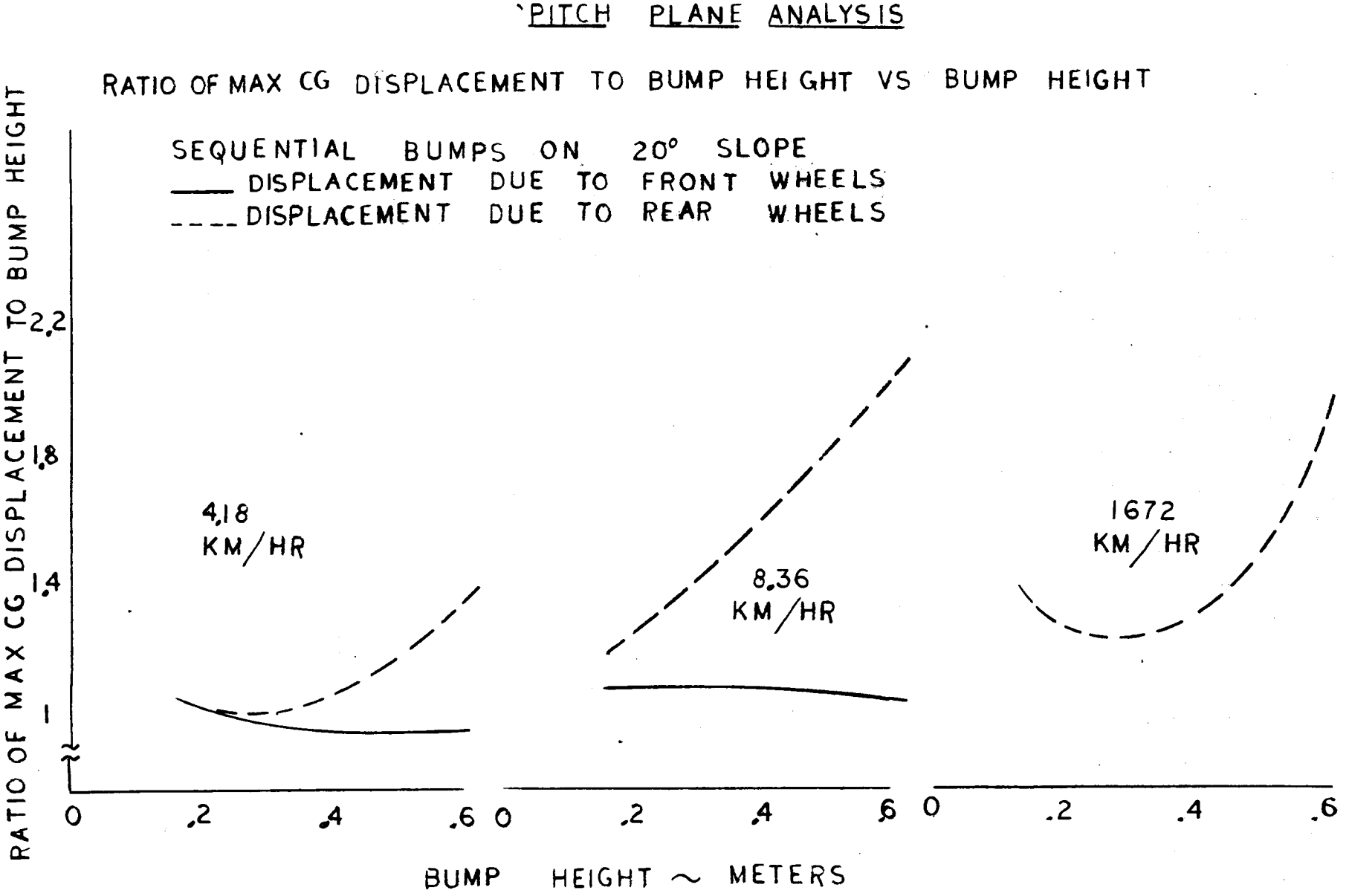

FIGURE 4C. MAXIMUM RATIO CG DISPLACEMENT TO BUMP HEIGHT VERSUS BUMP HEIGHT

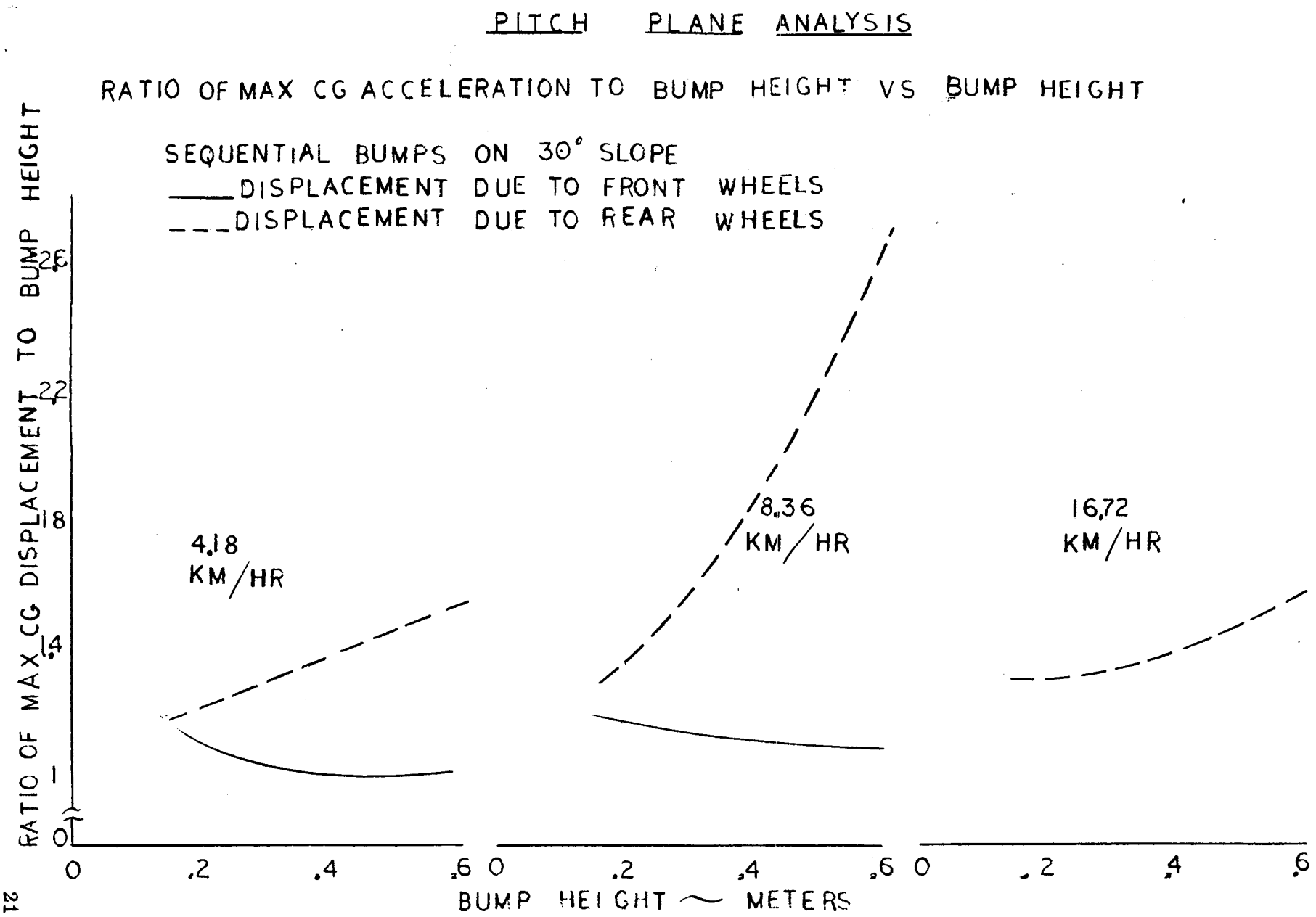

FIGURE 4D. MAXIMUM RATIO CG DISPLACEMENT TO BUMP HEIGHT VERSUS BUMP HEIGHT

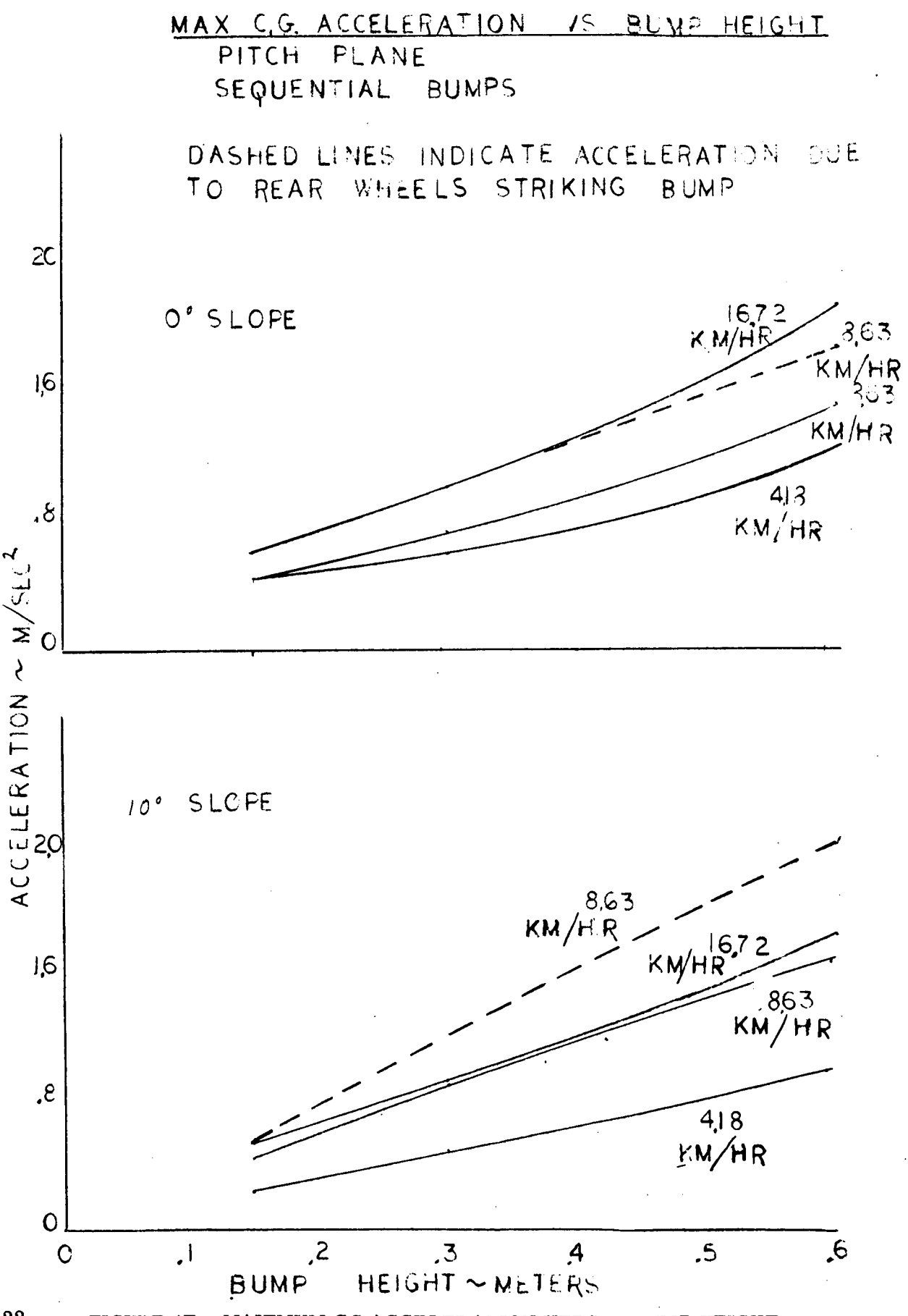

22 FIGURE 4E. MAXIMUM CG ACCELERATION VERSUS BUMP HEIGHT

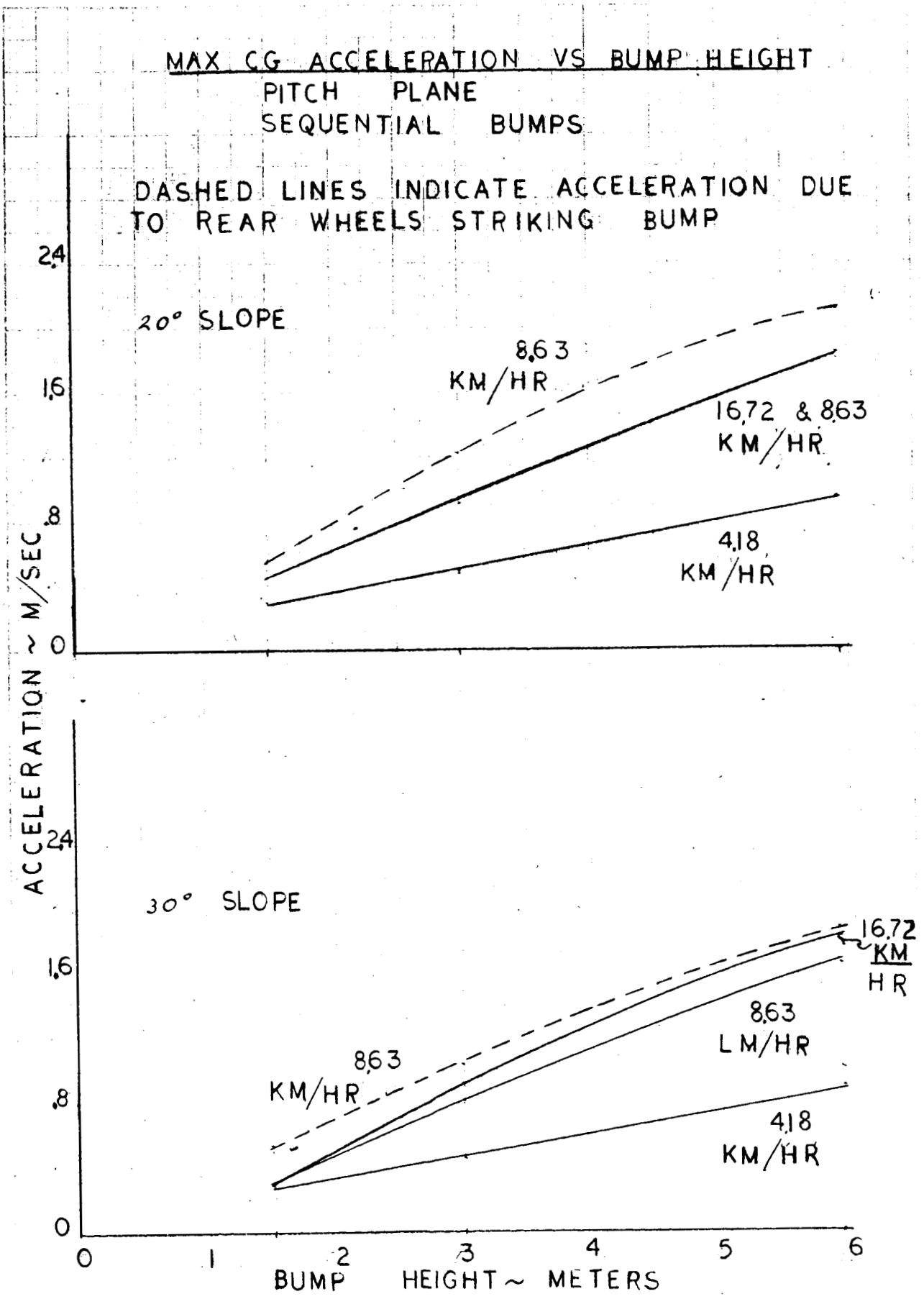

FIGURE 4F. MAXIMUM CG ACCELERATION VERSUS BUMP HEIGHT

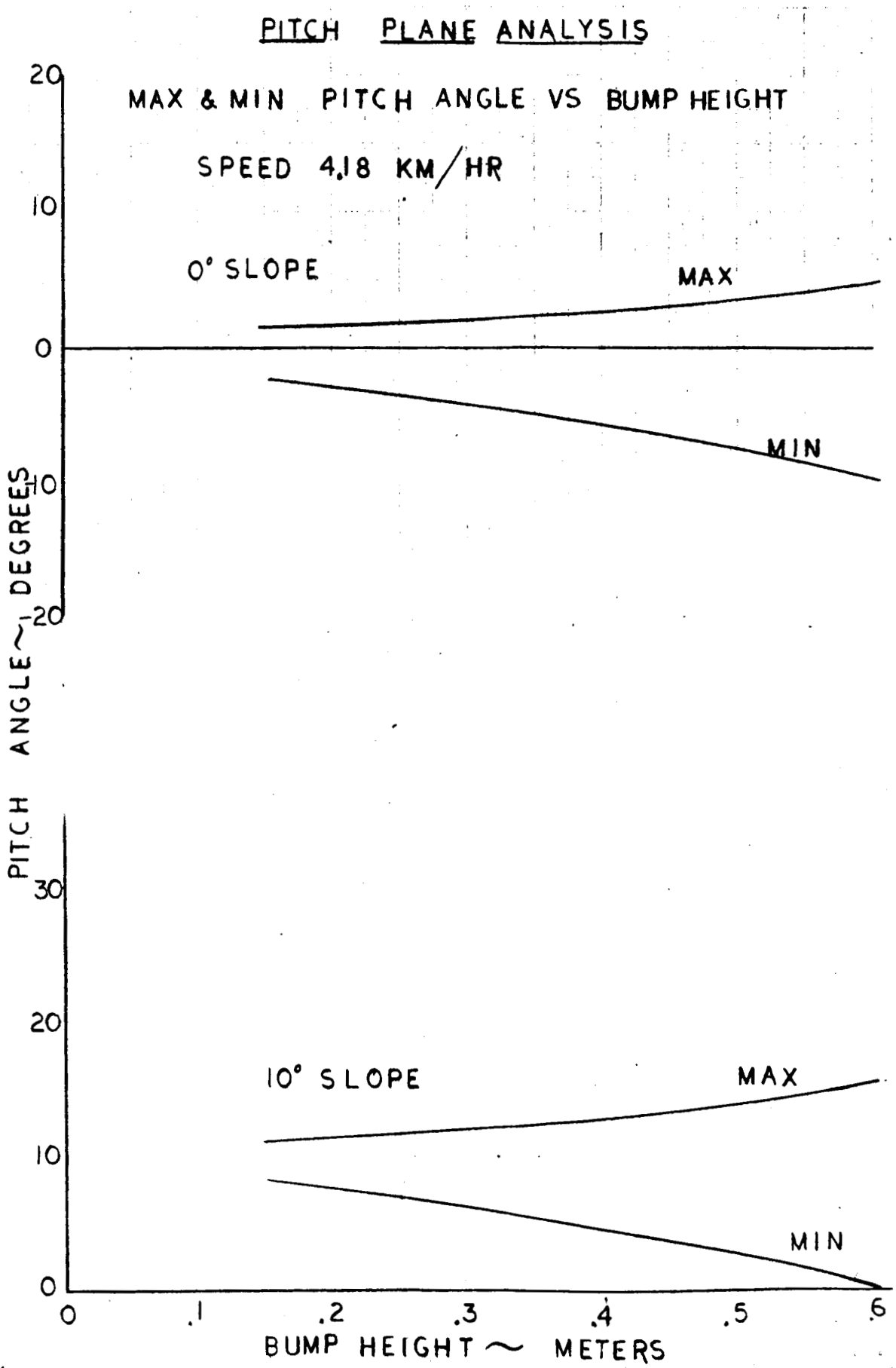

FIGURE 4G. MAXIMUM AND MINIMUM PITCH ANGLE VERSUS BUMP HEIGHT

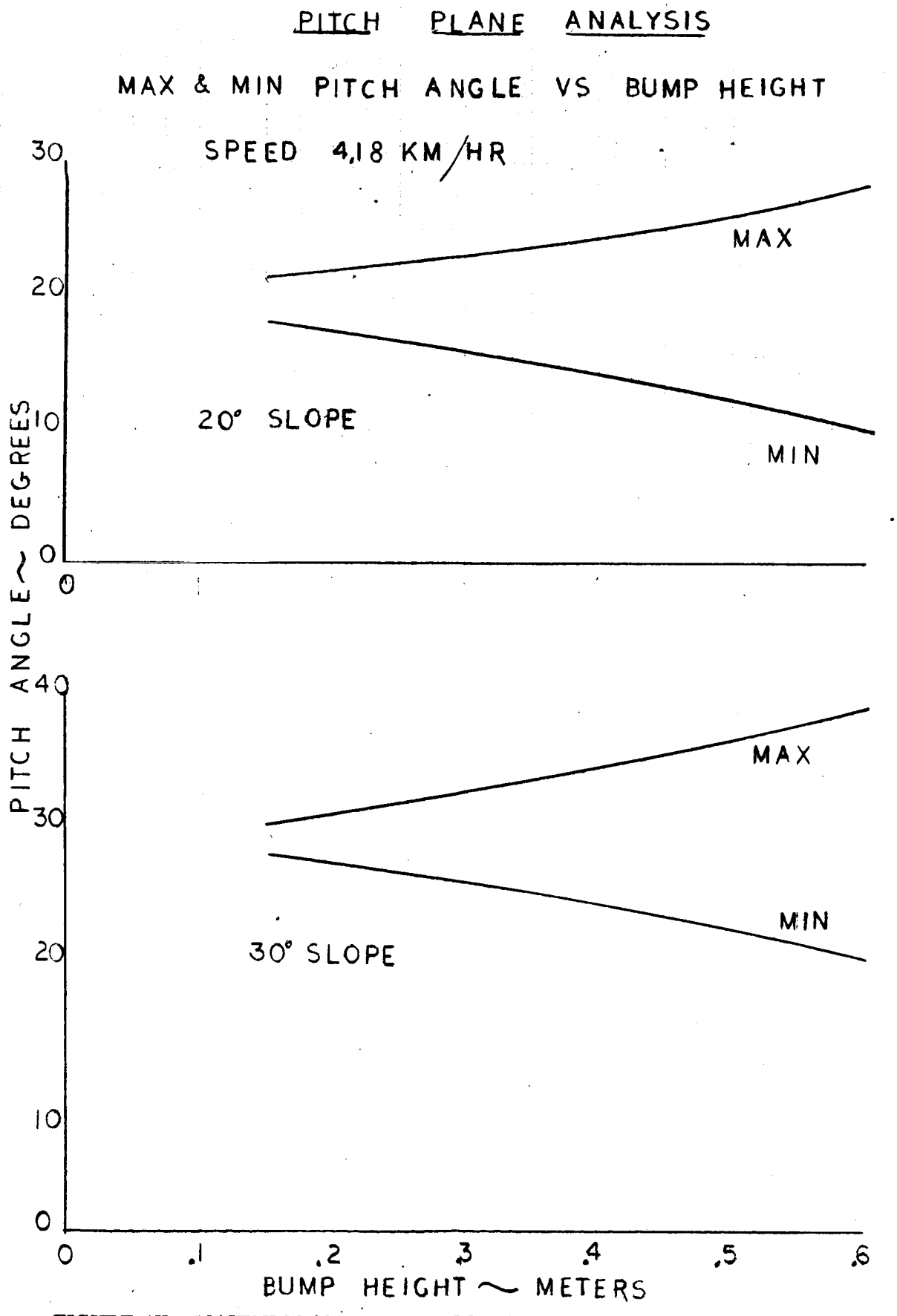

FIGURE 4H. MAXIMUM AND MINIMUM PITCH ANGLE VERSUS BUMP HEIGHT

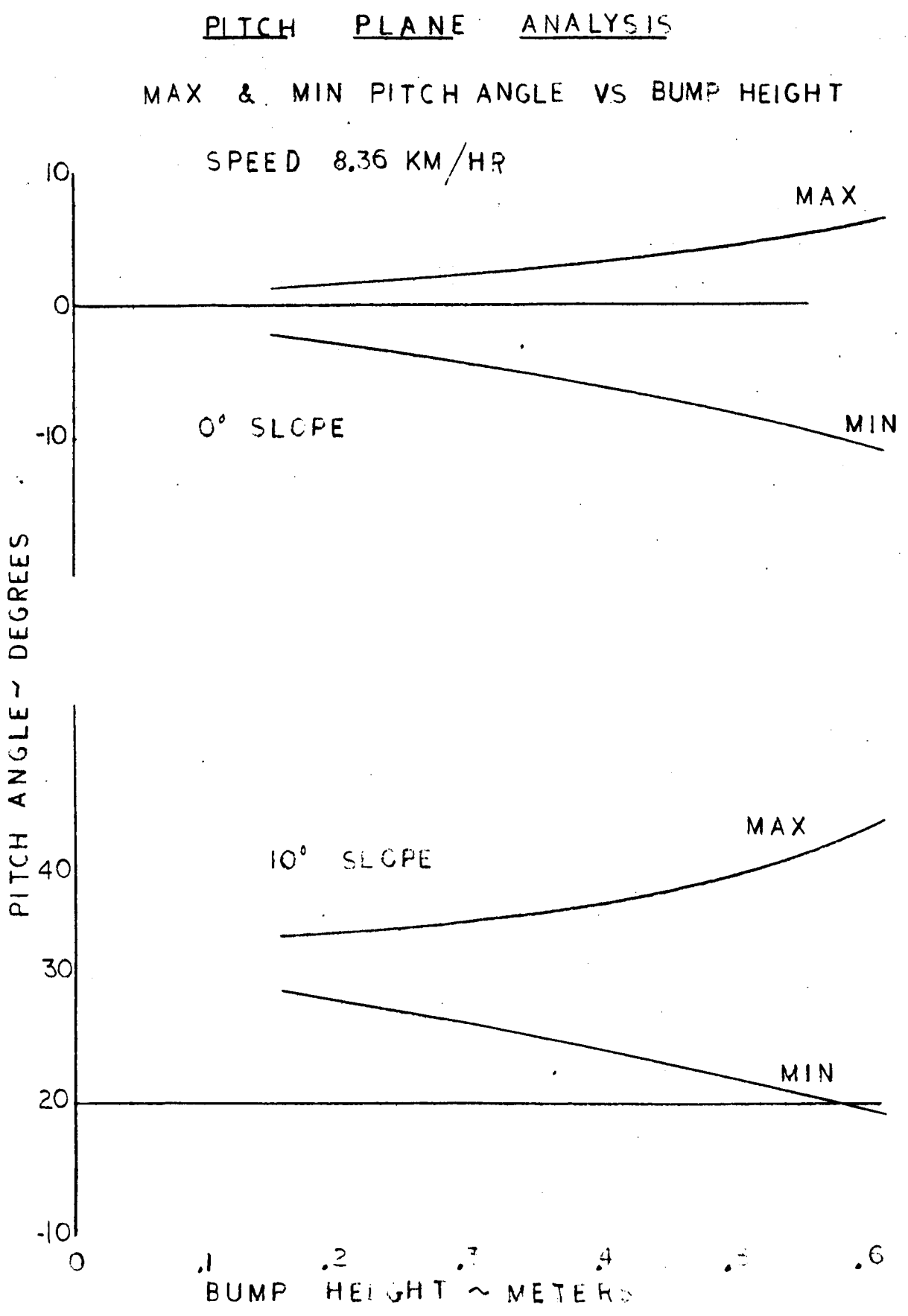

FIGURE 41. MAXIMUM AND MINIMUM PITCH ANGLE VERSUS BUMP HEIGHT

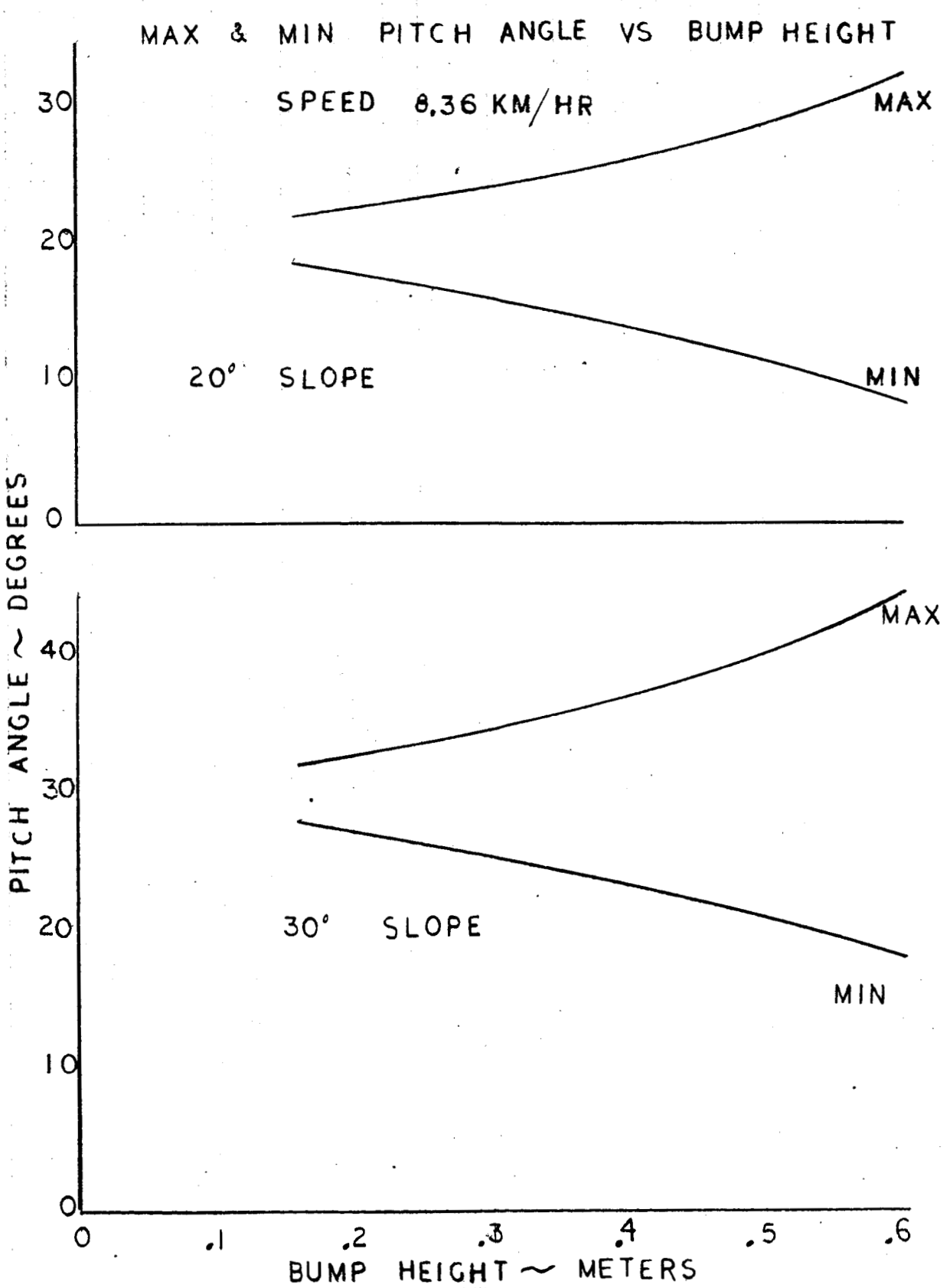

FIGURE 4J. MAXIMUM AND MINIMUM PITCH ANGLE VERSUS BUMP HEIGHT

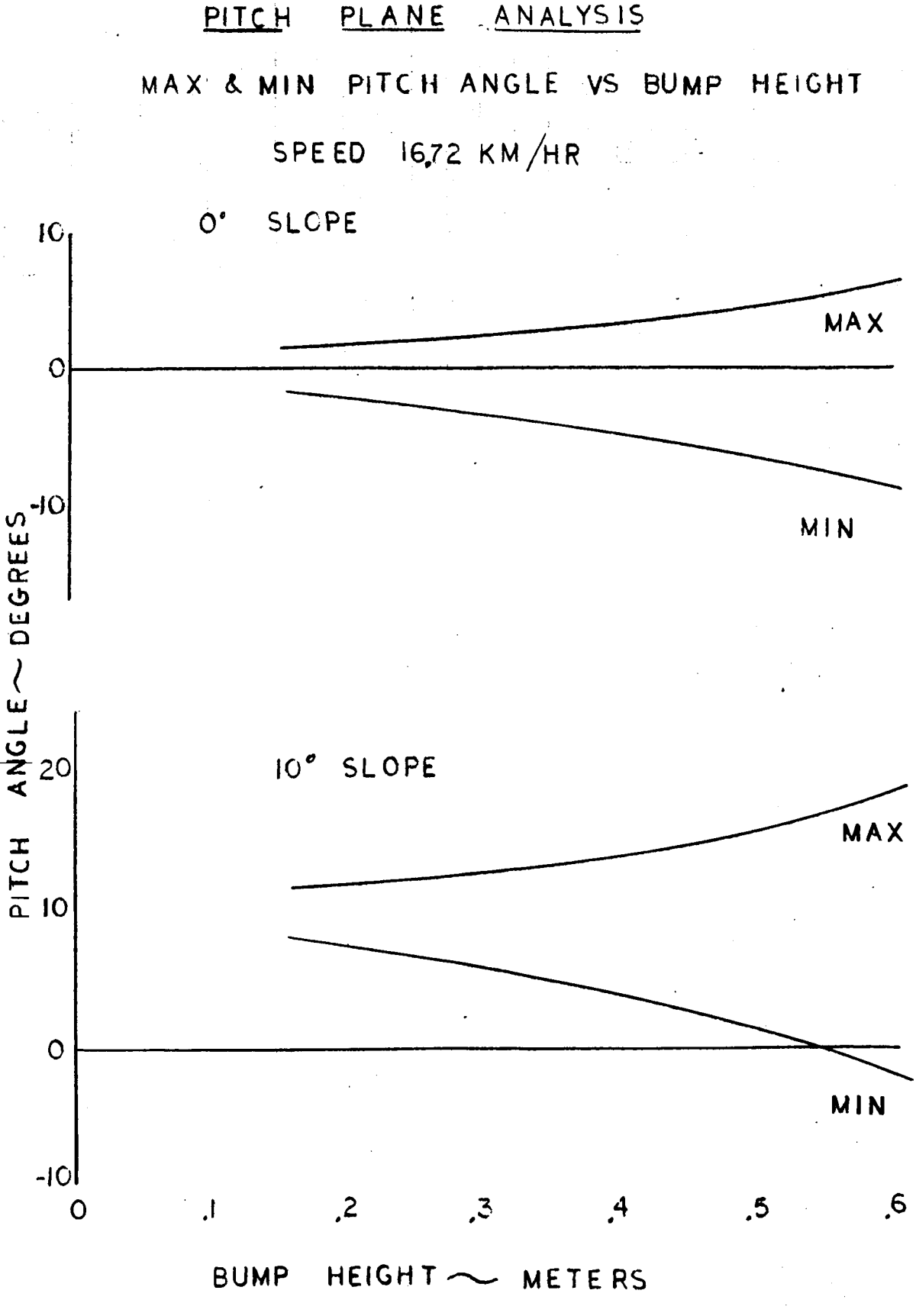

FIGURE 4K. MAXIMUM AND MINIMUM PITCH ANGLE VERSUS BUMP HEIGHT

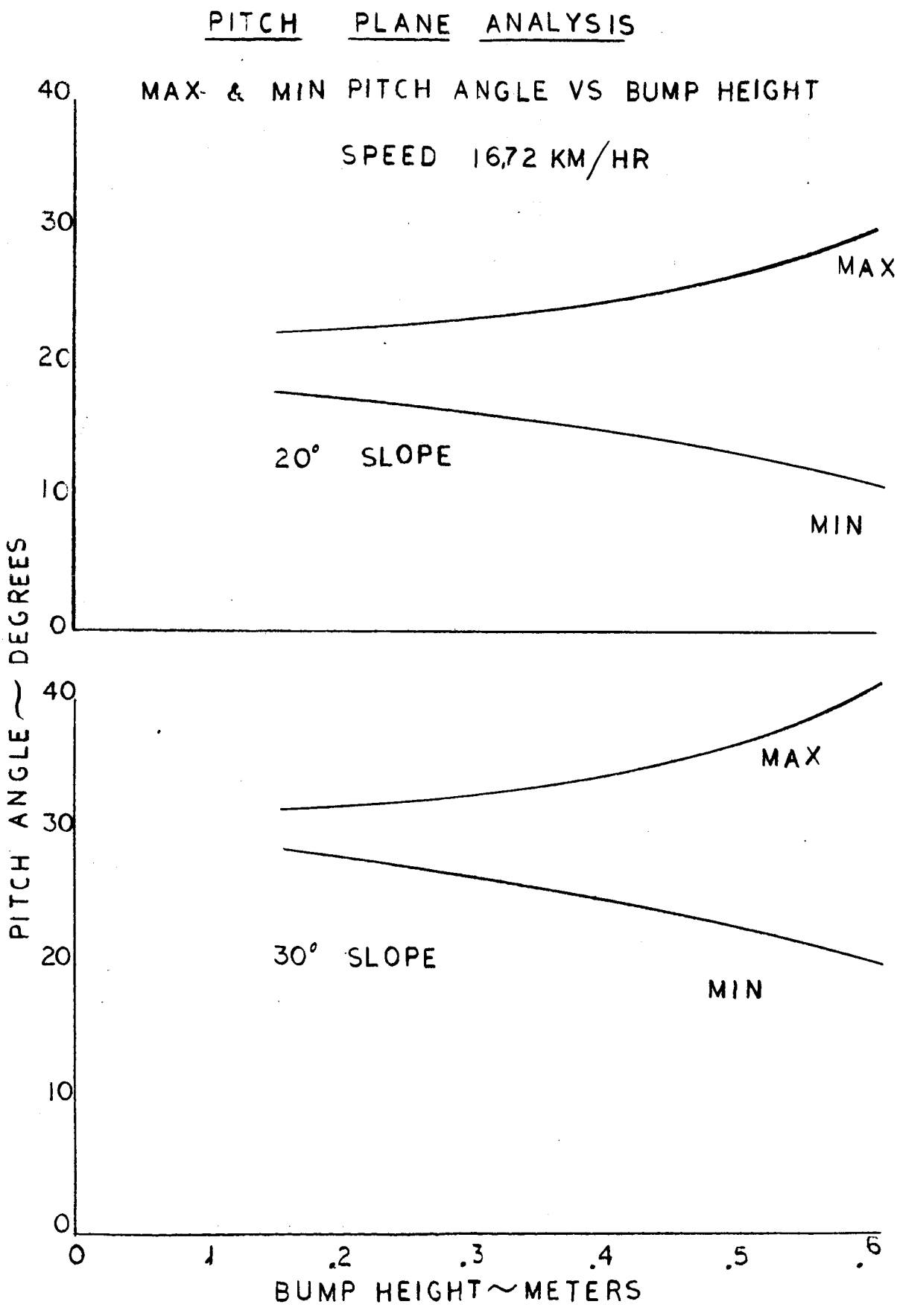

FIGURE 4L. MAXIMUM AND MINIMUM PITCH ANGLE VERSUS BUMP HEIGHT

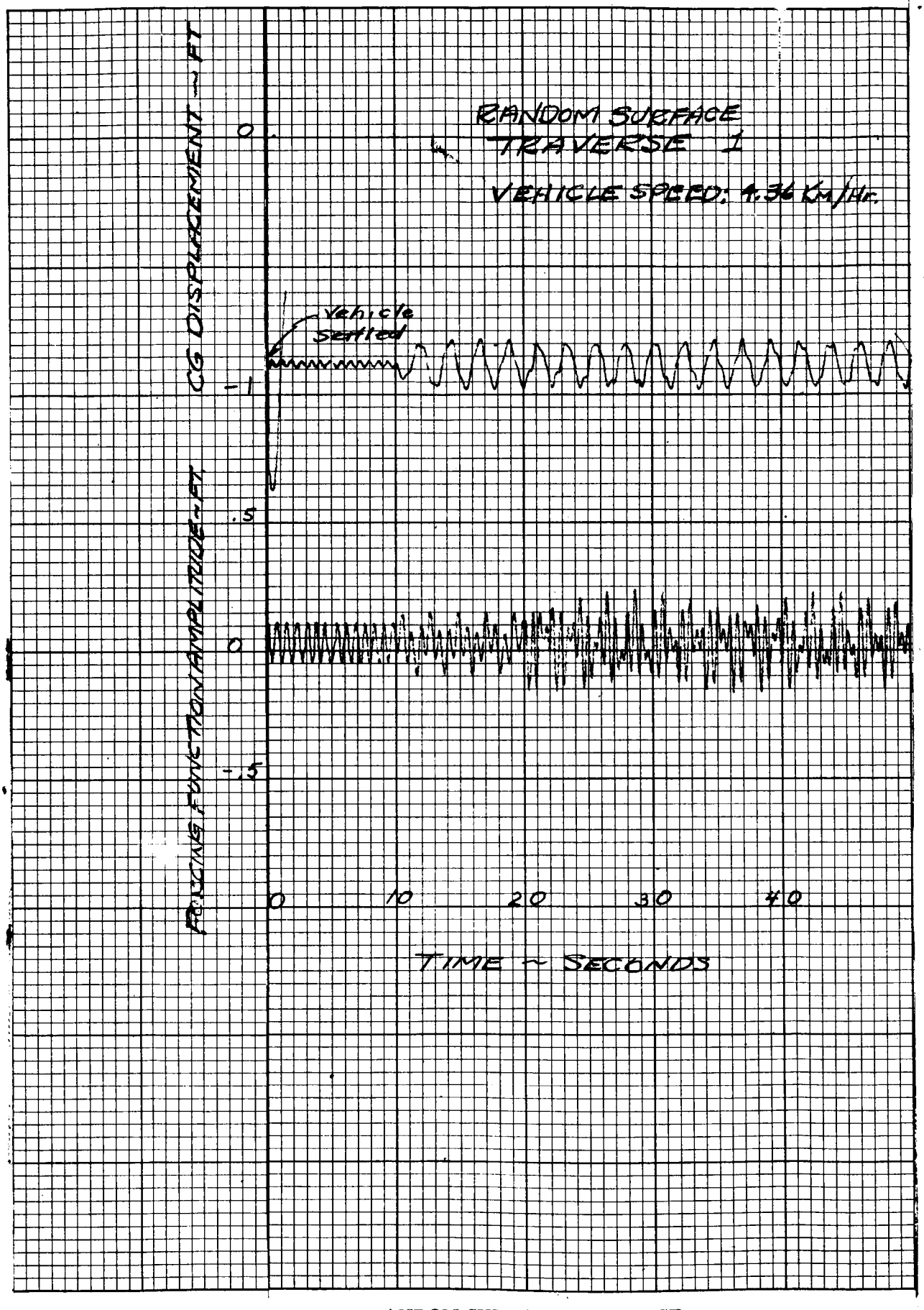

FIGURE 4M. RANDOM SURFACE TRAVERSE

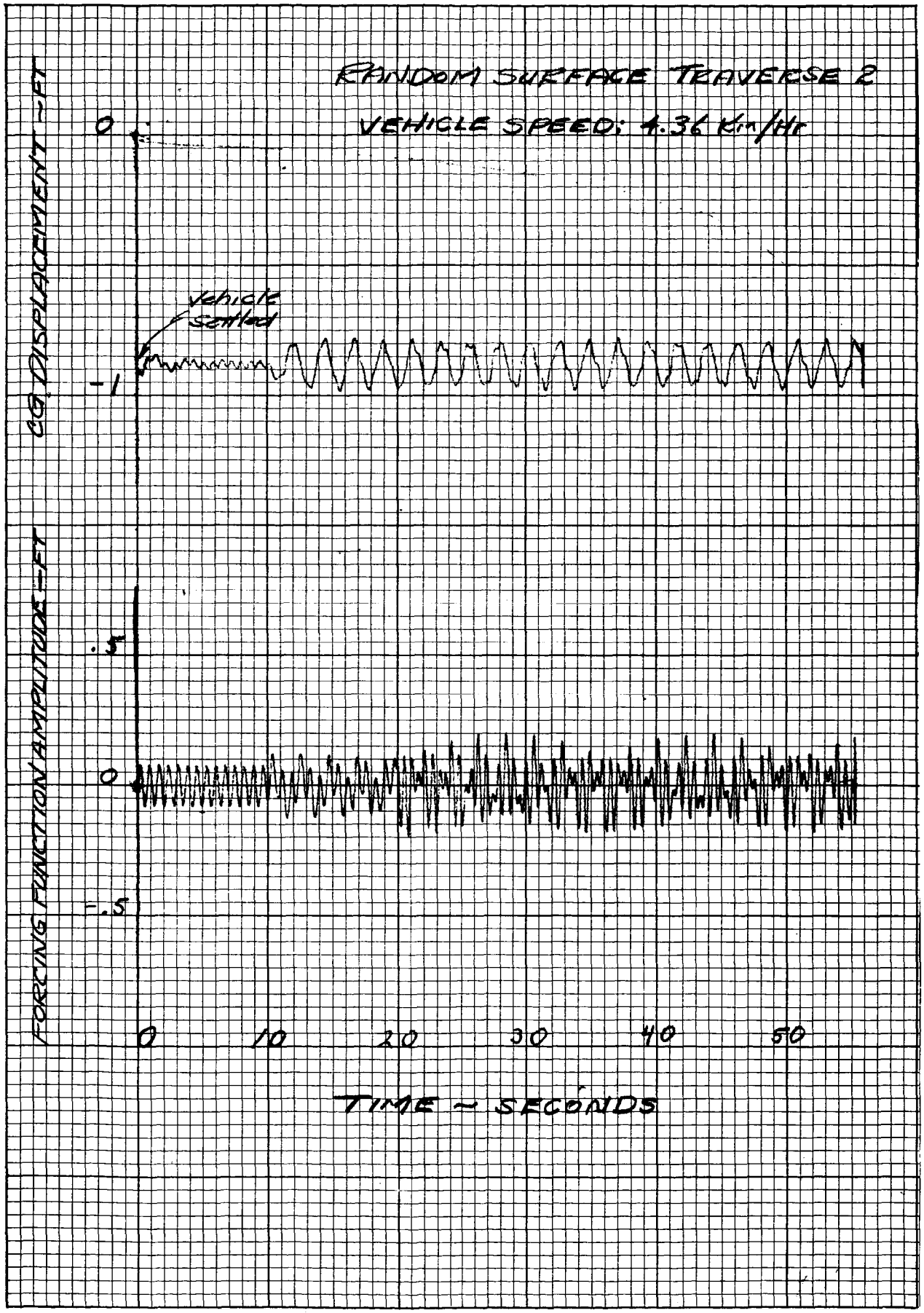

FIGURE 4N. RANDOM SURFACE TRAVERSE

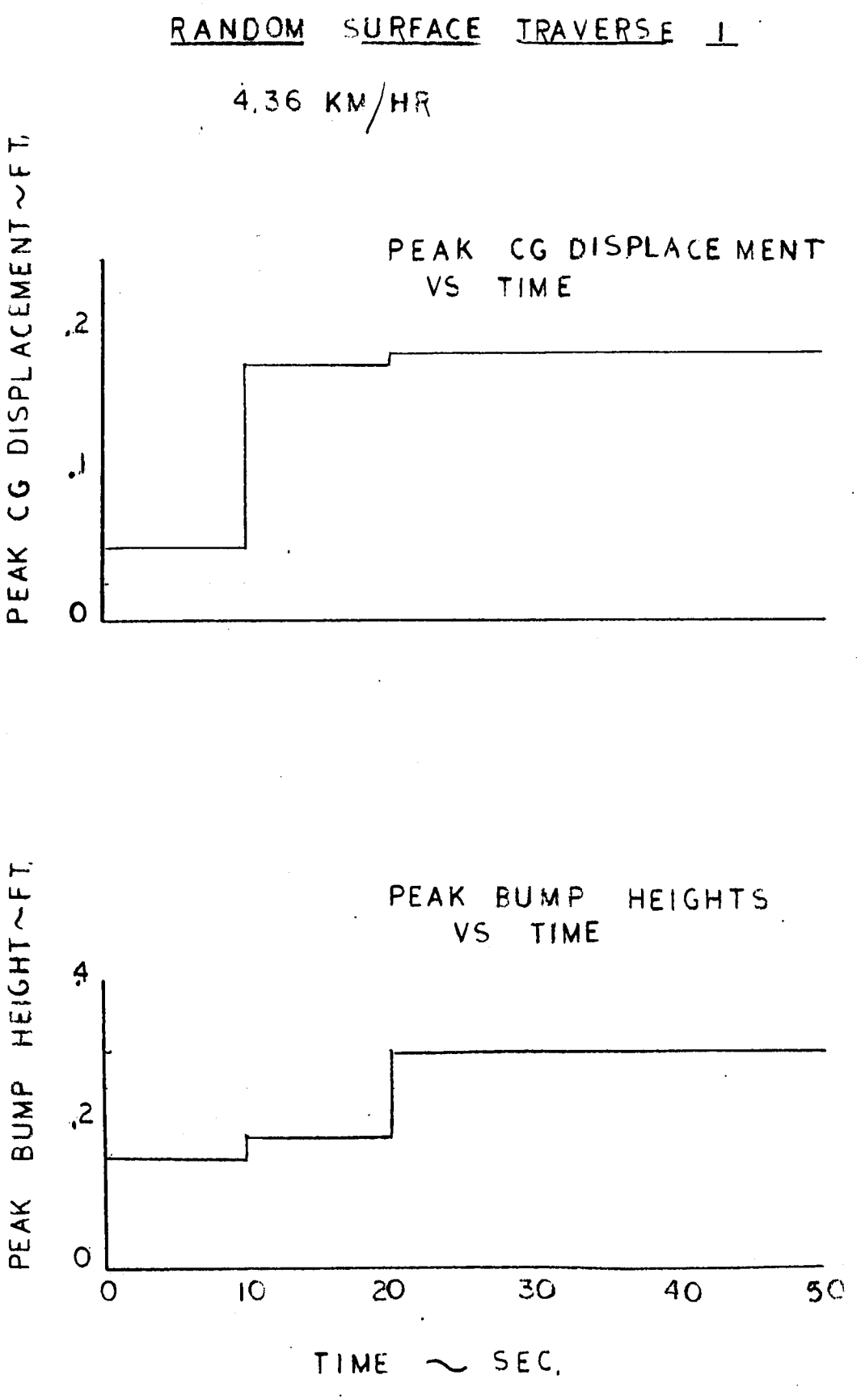

FIGURE 40. RANDOM SURFACE TRAVERSE

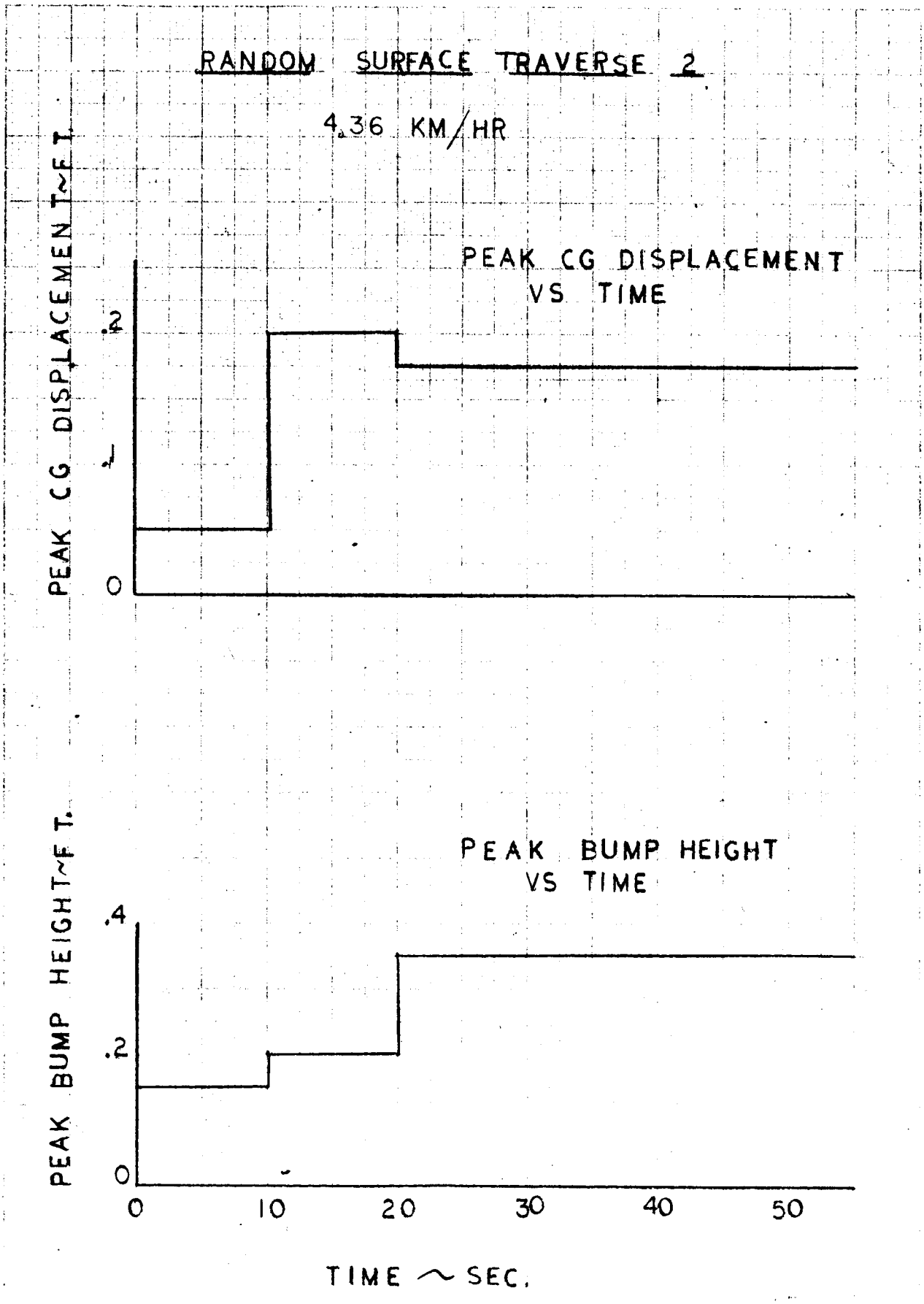

FIGURE 4P. RANDOM SURFACE TRAVERSE

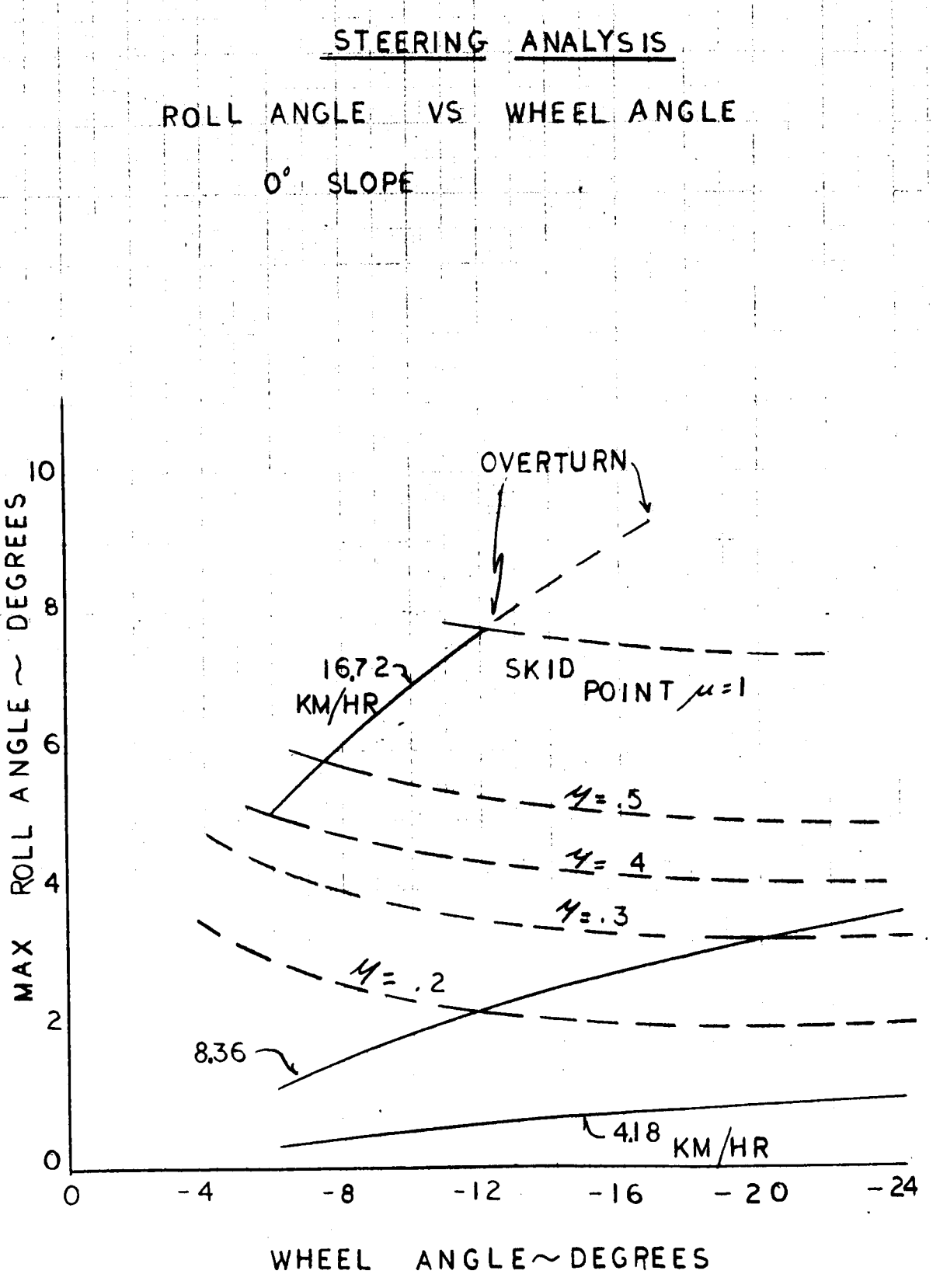

FIGURE 5A. ROLL ANGLE VERSUS WHEEL ANGLE

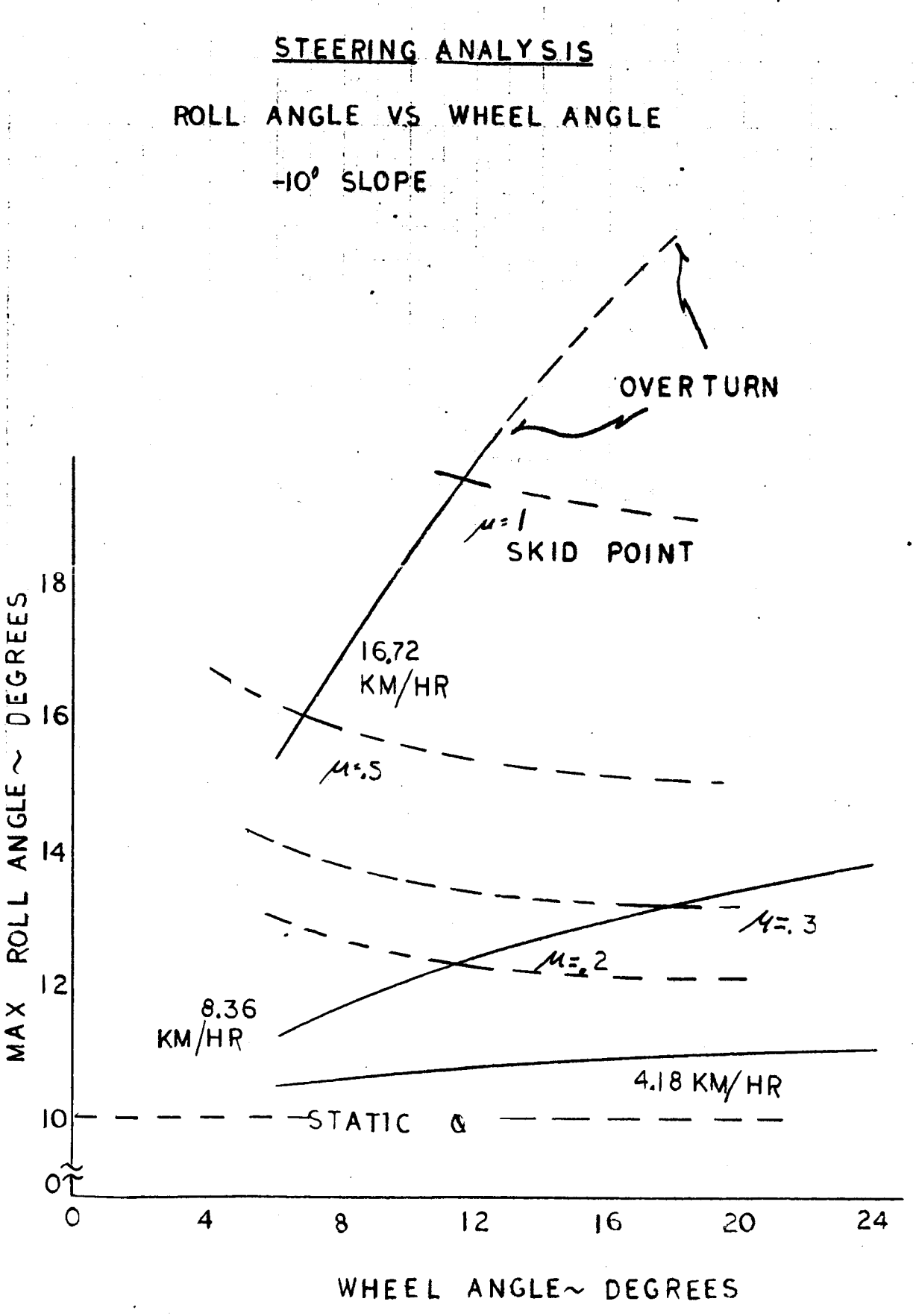

FIGURE 5B. ROLL ANGLE VERSUS WHEEL ANGLE

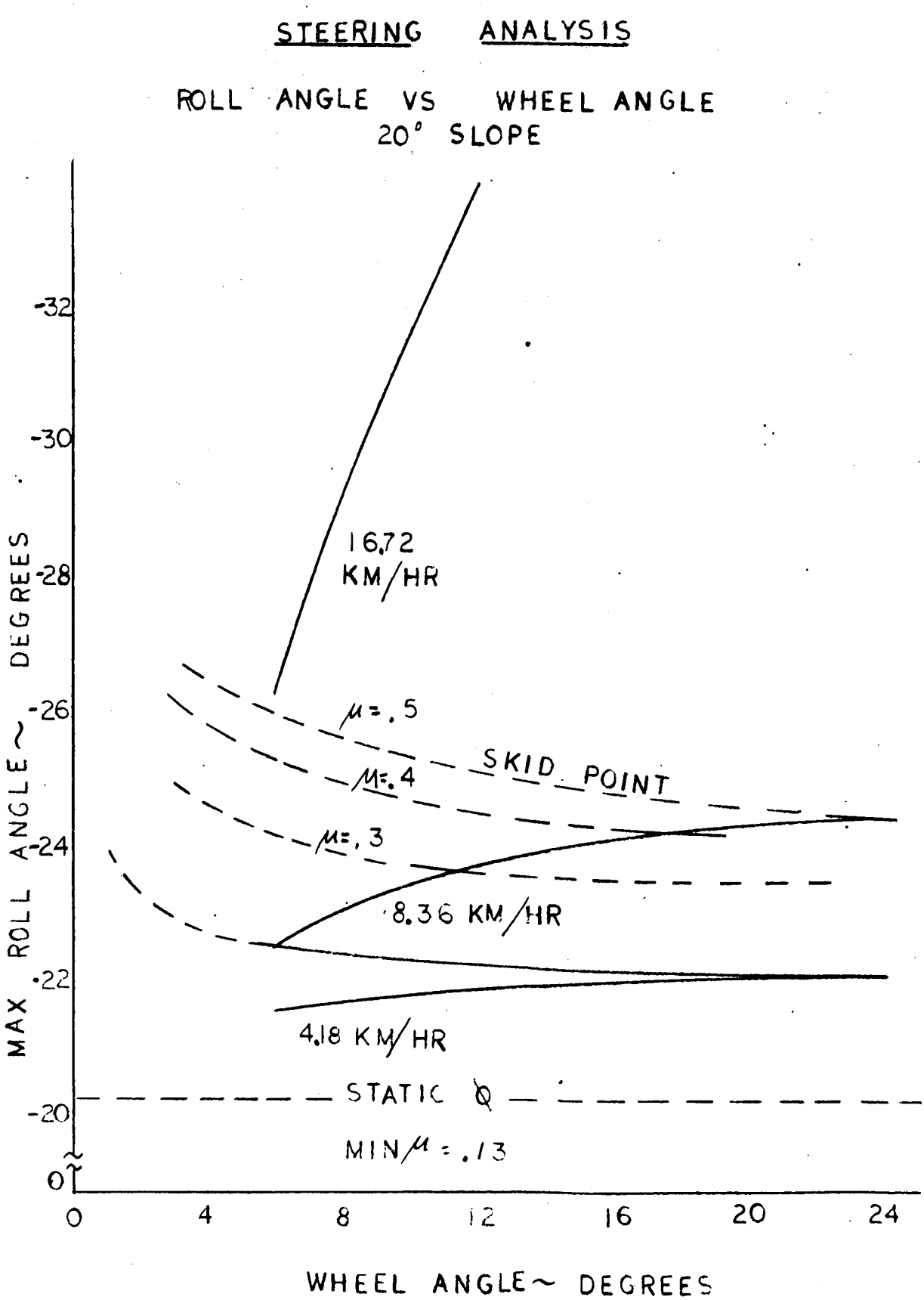

FIGURE 5C. ROLL ANGLE VERSUS WHEEL ANGLE

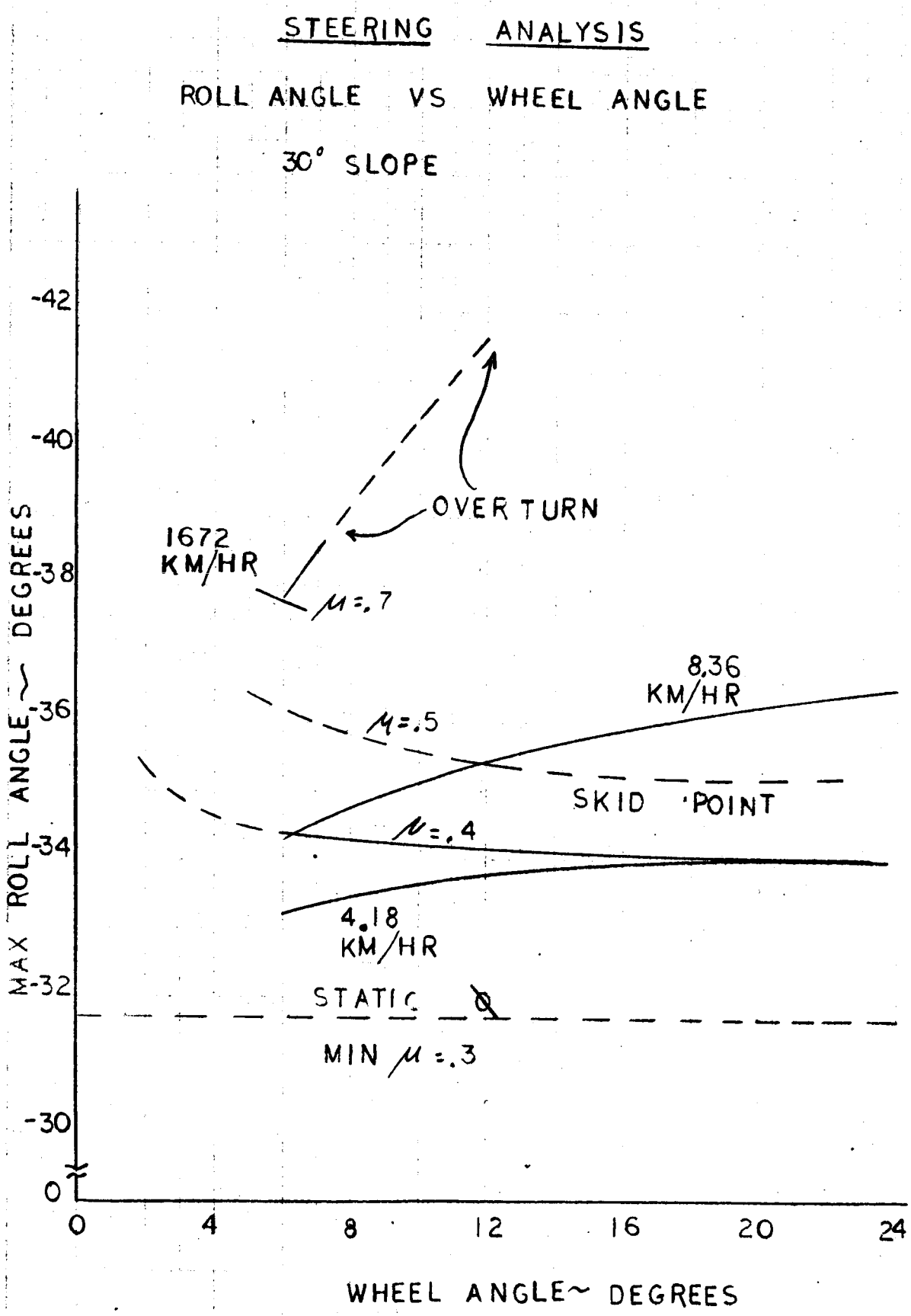

FIGURE 5D. ROLL ANGLE VERSUS WHEEL ANGLE

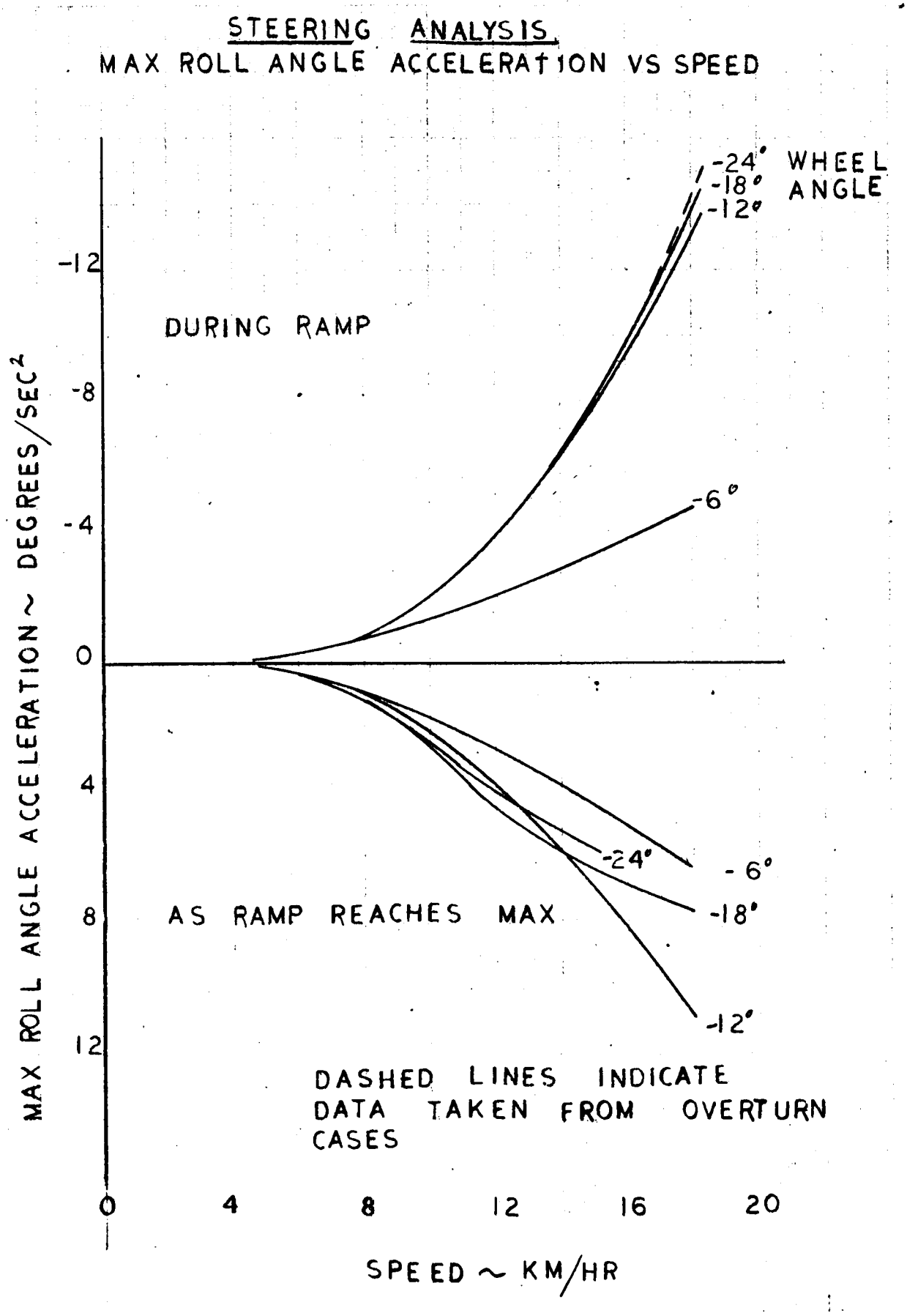

FIGURE 5E. MAXIMUM ROLL ANGLE ACCELERATIONS VERSUS SPEED

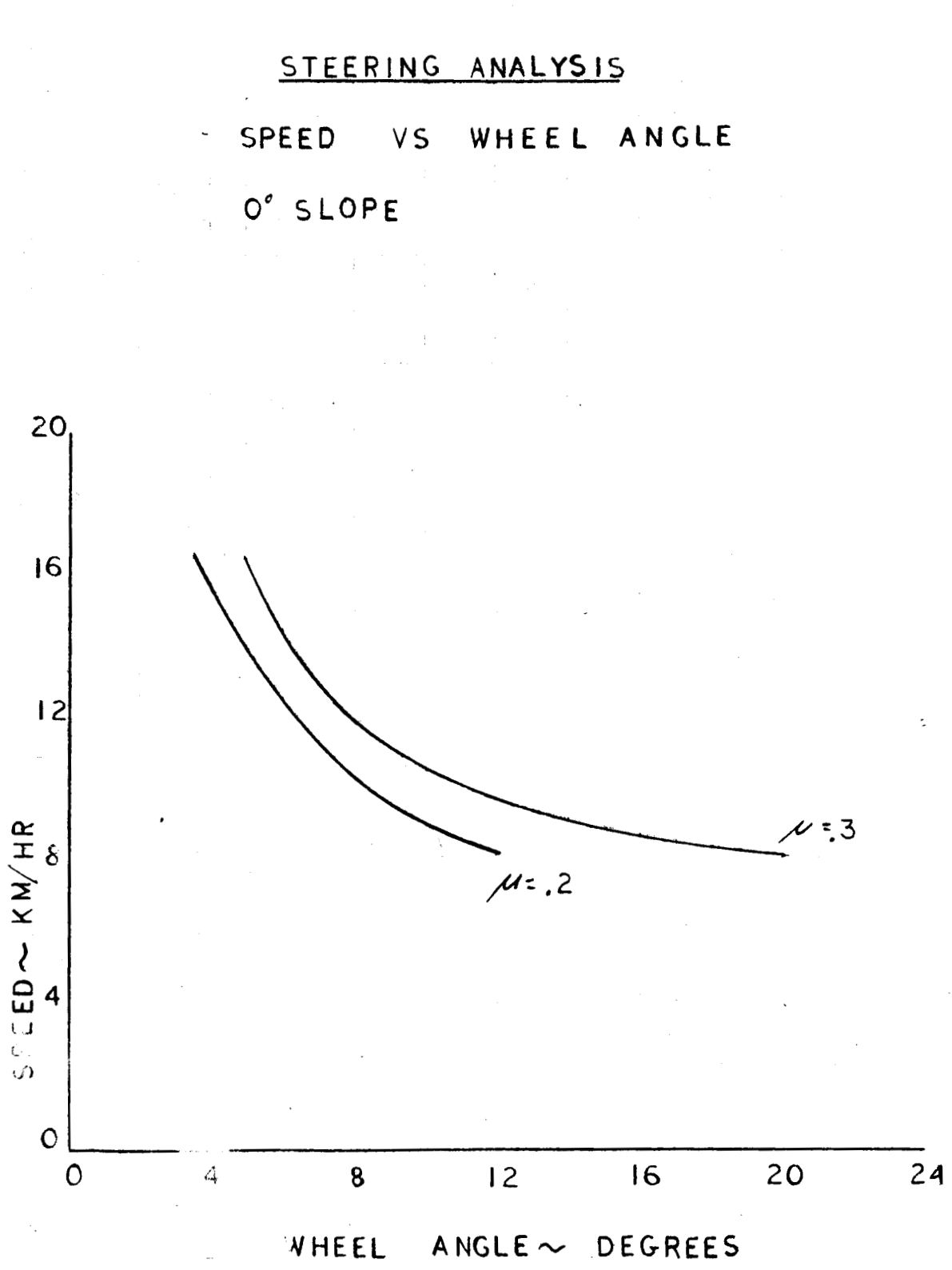

FIGURE 5F. SPEED VERSUS WHEEL ANGLE

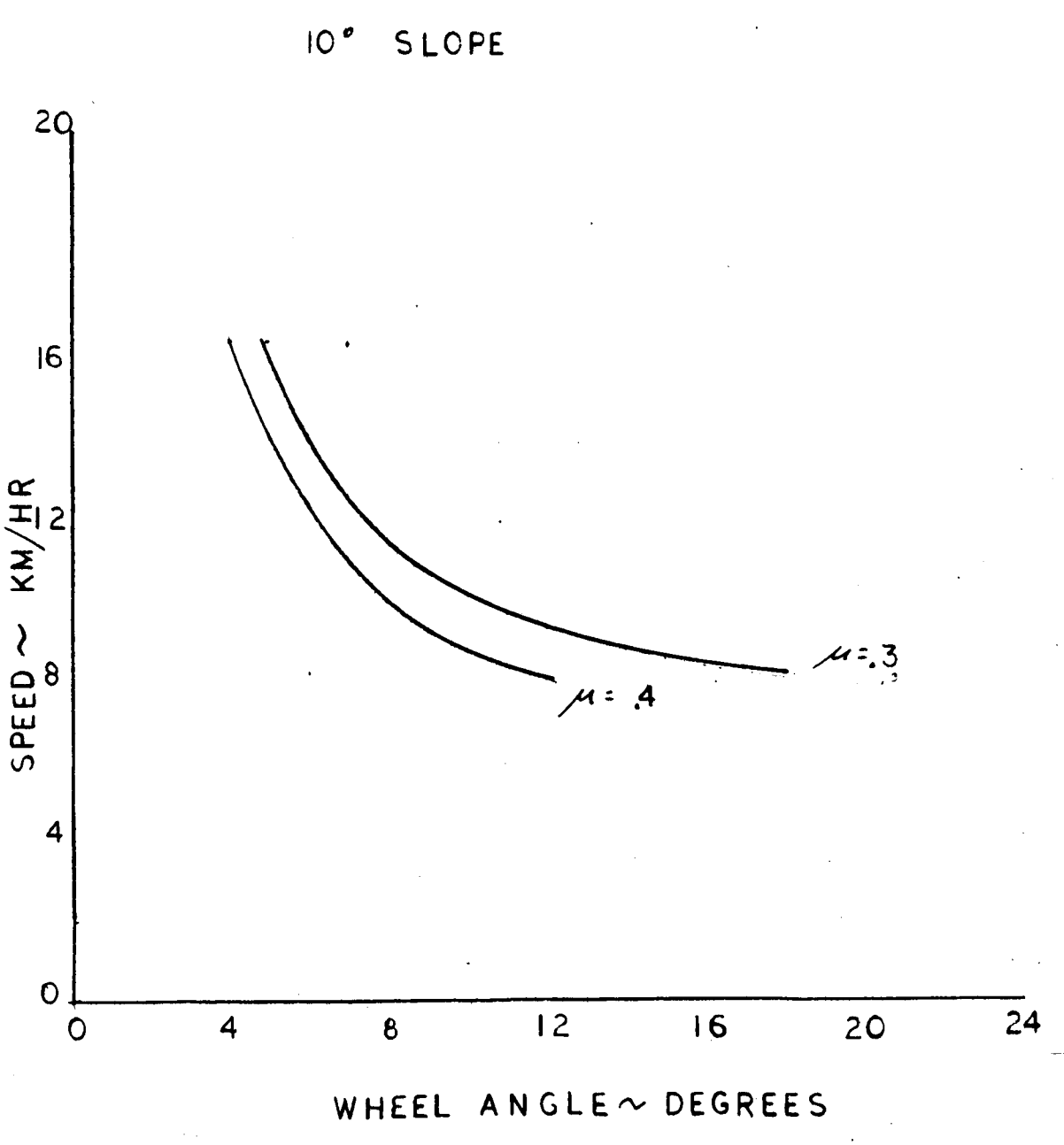

FIGURE 5G. SPEED VERSUS WHEEL ANGLE

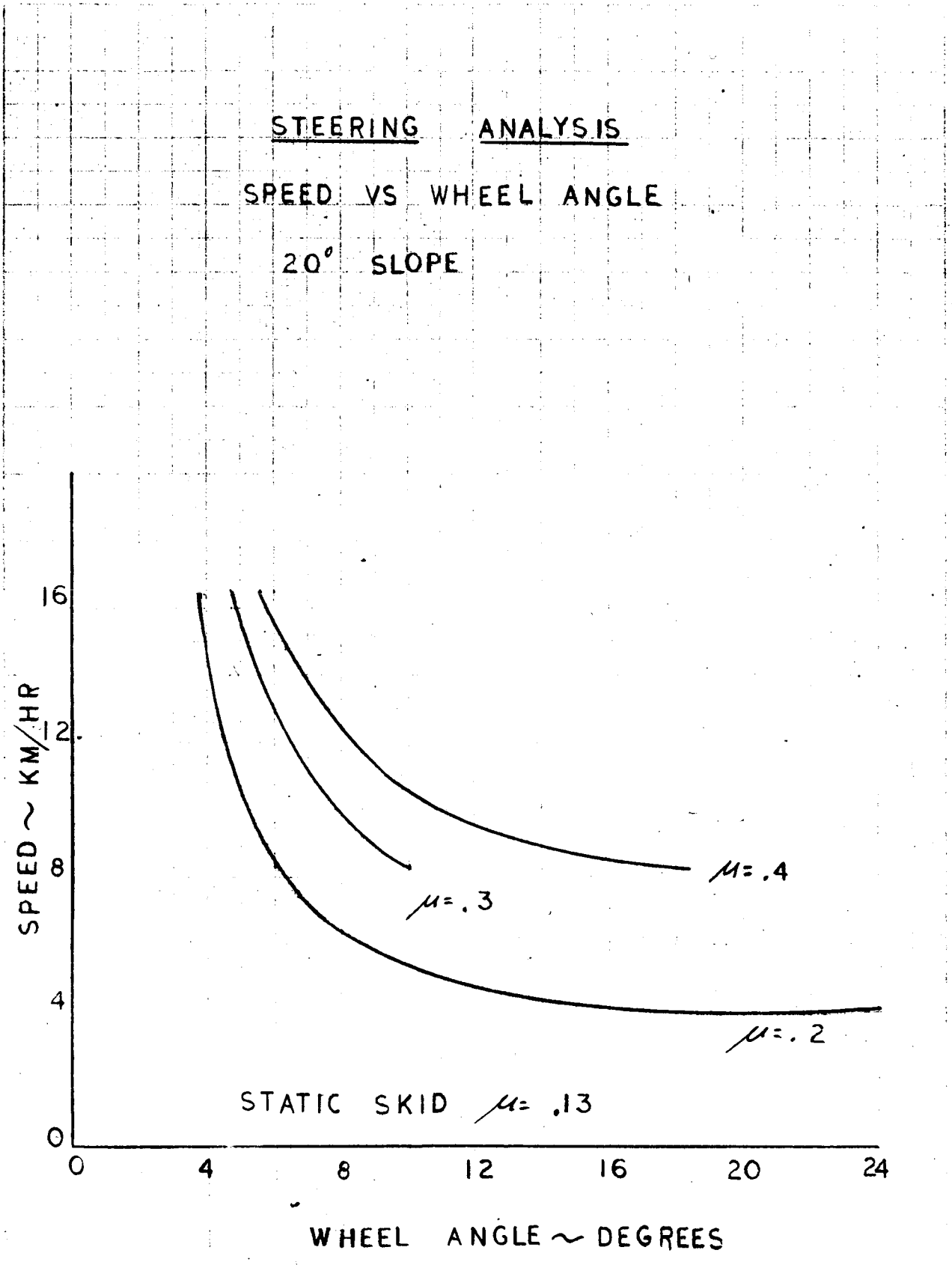

FIGURE 5H. SPEED VERSUS WHEEL ANGLE

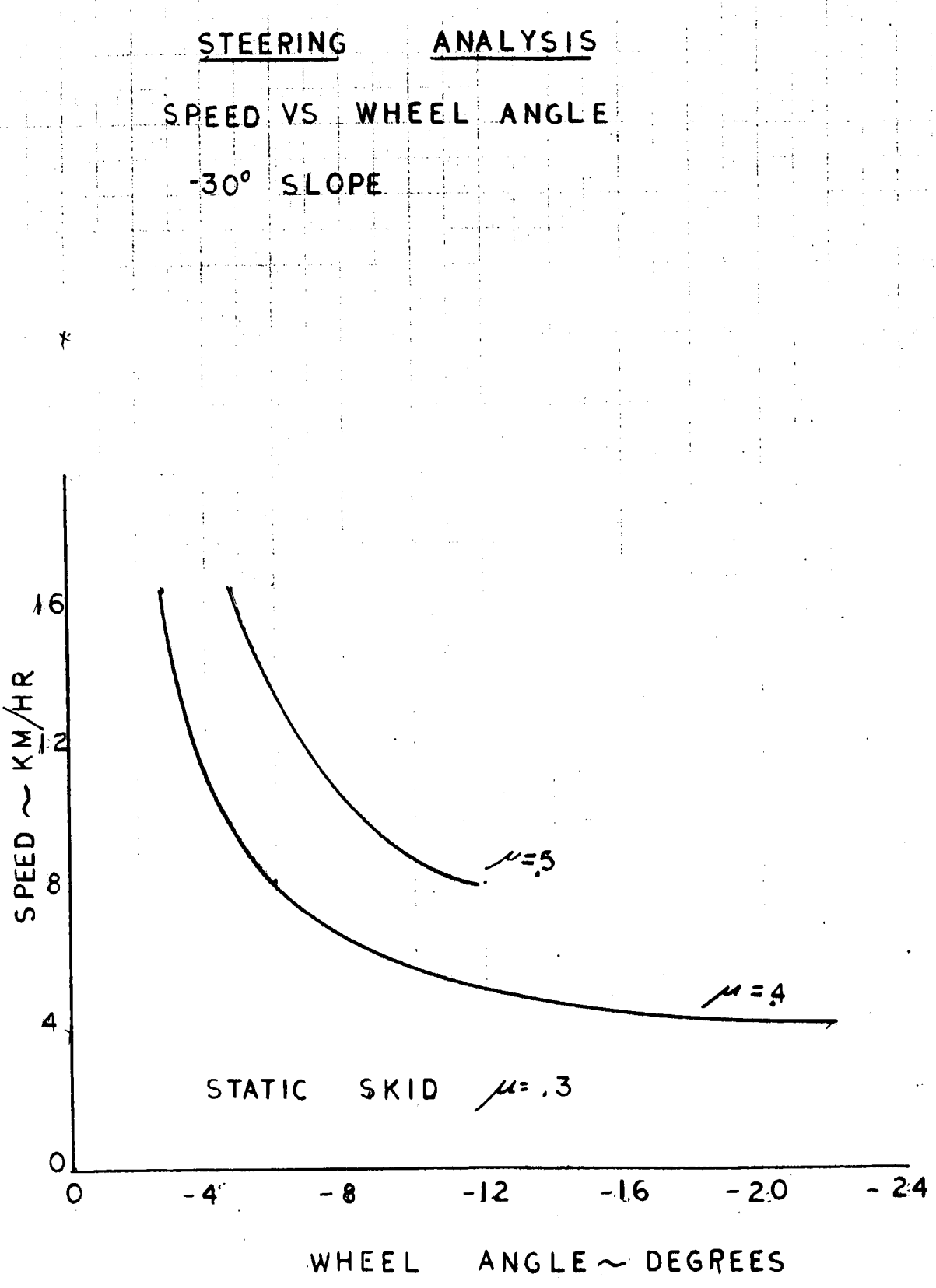

FIGURE 5I. SPEED VERSUS WHEEL ANGLE

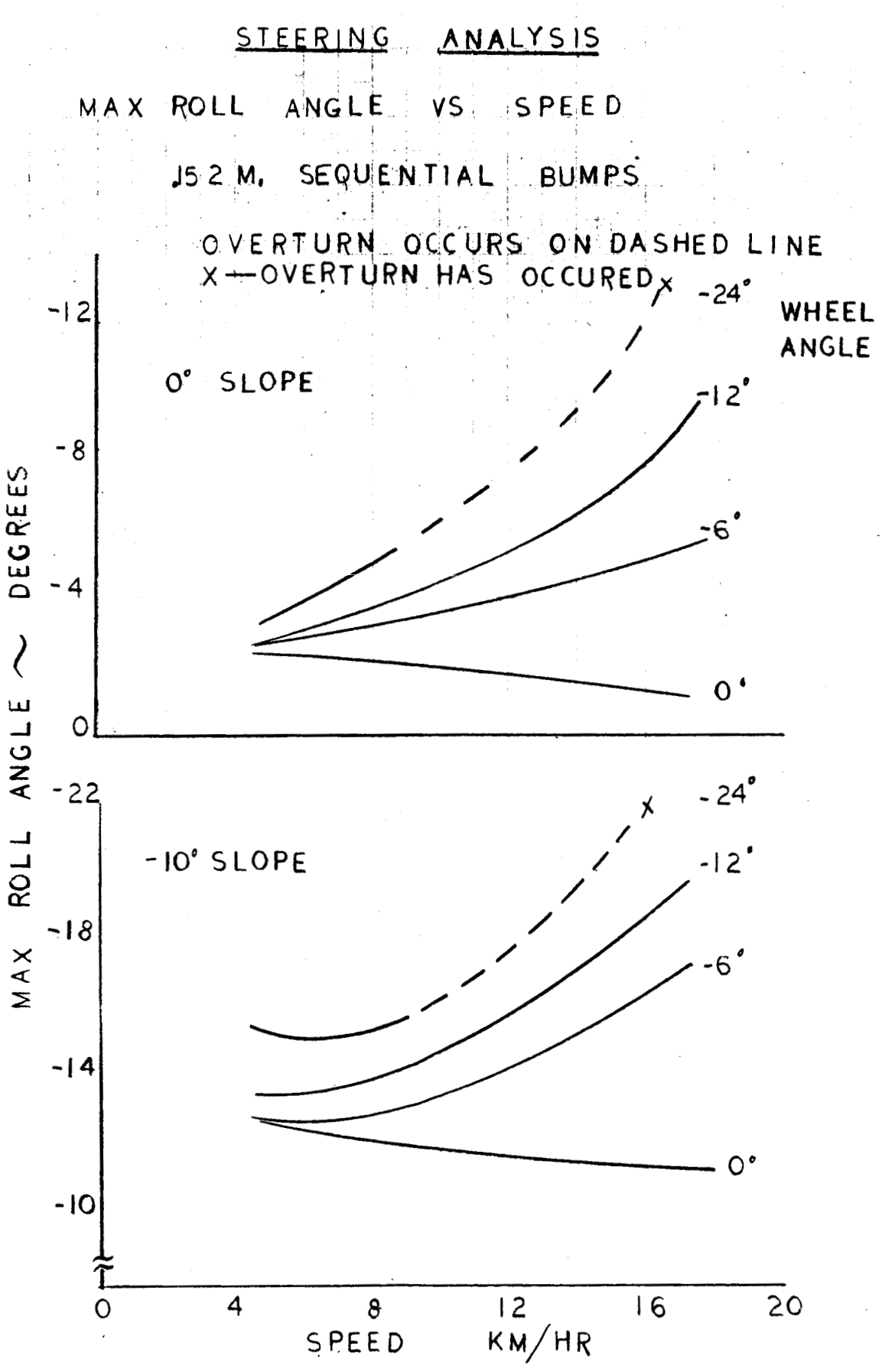

FIGURE 6A. MAXIMUM ROLL ANGLE VERSUS SPEED

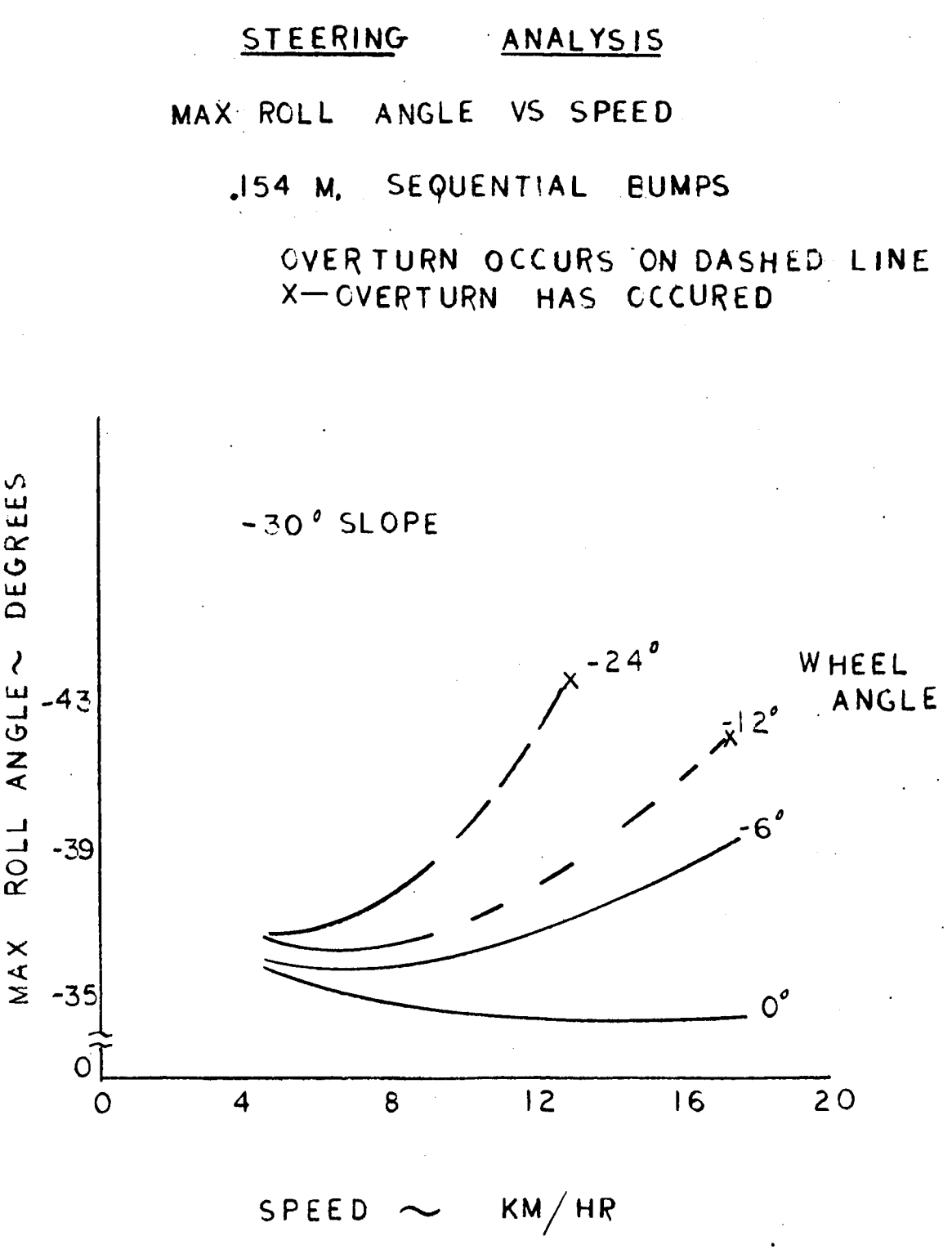

FIGURE 6B. MAXIMUM ROLL ANGLE VERSUS SPEED

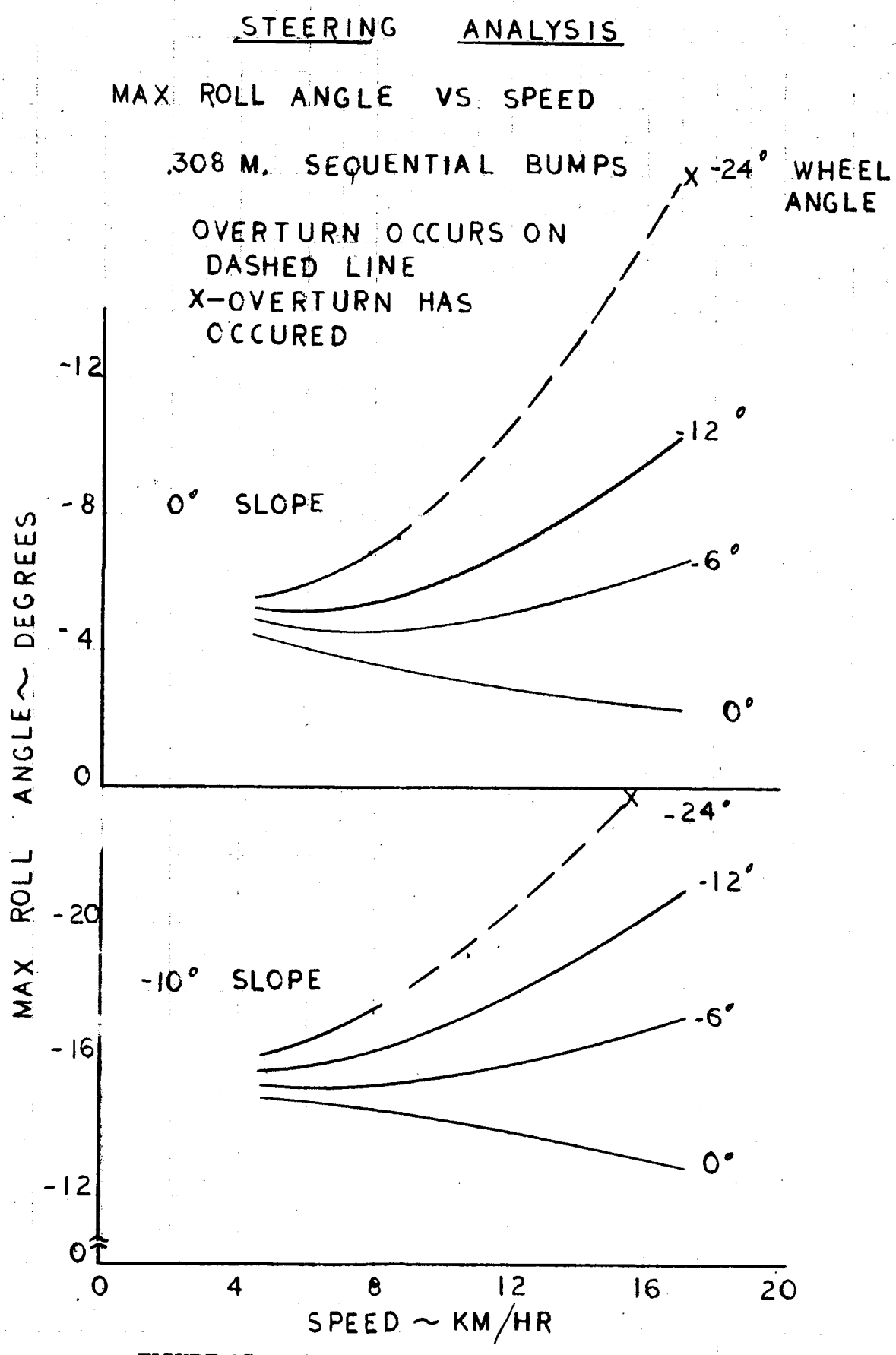

FIGURE 6C. MAXIMUM ROLL ANGLE VERSUS SPEED

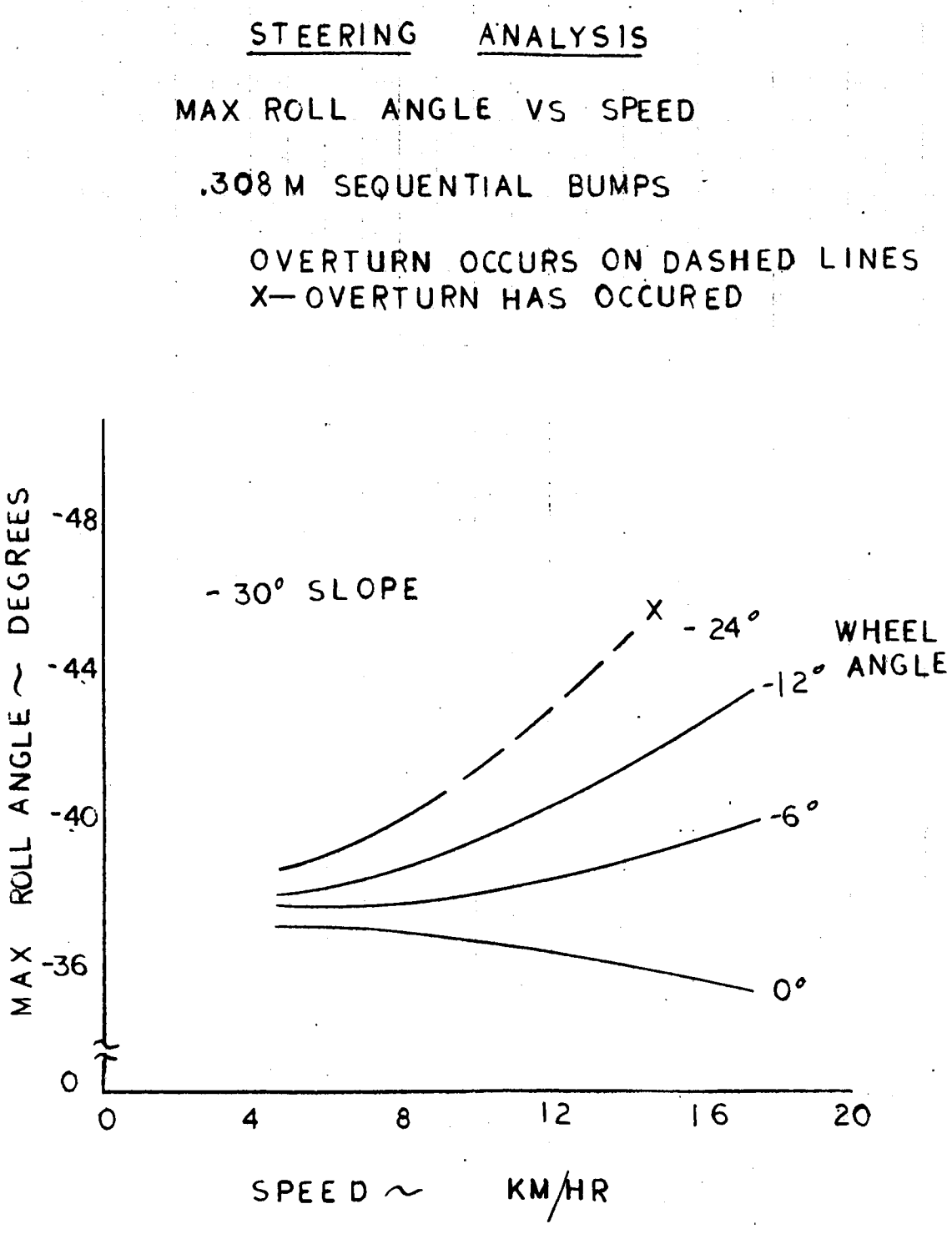

FIGURE 6D. MAXIMUM ROLL ANGLE VERSUS SPEED

STEERING ANALYSIS

MAX ROLL ANGLE VS SPEED

.61 M. SEQUENTIAL BUMPS

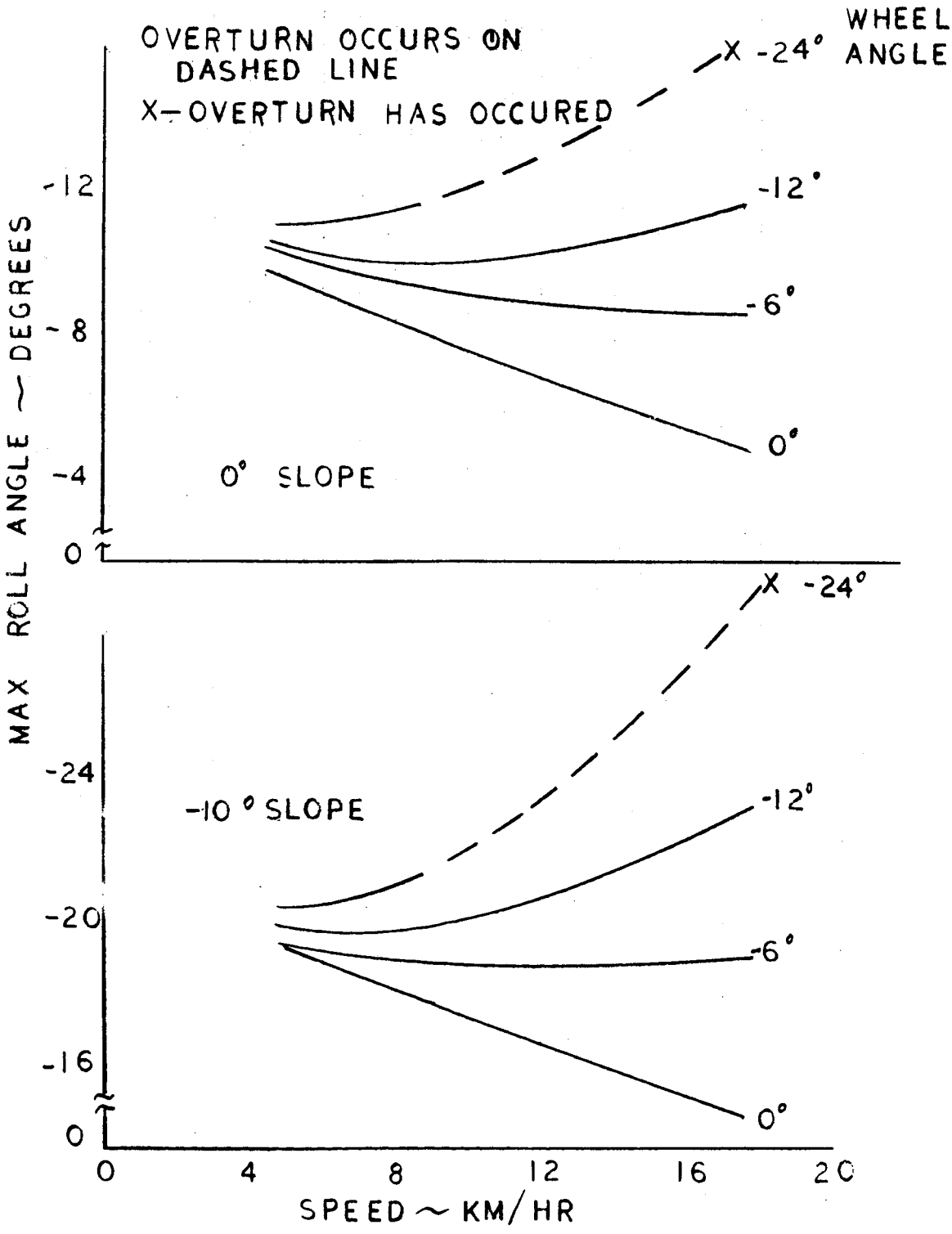

FIGURE 6E. MAXIMUM ROLL ANGLE VERSUS SPEED

STEERING ANALYSIS

MAX ROLL ANGLE VS SPEED

.61 M SEQUENTIAL BUMPS

OVERTURN OCCURS ON DASHED LINE
X—OVERTURN HAS OCCURED

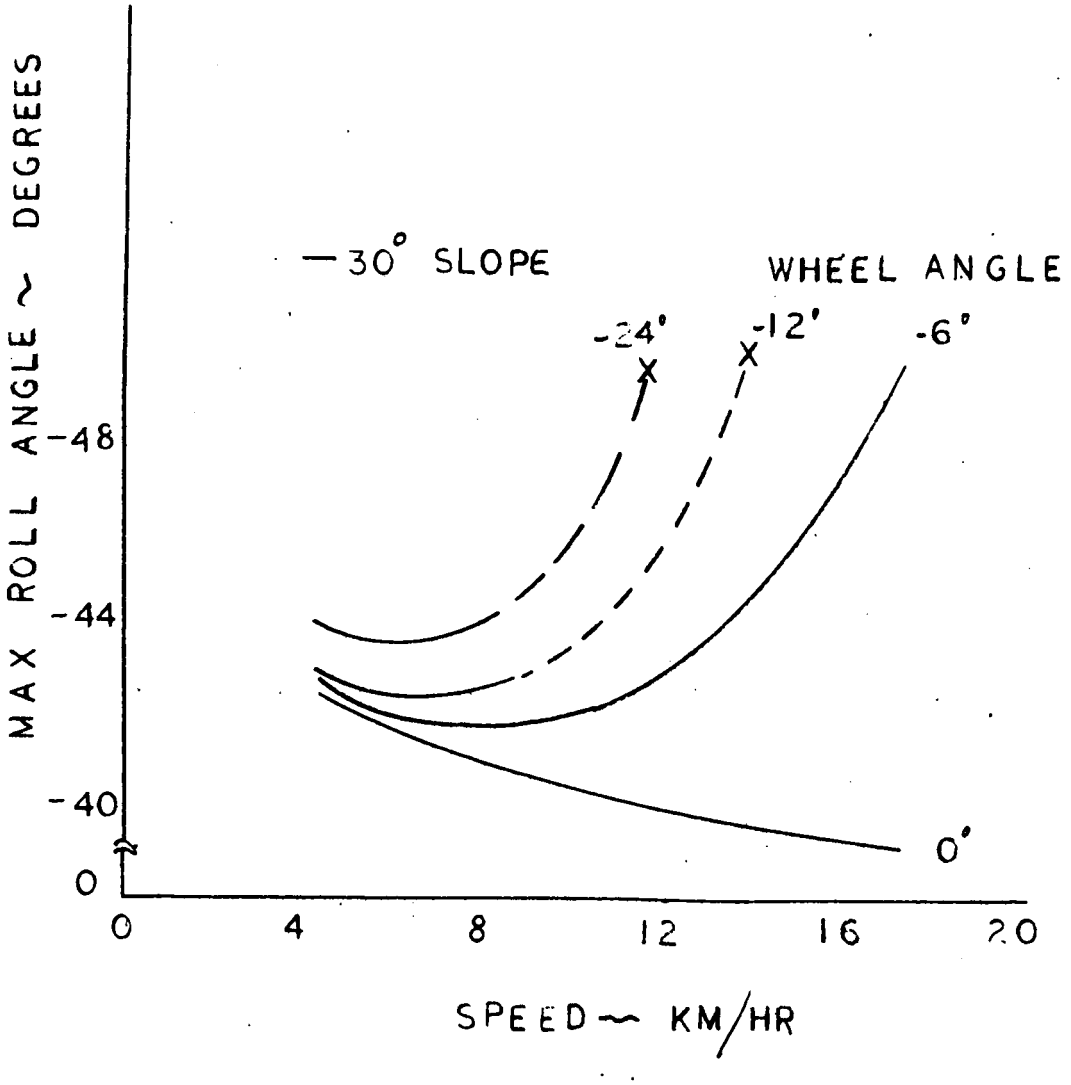

FIGURE 6F. MAXIMUM ROLL ANGLE VERSUS SPEED

TABLE I. COMPARISON OF THE 4-WHEEL VEHICLE WITH VEHICLES TESTED PREVIOUSLY

	Ref. 1 Vehicle	Ref. 1 Vehicle	Ref. 1 Vehicle	4-Wheel Vehicle
Suspension Constant, Lb/Ft.	1000	2000	1000	725
Tire Constant Lb/Ft.	500	500	500	600
Suspension Damping, Lb/Ft/Sec.	125	125	500	150
Tire Damping, Lb/Ft/Sec.	0	0	0	15
Max. CG Displacement, Meters	0.54	0.6	0.57	0.58
Settling Time, Seconds	9	25	12	7

PART II
SIX WHEEL ARTICULATED VEHICLE

3.1 ROLL PLANE ANALYSIS

The mathematical model and equations of motion for the roll plane analysis are shown in Figures 7A, 7B, 7C, and 7D. These equations were written primarily for studying the steering and studying the effects of LSV's traverse in an object with the wheels of only one side of the vehicle.

The use of the equation's elements which contain M_a and M_b will be explained in Section 3.2 and in (Figure C3) Appendix C. Otherwise, the equations are written in the usual manner.

The analog computer diagram and data for simulating the roll plane of the six wheel articulated vehicle are shown in (Figures D1 and D2) Appendix D.

3.2 PITCH PLANE ANALYSIS

The mathematical model and equations of motion for the pitch plane analysis are shown in Figures 7E and 7F. This model was primarily developed to examine the vehicle resonance, the vehicle displacement and pitch angle resulting from a forcing function applied to all wheels simultaneously, and the vehicle response to forcing functions applied to three sets of wheels (The wheels of an axle form a set), sequentially. The latter simulates the LSV's striking a ledge.

The only unusual features of the equations of motion are the last two elements of equation (5) and the last element of equation (6) (Figure 7F). The M_a and M_b of these equations are developed as equations (7) and (8) of Figure 7F. These equations were developed, as shown in Figure C3 of Appendix C, to simulate the results of bending modes in the vehicle spring coupling bar. The true representation of the latter is a fourth-or higher order-equation which makes it impractical for a medium-sized analog computer. The last element of equation (5) represents forces set-up by the shear at the point of spring bar and the main module contact, and the element preceding the last element represents the moment on the spring bar at the same point of contact. The last element of equation (6) represents the main module force on the trailer module.

The computer diagram and data to be used in the pitch plane analysis are shown in (Figures C1 and C2) Appendix C.

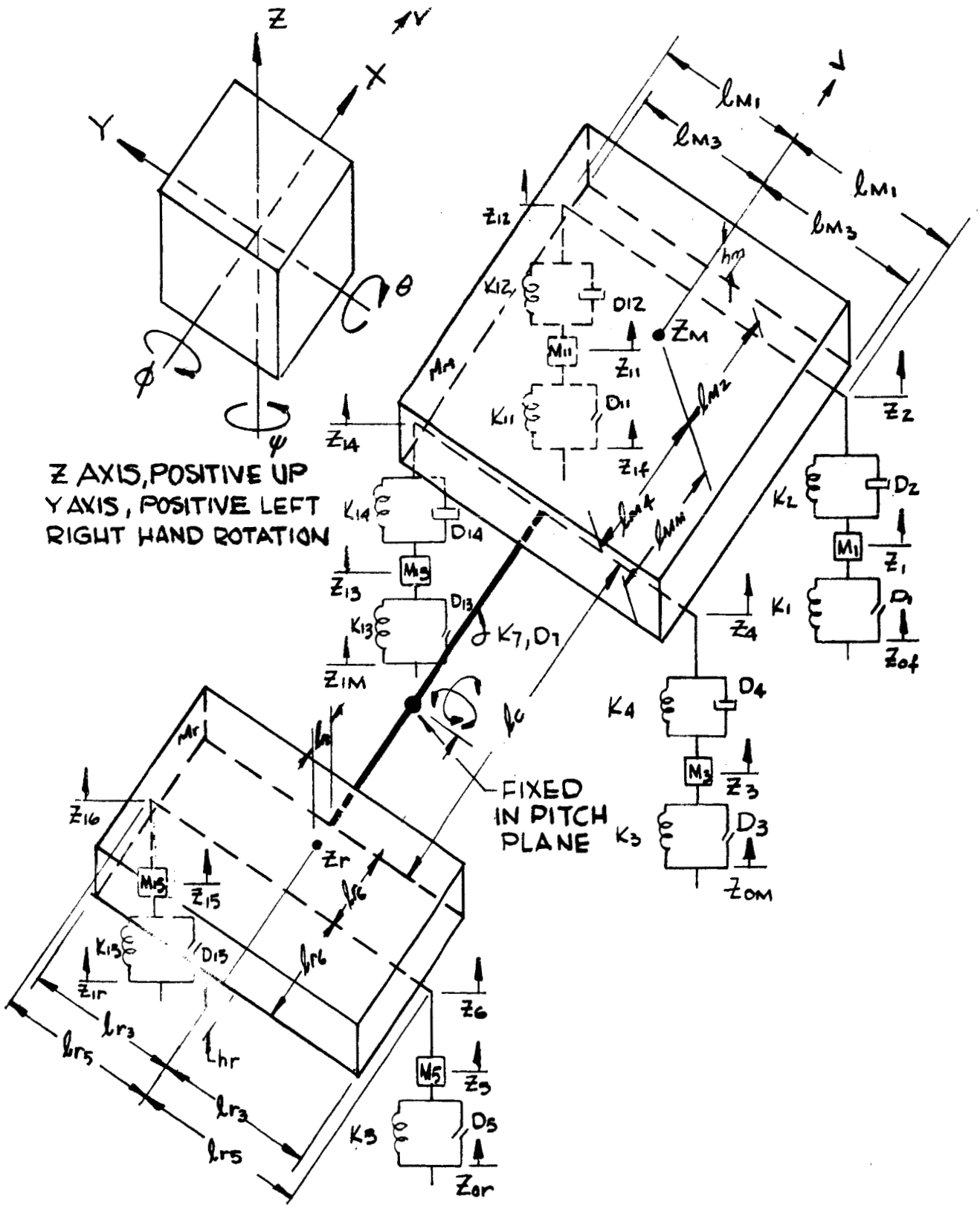

FIGURE 7A. LSV-6 WHEEL -ARTICULATED, MATHEMATICAL MODEL

$$(1)\quad \ddot{z}_1 = \frac{K_1}{M_1}(z_{0f} - z_1) + \frac{D_1}{M_1}(\dot{z}_{0f} - \dot{z}_1) - \frac{K_2}{M_1}(z_1 - z_2) - \frac{D_2}{M_1}(\dot{z}_1 - \dot{z}_2) - g$$

$$(2)\quad \ddot{z}_3 = \frac{K_3}{M_3}(z_{0m} - z_3) + \frac{D_3}{M_3}(\dot{z}_{0m} - \dot{z}_3) - \frac{K_4}{M_3}(z_3 - z_4) - \frac{D_4}{M_3}(\dot{z}_3 - \dot{z}_4) - g$$

$$(3)\quad \ddot{z}_{11} = \frac{K_{11}}{M_{11}}(z_{1f} - z_{11}) + \frac{D_{11}}{M_{11}}(\dot{z}_{1f} - \dot{z}_{11}) - \frac{K_{12}}{M_{11}}(z_{11} - z_{12}) - \frac{D_{12}}{M_{11}}(\dot{z}_{11} - \dot{z}_{12}) - g$$

$$(4)\quad \ddot{z}_{13} = \frac{K_{13}}{M_{13}}(z_{1M} - z_{13}) + \frac{D_{13}}{M_{13}}(\dot{z}_{1M} - \dot{z}_{13}) - \frac{K_{14}}{M_{13}}(z_{13} - z_{14}) - \frac{D_{14}}{M_{13}}(\dot{z}_{13} - \dot{z}_{14}) - g$$

$$(5)\quad \ddot{z}_M = \frac{K_2}{M_M}(z_1 - z_2) + \frac{D_2}{M_M}(\dot{z}_1 - \dot{z}_2) + \frac{K_4}{M_M}(z_3 - z_4) + \frac{D_4}{M_M}(\dot{z}_3 - \dot{z}_4)$$

$$+ \frac{K_{12}}{M_M}(z_{11} - z_{12}) + \frac{D_{12}}{M_M}(\dot{z}_{11} - \dot{z}_{12}) + \frac{K_{14}}{M_M}(z_{13} - z_{14}) + \frac{D_{14}}{M_M}(\dot{z}_{13} - \dot{z}_{14})$$

$$+ \frac{K_5}{M_M}(z_{0r} - z_5) + \frac{D_5}{M_M}(\dot{z}_{0r} - \dot{z}_5) + \frac{K_{15}}{M_M}(z_{1r} - z_{15}) + \frac{D_{15}}{M_M}(\dot{z}_{1r} - \dot{z}_{15})$$

$$- \ddot{z}_r\left(\frac{M_r + M_5}{M_M}\right) - \left(\frac{M_r + M_5}{M_M}\right)g - g$$

$$(6)\quad \ddot{\theta}_M = \frac{\ell_{M_2}}{I_{YM}}\left[K_4(z_3 - z_4) + D_4(\dot{z}_3 - \dot{z}_4\right] - \frac{\ell_{M_2}}{I_{YM}}\left[K_2(z_1 - z_2) + D_2(\dot{z}_1 - \dot{z}_2)\right]$$

$$+ \frac{h_M D_5}{I_{YM}}(\dot{\theta}_r - \dot{\theta}_M) - \frac{\ell_{M_2}}{I_{YM}}\left[K_5(z_{0r} - z_5) + D_5(\dot{z}_{0r} - \dot{z}_5)\right.$$

$$\left. - (M_5 + M_r)g\right] - \frac{M_\theta}{I_{YM}} - \frac{M_\theta \ell_2}{I_{YM}\ell_{M_4}}$$

FIGURE 7B. LSV-6 WHEEL -ARTICULATED, ROLL EQUATIONS

$$(7)\quad \ddot{\phi}_M = \frac{\ell_{M_1}}{I_{RM}}\left[-K_2(z_1-z_2) - D_2(\dot{z}_1-\dot{z}_2) - K_4(z_3-z_4) - D_4(\dot{z}_3-\dot{z}_4)\right.$$

$$\left. + K_{12}(z_{11}-z_{12}) + D_{12}(\dot{z}_{11}-\dot{z}_{12}) + K_{14}(z_{13}-z_{14}) + D_{14}(\dot{z}_{13}-\dot{z}_{14})\right]$$

$$(8)\quad \ddot{z}_2 = \ddot{z}_M - \ell_{M_2}\ddot{\theta}_M - \ell_{M_1}\ddot{\phi}_M \qquad (9)\quad \ddot{z}_4 = \ddot{z}_M + \ell_{M_4}\ddot{\theta}_M - \ell_{M_1}\ddot{\phi}_M$$

$$\dot{z}_2 = \dot{z}_M - \ell_{M_2}\dot{\theta}_M - \ell_{M_1}\dot{\phi}_M \qquad \dot{z}_4 = \dot{z}_M + \ell_{M_4}\dot{\theta}_M - \ell_{M_1}\dot{\phi}_M$$

$$z_2 = z_M - \ell_{M_2}\theta_M - \ell_{M_1}\phi_M \qquad z_4 = z_M + \ell_{M_4}\theta_M - \ell_{M_1}\phi_M$$

$$(10)\quad \ddot{z}_{12} = \ddot{z}_M - \ell_{M_2}\ddot{\theta}_M + \ell_{M_1}\ddot{\phi}_M \qquad (11)\quad \ddot{z}_{14} = \ddot{z}_M + \ell_{M_4}\ddot{\theta}_M + \ell_{M_1}\ddot{\phi}_M$$

$$\dot{z}_{12} = \dot{z}_M - \ell_{M_2}\dot{\theta}_M + \ell_{M_1}\dot{\phi}_M \qquad \dot{z}_{14} = \dot{z}_M + \ell_{M_4}\dot{\theta}_M + \ell_{M_1}\dot{\phi}_M$$

$$z_{12} = z_M - \ell_{M_2}\theta_M + \ell_{M_1}\phi_M \qquad z_{14} = z_M + \ell_{M_4}\theta_M + \ell_{M_1}\phi_M$$

$$(12)\quad \ddot{z}_r = \frac{K_5}{(M_r+M_5)}(z_{or}-z_5) + \frac{D_5}{(M_r+M_5)}(\dot{z}_{or}-\dot{z}_5) + \frac{M_A}{(M_r+M_5)\ell_{r_1}}$$

$$(13)\quad \ddot{\theta}_r = \left[\frac{\ell_{r_5}}{I_{Yr}}\right]\left[K_5(z_{or}-z_5) + D_5(\dot{z}_{or}-\dot{z}_5)\right] - \frac{\ell_{r_1}}{I_{Yr}}\left[(M_r+M_5)g\right]$$

$$- \frac{M_A}{I_{Yr}} - \frac{D_r}{I_{Yr}}(\dot{\theta}_r - \dot{\theta}_M)\ell_M$$

$$(14)\quad \ddot{\phi}_r = \frac{\ell_{r_5}}{I_{xr}}\left[-K_5(z_{or}-z_5) - D_5(\dot{z}_{or}-\dot{z}_5) + K_{15}(z_{1r}-z_{15})\right.$$

$$\left. + D_{15}(\dot{z}_{1r}-\dot{z}_{15})\right]$$

$$(15)\quad M_A = \frac{EI}{\ell_c^2}\left[(\ell_c+\ell_{M_4})\theta_M + \ell_{r_1}\theta_r - (z_r - z_M)\right]$$

$$(16)\quad M_B = \frac{EI}{\ell_c^2}\left[(\ell_c+\ell_{r_1})\theta_r + \ell_{M_4}\theta_M - (z_r - z_M)\right]$$

FIGURE 7C. LSV-6 WHEEL - ARTICULATED, ROLL EQUATIONS

$$(17)\quad \ddot{z}_5 = \ddot{z}_r + (l_{r6} - l_{r1})\ddot{\theta}_r - l_{r5}\ddot{\phi}_r \qquad \ddot{z}_5 = \ddot{z}_6$$

$$\dot{z}_5 = \dot{z}_r + (l_{r6} - l_{r1})\dot{\theta}_r - l_{r5}\dot{\phi}_r \qquad \dot{z}_5 = \dot{z}_6$$

$$z_5 = z_r + (l_{r6} - l_{r1})\theta_r - l_{r5}\phi_r \qquad z_5 = z_6$$

$$(18)\quad \ddot{z}_{15} = \ddot{z}_r + (l_{r6} - l_{r1})\ddot{\theta}_r + l_{r5}\ddot{\phi}_r \qquad \ddot{z}_{15} = \ddot{z}_{16}$$

$$\dot{z}_{15} = \dot{z}_r + (l_{r6} - l_{r1})\dot{\theta}_r + l_{r5}\dot{\phi}_r \qquad \dot{z}_{15} = \dot{z}_{16}$$

$$z_{15} = z_r + (l_{r6} - l_{r1})\theta_r + l_{r5}\phi_r \qquad z_{15} = z_6$$

NOTE: $(z_1 - z_2)$, $(z_3 - z_4)$, $(z_{11} - z_{12})$, $(z_{13} - z_{14})$ are limited to (+) 8 inch and (−) 6 inch travel

FIGURE 7D. LSV-6 WHEEL - ARTICULATED, ROLL EQUATIONS

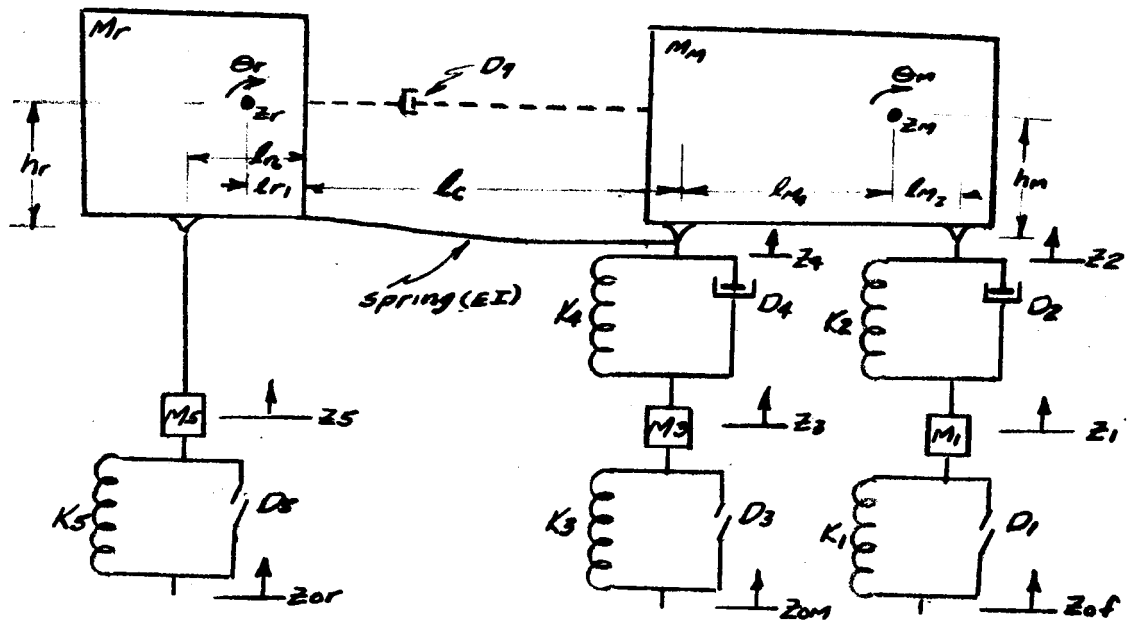

$$(1)\quad \ddot{z}_1 = \frac{K_1}{M_1}(z_{of} - z_1) + \frac{D_1}{M_1}(\dot{z}_{of} - \dot{z}_1) - \frac{K_2}{M_1}(z_1 - z_2) - \frac{D_2}{M_1}(\dot{z}_1 - \dot{z}_2) - g$$

$$(2)\quad \ddot{z}_3 = \frac{K_3}{M_3}(z_{om} - z_3) + \frac{D_3}{M_3}(\dot{z}_{om} - \dot{z}_3) - \frac{K_4}{M_3}(z_3 - z_4) - \frac{D_3}{M_3}(\dot{z}_3 - \dot{z}_4) - g$$

$$(3)\quad \ddot{z}_m = \frac{K_2}{M_m}(z_1 - z_2) + \frac{D_2}{M_m}(\dot{z}_1 - \dot{z}_2) + \frac{K_4}{M_m}(z_3 - z_4) + \frac{D_4}{M_m}(\dot{z}_3 - \dot{z}_4)$$

$$+ \frac{K_5}{M_m}(z_{or} - z_5) + \frac{D_5}{M_m}(\dot{z}_{or} - \dot{z}_5) - \left(\frac{M_r + M_5}{M_m}\right)g - \ddot{z}_r\left(\frac{M_r + M_5}{M_m}\right) - g$$

FIGURE 7E. LSV-6 WHEEL - ARTICULATED, MATHEMATICAL MODEL, PITCH PLANE

$$(4)\ \ddot{\theta}_r = \left[\frac{\ell_{r2}}{I_{yr}}\right]\left[K_5(z_{or}-z_5)+D_5(\dot{z}_{or}-\dot{z}_5)\right]-\frac{\ell_{r1}}{I_{yr}}\left[(M_r+M_5)g\right]$$

$$-\frac{M_B}{I_{yr}}-\frac{D_7}{I_{yr}}(\dot{\theta}_r-\dot{\theta}_m)h_m$$

$$(5)\ \ddot{\theta}_m = \frac{\ell_{m4}}{I_{ym}}\left[K_4(z_3-z_4)+D_4(\dot{z}_3-\dot{z}_4)\right]-\frac{\ell_{m2}}{I_{ym}}\left[K_2(z_1-z_2)+D_2(\dot{z}_1-\dot{z}_2)\right]$$

$$+\frac{D_7}{I_{ym}}(\dot{\theta}_r-\dot{\theta}_m)h_m-\frac{\ell_{m4}}{I_{ym}}\left[K_5(z_{or}-z_5)+D_5(\dot{z}_{or}-\dot{z}_5)\right.$$

$$\left.-(M_5+M_r)g\right]-\frac{M_B}{I_{ym}}-\frac{M_B\ell_{m2}}{I_{ym}\ell_{m4}}$$

$$(6)\ \ddot{z}_r = \frac{K_5}{(M_r+M_5)}(z_{or}-z_5)+\frac{D_5}{(M_r+M_5)}(\dot{z}_{or}-\dot{z}_5)+\frac{M_B}{(M_r+M_5)(\ell_{r1})}$$

$$(7)\ M_A = \frac{2EI}{\ell_c^2}\left[(\ell_c+\ell_{m4})\theta_m+\ell_{r1}\theta_r-(z_r-z_m)\right]$$

$$(8)\ M_B = \frac{2EI}{\ell_c^2}\left[(\ell_c+\ell_{r1})\theta_r+\ell_{m4}\theta_m-(z_r-z_m)\right]$$

$$(9)\quad \ddot{z}_5=\ddot{z}_r \quad ; \quad \ddot{z}_4=\ddot{z}_m+\ell_{m4}\ddot{\theta}_m \quad ; \quad \ddot{z}_2=\ddot{z}_m-\ell_{m2}\ddot{\theta}_m$$

$$\dot{z}_5=\dot{z}_r \qquad \dot{z}_4=\dot{z}_m+\ell_{m4}\dot{\theta}_m \qquad \dot{z}_2=\dot{z}_m-\ell_{m2}\dot{\theta}_m$$

$$z_5=z_r \qquad z_4=z_m+\ell_{m4}\theta_m \qquad z_2=z_m-\ell_{m2}\theta_m$$

NOTE: (z_1-z_2), (z_3-z_4) are limited to

+8 inch and -6 inch travel

FIGURE 7F. LSV-6 WHEEL - ARTICULATED, PITCH EQUATIONS

PART III

PRELIMINARY STUDY OF LSV STEERING CONTROL

PRELIMINARY STUDY OF LSV STEERING CONTROL

Figure 8 is a preliminary block diagram to be used as a basis for studying the LSV steering control. Only the major loops of the control are shown. The system, as shown, is general in all areas concerning sensors, instruments and limits. A digital, analog--or combination digital-analog-control system can be studied by proper models in the appropriate blocks.

Two modes of operation are shown--remote and manual. The remote loop, marked "Mode 2", is shown for Earth-remote study purposes. However, by changing time delays the same loop can be used for Lunar-remote surface operations. "Mode 1" is the manual control loop operated by the astronaut, and with the exception of the coding, decoding (computer) and radio transmission functions, is similar to Mode 2. Only one of the modes of steering (remote or manual) can be used at any time.

Speed is a parameter which directly affects the ability to steer. It is not part of the direct steering control, but is added for both modes where it is applicable.

The capability for changing steering modes is shown. Although scuff steering is not shown, it could easily be added to the steering mode block which controls the "Master Wheel Position".

In all steering modes, except scuff steering, it will be necessary to control both front wheels as a unit and both rear wheels as a unit. This is shown on the schematic as a synchronizer in the steering motor loops feedback.

Speed, roll, and pitch limits which have been found from dynamic studies to be very desirable, have been included in the study diagram. Other features resulting from the completed dynamic studies can be shown in the expansion of the block marked "Vehicle Position".

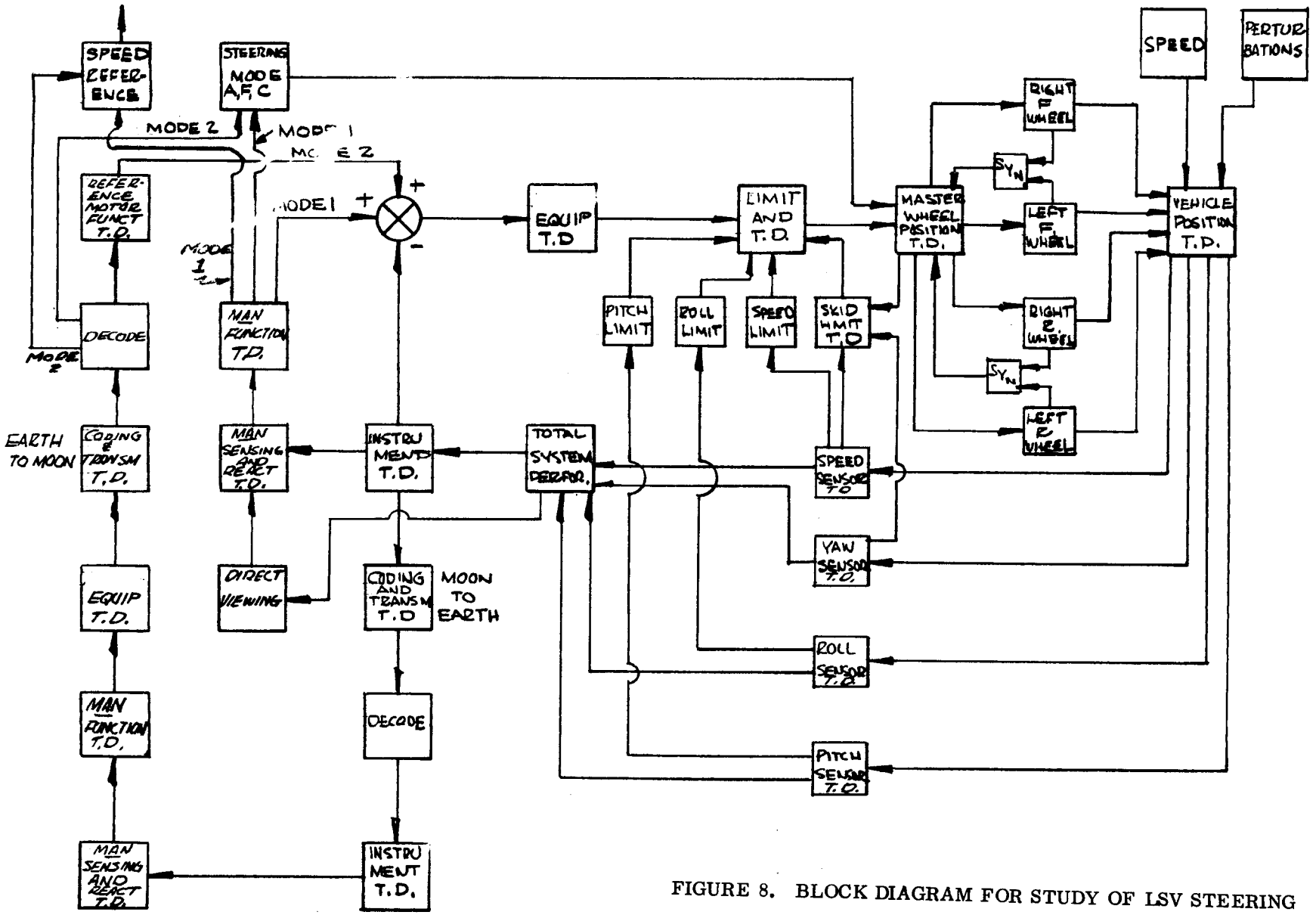

FIGURE 8. BLOCK DIAGRAM FOR STUDY OF LSV STEERING

5.0 SYMBOLS

C. G.	Center of Gravity
$D_{(\ )}$	Damping constant, lb/ft/sec
EI	Module of Elasticity, $lb\text{-}ft^2$
g	Gravity, ft/sec^2
h	Height of C. G, Ft.
Ix	Moment of Inertia about X axis (Roll Plane), $Slug\text{-}ft^2$
Iy	Moment of Inertia about Y axis (Pitch plane), $Slug\text{-}ft^2$
$K_{(\ )}$	Spring constant, lb/fg
$lm_{(\ )}$	Dimension (Main Module), ft
$lr_{(\ )}$	Dimension (Rear Module), ft
$M_{(\ )}$	Mass, Slugs
t	TIME, seconds
V	Vehicle velocity, Km (miles) per hour
$X_{(\ )}$	Length Dimension (4 wheel vehicle), ft
$Y_{(\ )}$	Width dimension (4 wheel vehicle), ft
$Z_{(\ )}$	Vertical Displacement, ft
θ	Pitch angle, degrees
ϕ	Roll angle, degrees
ψ	Yaw angle, degrees

Subscripts:

1	Right Front Wheel Main Module
2	Right Front Chassis Main Module
3	Right Rear Wheel Main Module
4	Right Rear Chassis Main Module

5	Right Trailer Wheel
6	Right Trailer Chassis
7	Coupling Between Main Module and Trailer
11	Left Front Wheel Main Module
12	Left Front Chassis Main Module
13	Left Rear Wheel Main Module
14	Left Rear Chassis Main Module
15	Left Rear Trailer Wheel
16	Left Rear Trailer Chassis
m	Main Module
of	Bottom of Right Front Wheel
lf	Bottom of Left Front Wheel
om	Bottom of Right Rear Wheel (6 wheel vehicle)
im	Bottom of Left Rear Wheel (6 Wheel vehicle)
or	Bottom of Right Trailer Wheel (6 wheel vehicle)
	Bottom of Right Rear Wheel (4 wheel vehicle)
ir	Bottom of Left Trailer Wheel (6 wheel vehicle)
	Bottom of Left Rear Wheel (4 wheel vehicle)
r	Rear Module (Trailer)

REFERENCES

1. "Apollo Logistics Support Systems MOLAB Studies-Mission Command and Control" by Arch W. Meagher and Harvey Ryland, ALLS BULLENTIN 006, September, 1964.

BIBLIOGRAPHY

1. "Elements of Strength of Materials", by Timoshienko and MacCullough, D. VanNostrand Co., Inc.

6.0 APPENDICES

INDEX

APPENDIX A

FOUR WHEEL VEHICLE--PITCH PLANE DATA AND COMPUTER MODELS

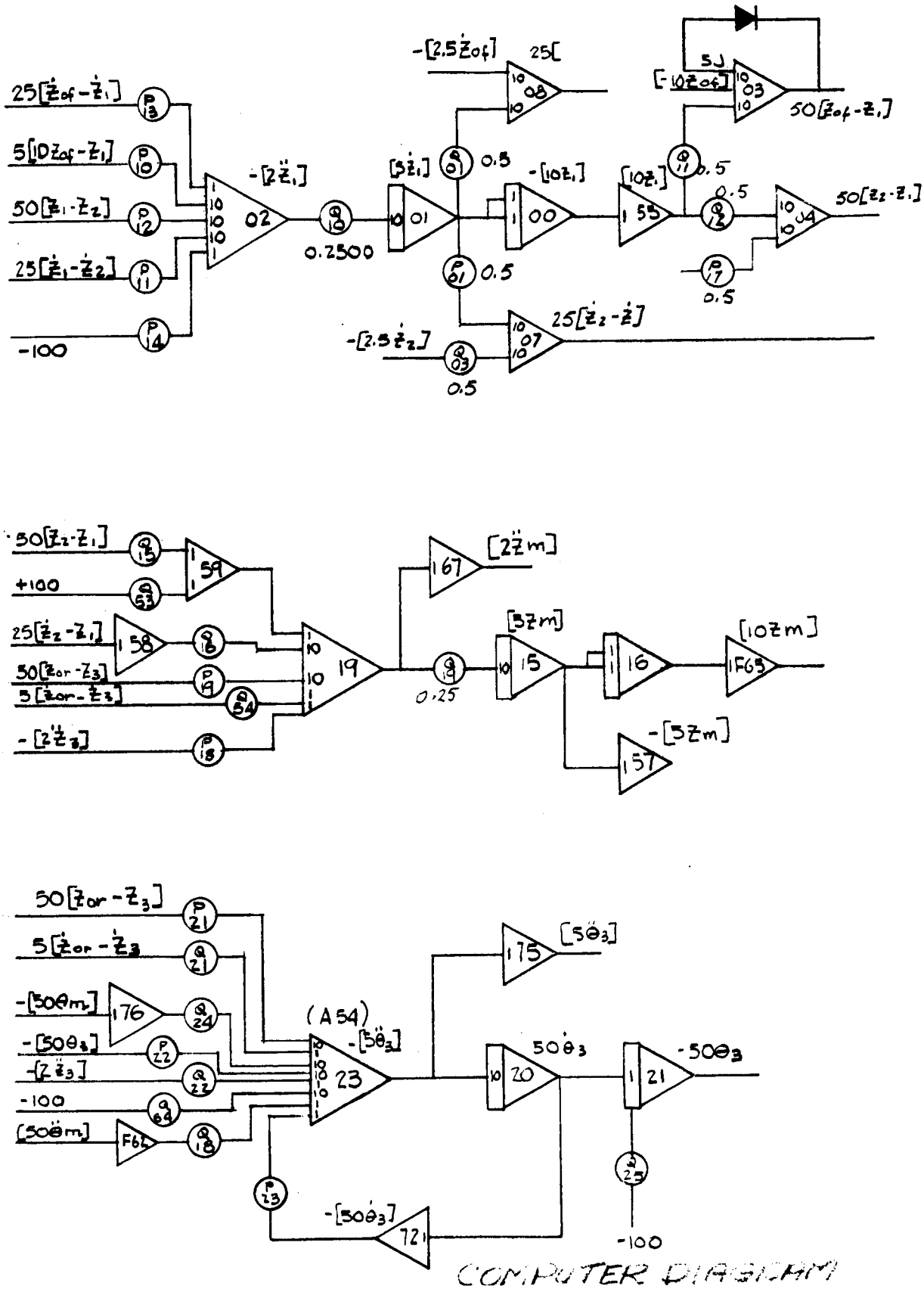

FIGURE A1A. FOUR WHEEL VEHICLE (PITCH PLANE)

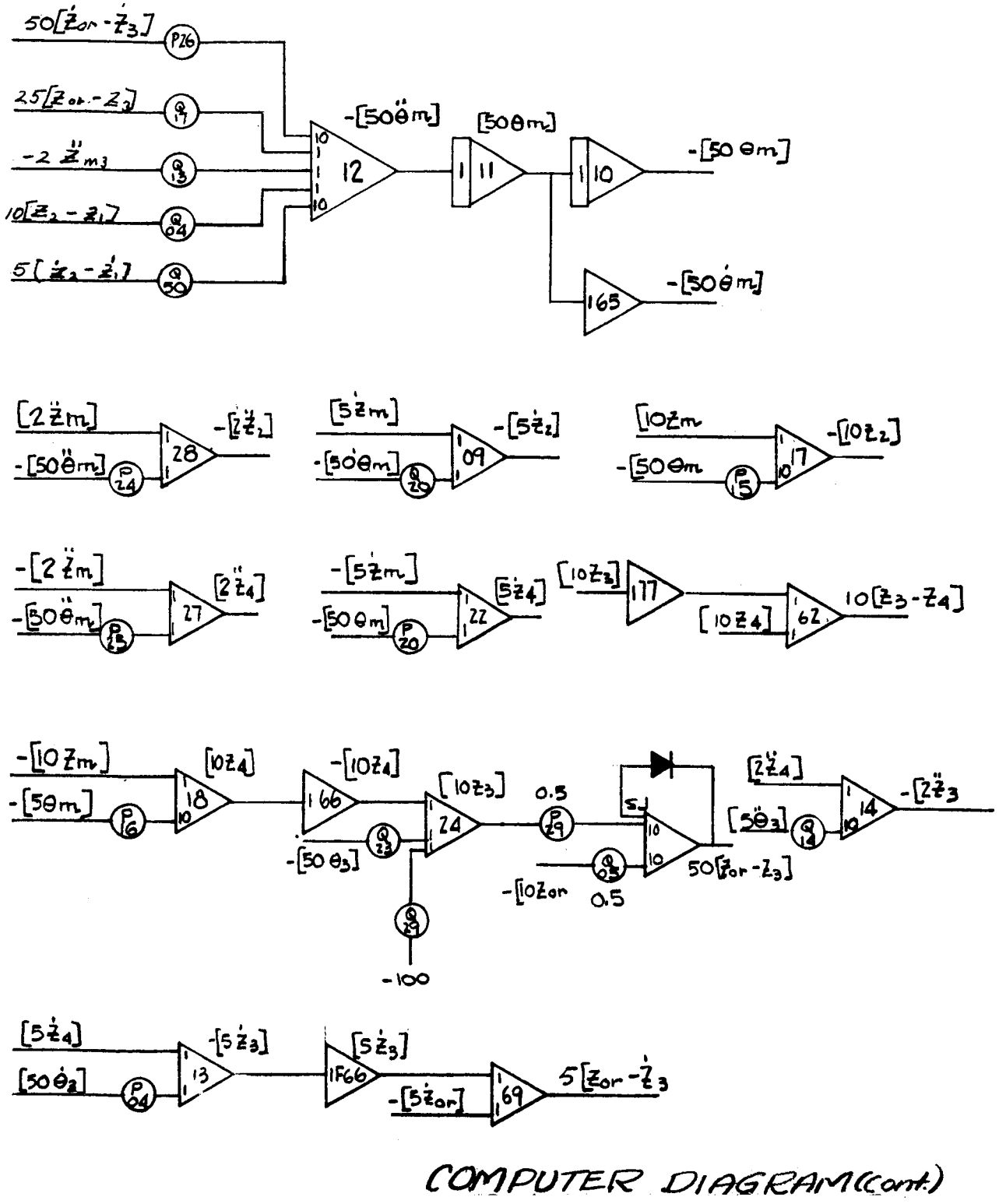

COMPUTER DIAGRAM (cont.)

FIGURE A1B. FOUR WHEEL VEHICLE (PITCH PLANE)

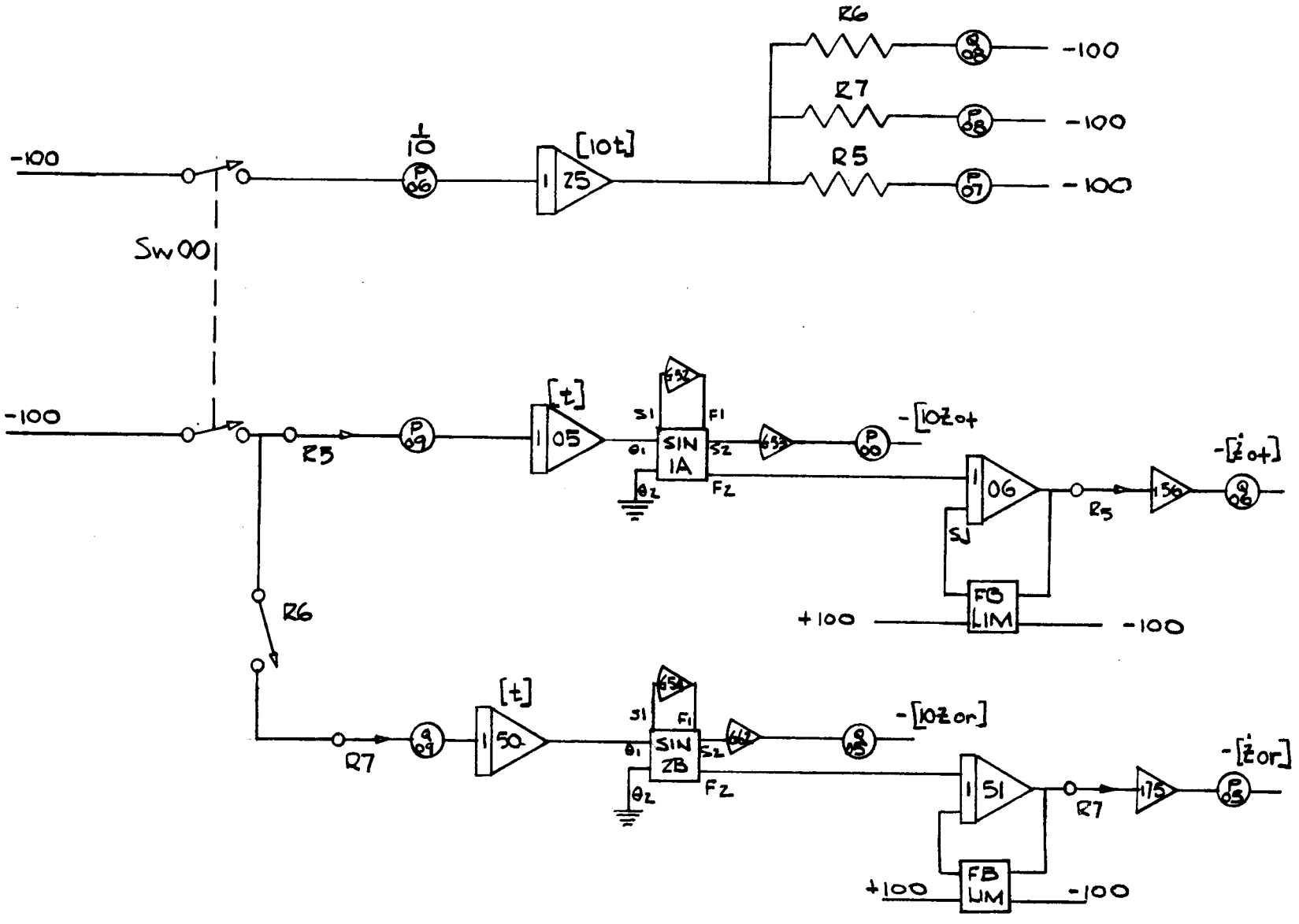

FIGURE A1C. SEQUENTIAL LEDGE FORCING FUNCTION (PITCH PLANE)

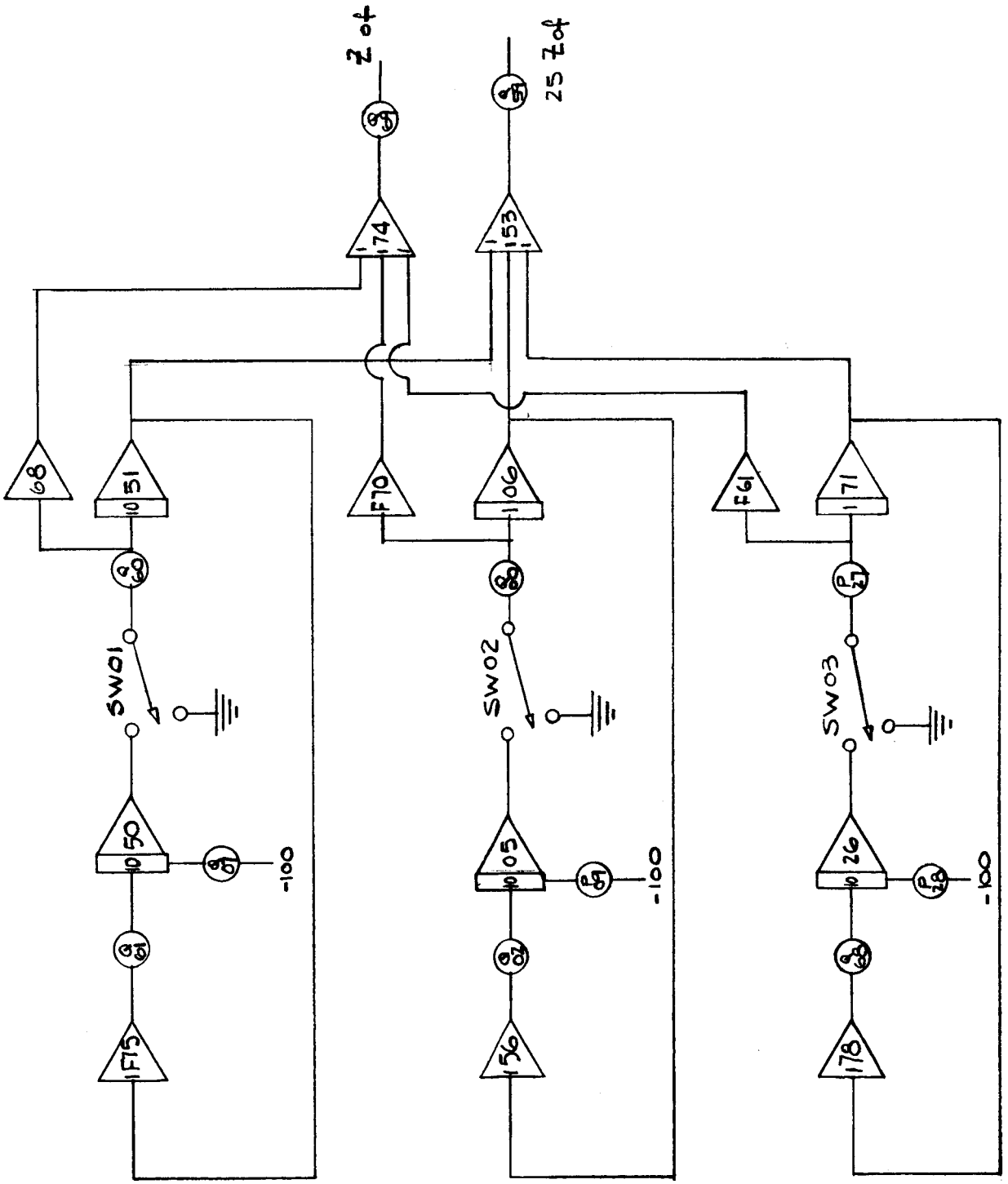

FIGURE A1D. RANDOM SURFACE FORCING FUNCTION - FOUR WHEEL VEHICLE (PITCH PLANE)

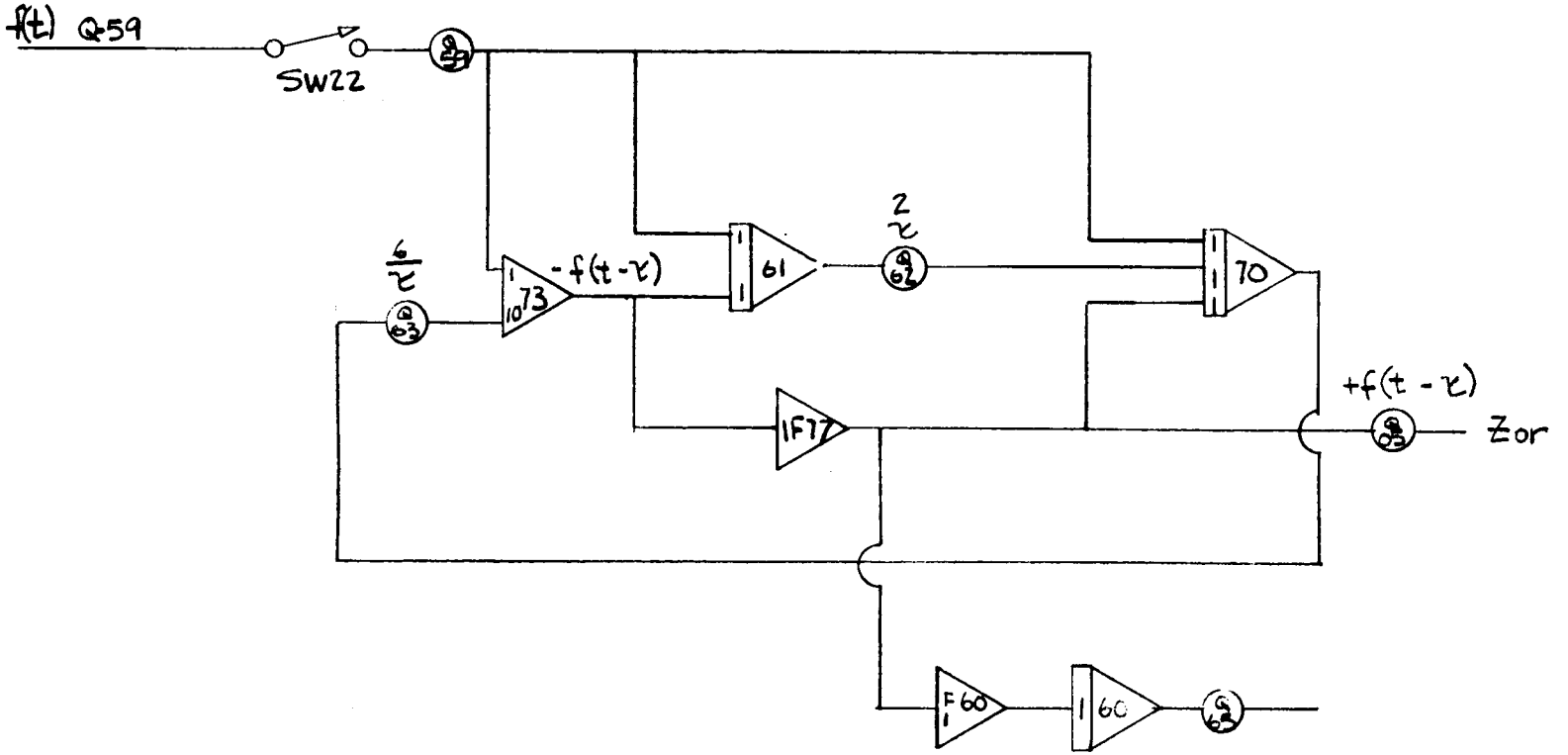

FIGURE A1E. DELAY CIRCUIT FOUR WHEEL VEHICLE - PITCH PLANE (SEQUENTIAL BUMPS)

P04	$X_5/10$
P10	$K_1/5M_1$
P11	$2D_1/5M_1$
P12	$K_2/5M_1$
P13	$2D_2/5M_1$
P14	$29/100$
P15	$X_2/5$
P16	$X_1/5$
P17	0.5
P18	M_3/M_m
P19	$K_3/5M_m$
P20	$X_1/10$
P21	$5X_5K_3/I_{ym+3}$
P23	$D_4/10I_{ym+8}$
P24	$X_2/25$
P25	$X_1/25$
P26	$X_2 K_3 5/I_{ym}$

Q04	$25X_2 M_3/I_{ym}$
Q13	$5X_1 K_2/I_{ym}$
Q14	$X_5/5$
Q15	$K_2/5M_m$
Q16	$2D_2/5M_m$
Q17	$10D_3X_2/I_{ym}$
Q20	$X_2/10$
Q21	$5X_5D_3/I_{ym+8}$
Q22	$K_4/10I_{ym+8}$
Q23	$X_5/5$
Q50	$10D_2X_1/I_{ym}$
Q53	$29/100$
Q54	$2D_2/5M_m$

FIGURE A1F. COMPUTER POT-SETTING QUANTITIES - 4 WHEEL VEHICLE (PITCH PLANE ANALYSIS)

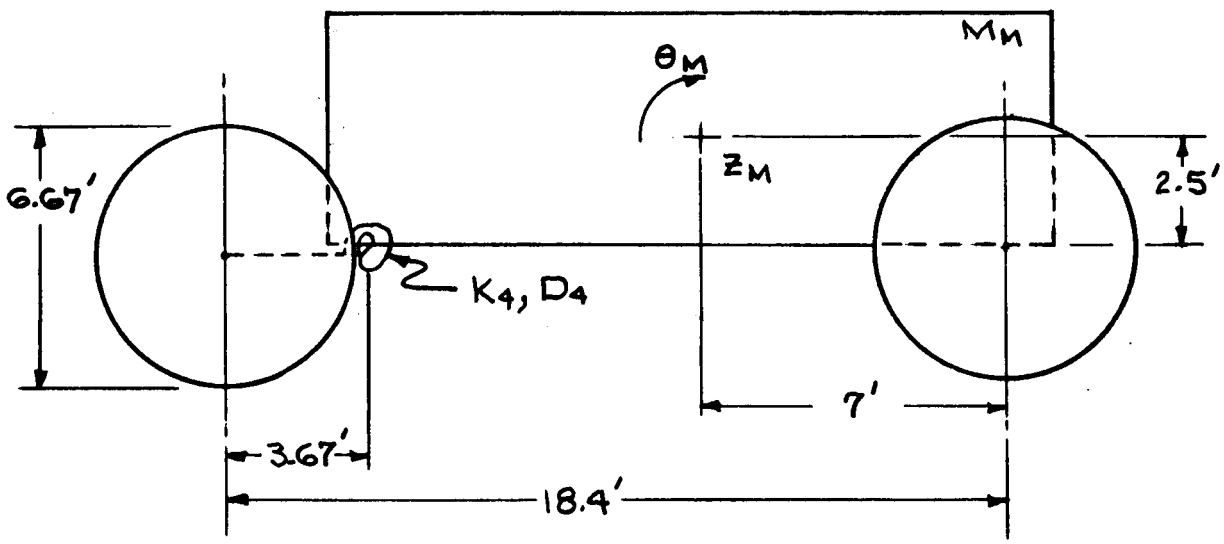

$M_1 = M_3 = 4.34$ SLUGS $\quad I_{Y\,BAR+MS} = 86.29$ SLUG FT^2

$M_M = 185$ SLUGS , $I_{Ym} = 8116$ SLUG-FT^2

DATA REFERRED TO MATHEMATICAL MODEL
(SEE TEXT, PAGE 9)

$K_1 = K_3 = 600$ #/FT , $D_1 = D_3 = 15$ #/FT/sec.

$K_3 = 725$ #/FT , $D_2 = 150$ #/FT/sec.

$K_4 = 7620$ #/rad $= 2075$ #/FT, $D_4 = 520$ #/FT/sec.

$X_1 = 7$ FT , $X_2 = 6.92$ FT, $X_5 = 3.67$ FT

$h = 5.83$ FT.

FIGURE A2. DATA AND CALCULATIONS - 4 WHEEL VEHICLE
(PITCH PLANE ANALYSIS)

APPENDIX B

FOUR WHEEL VEHICLE
ROLL PLANE DATA AND COMPUTER MODELS

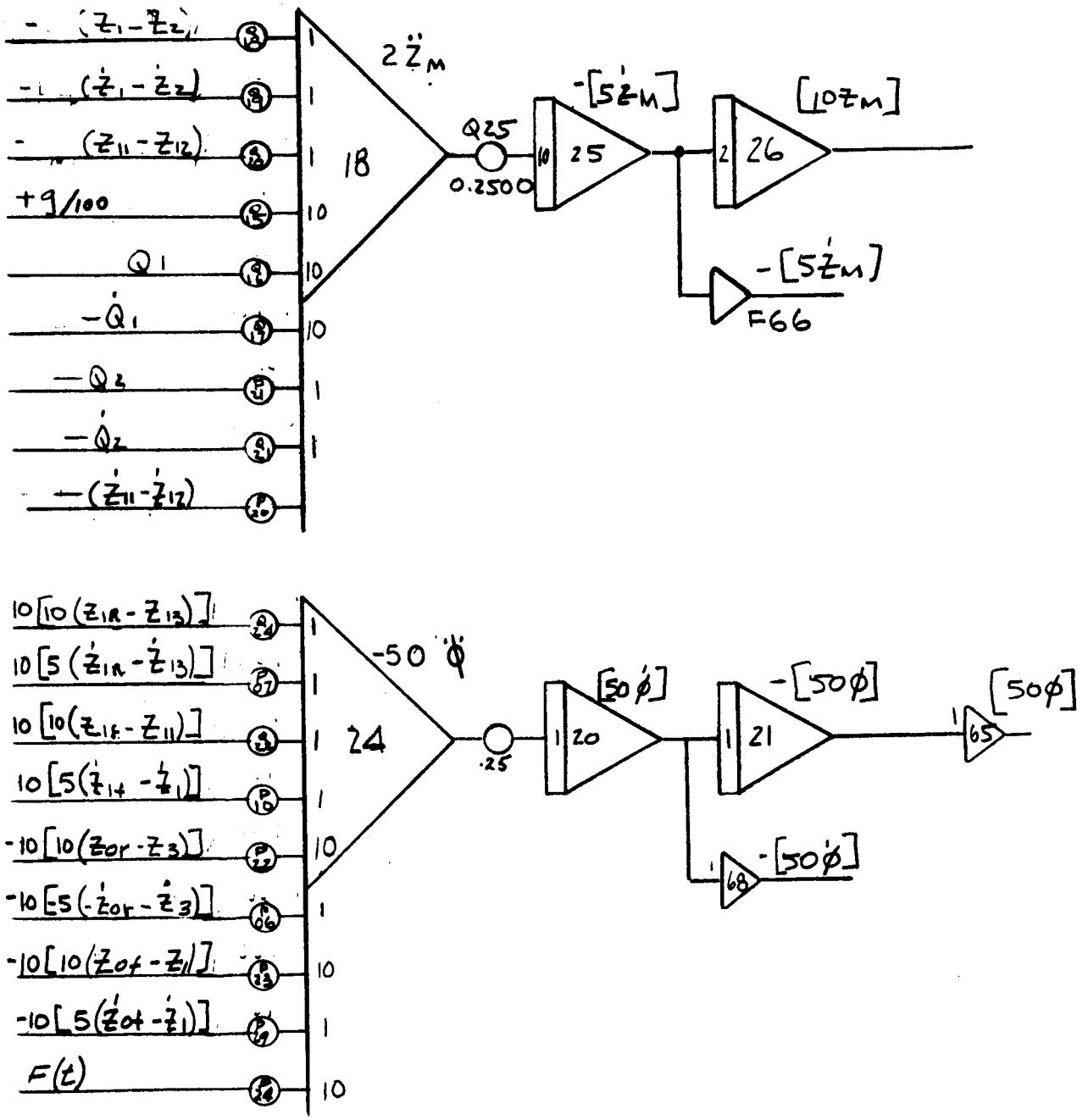

FIGURE B1A. ROLL PLANE - 4 WHEEL VEHICLE

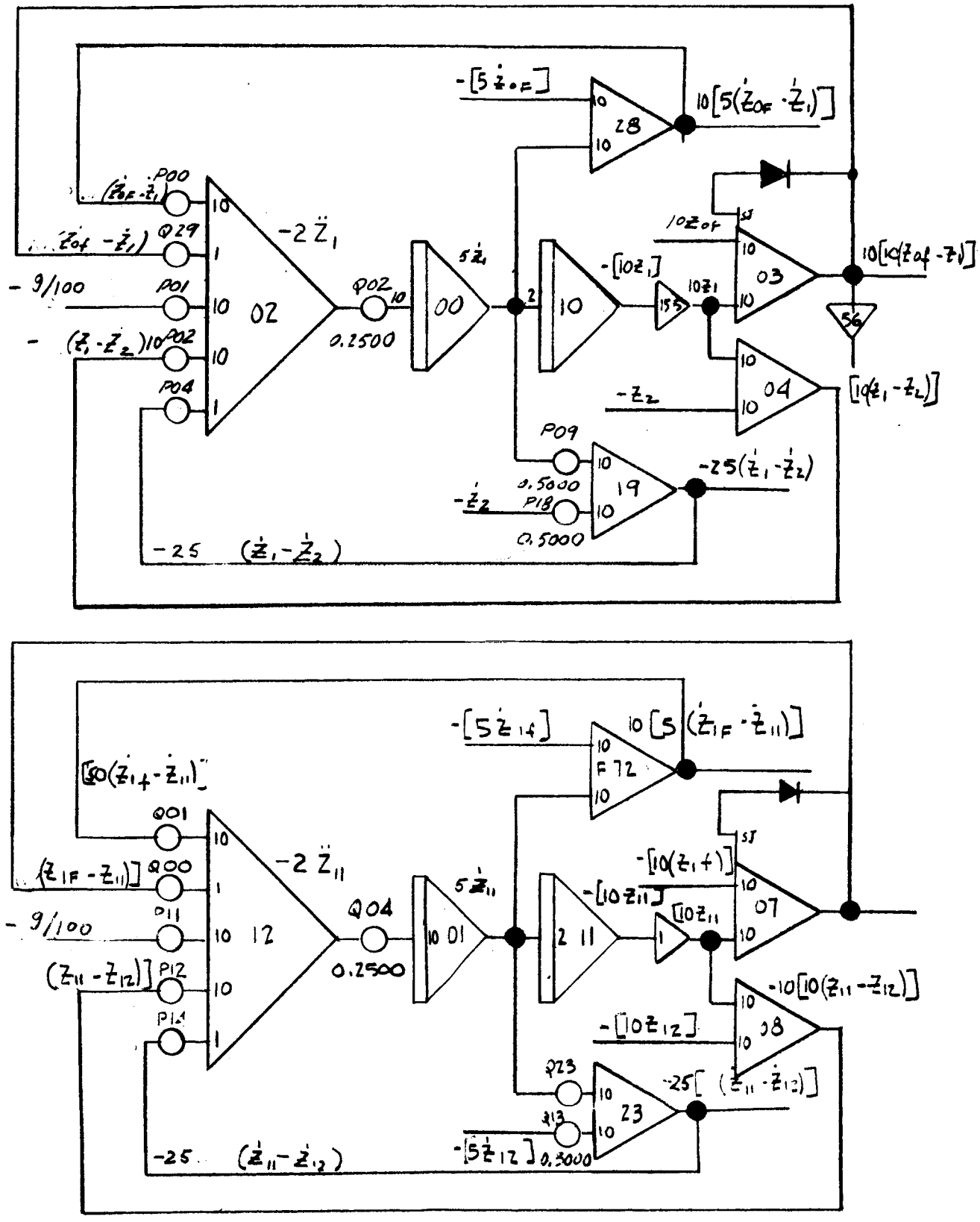

FIGURE B1B. ROLL PLANE - 4 WHEEL VEHICLE

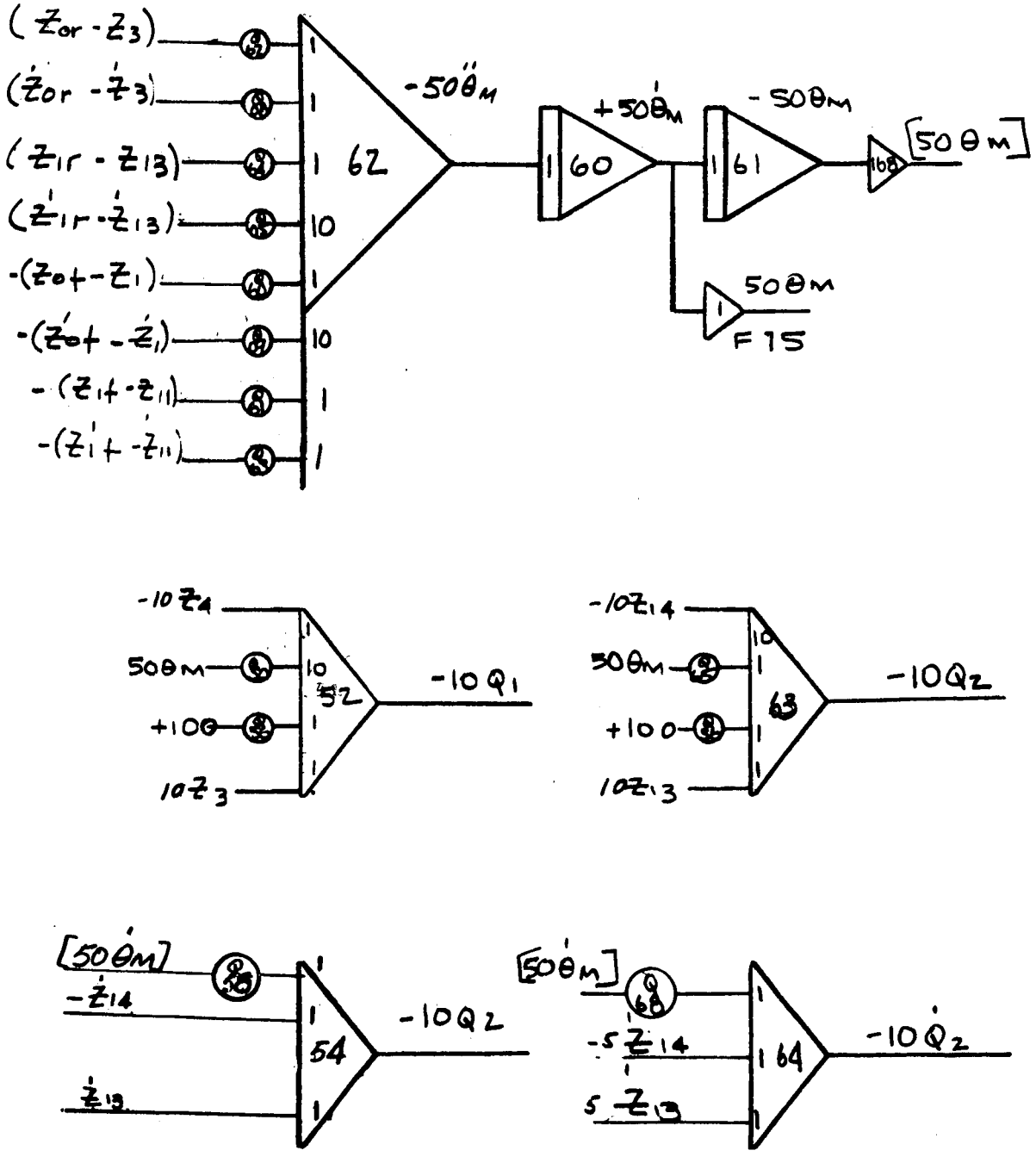

FIGURE B1C. ROLL PLANE - 4 WHEEL VEHICLE

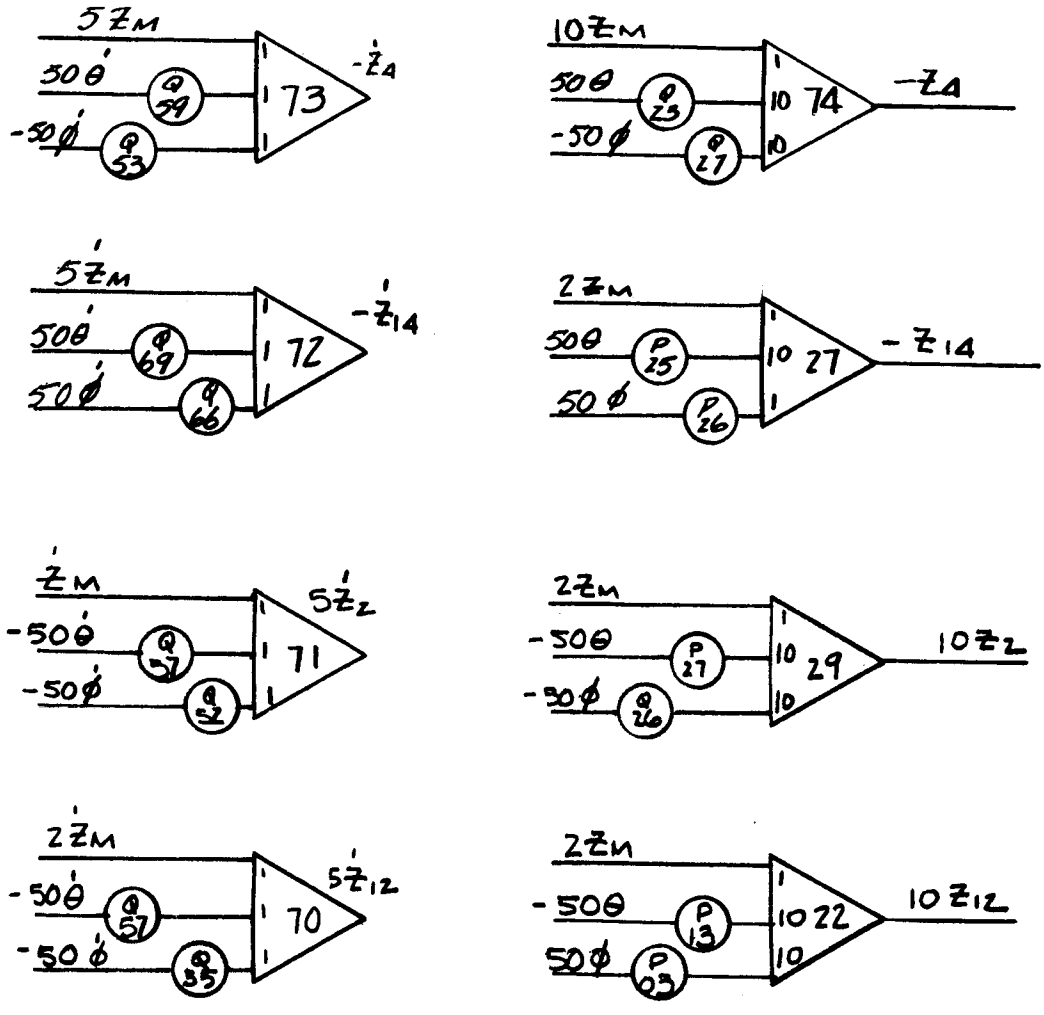

FIGURE B1D. ROLL PLANE - 4 WHEEL VEHICLE

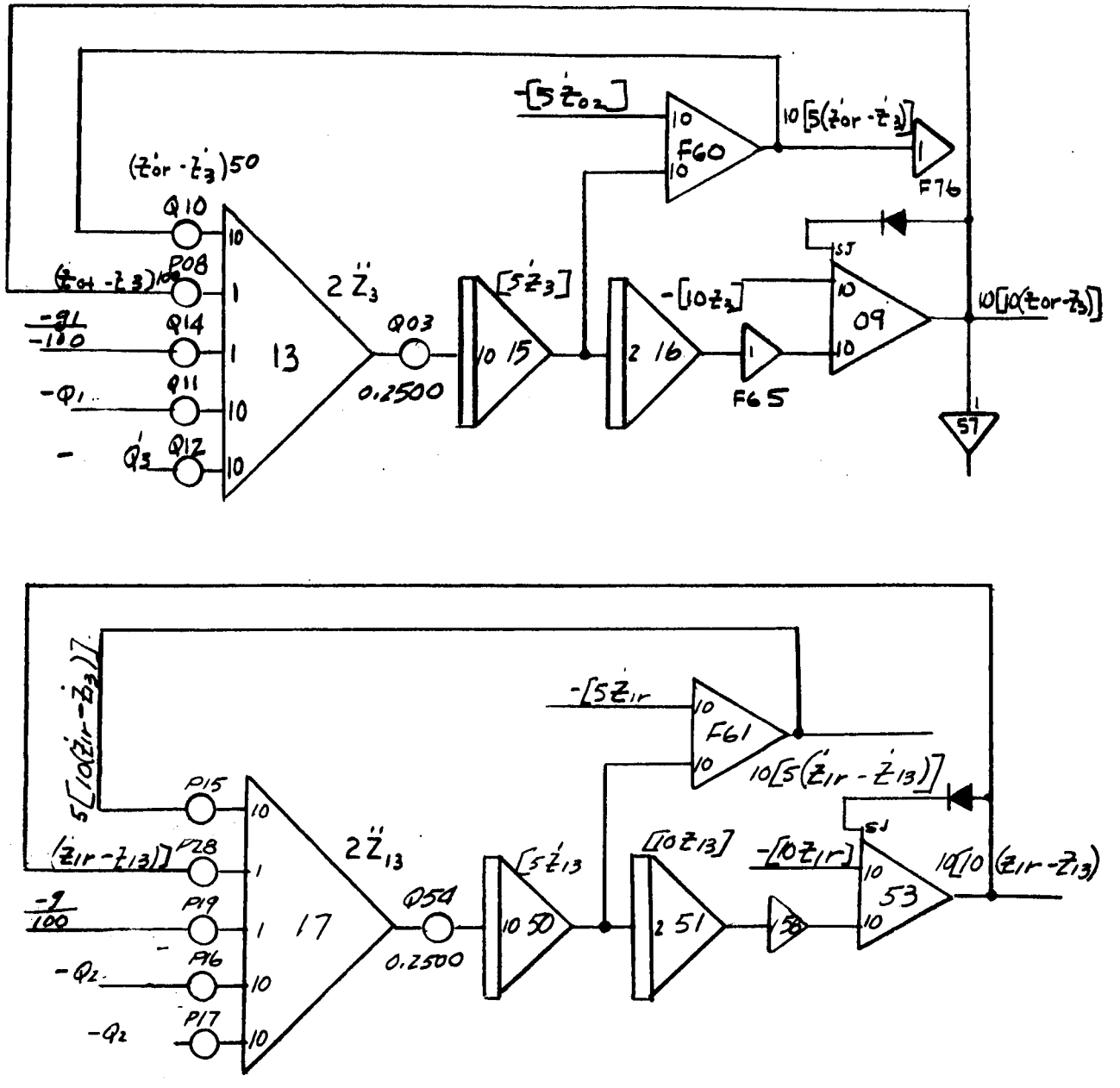

FIGURE B1E. ROLL PLANE - 4 WHEEL VEHICLE

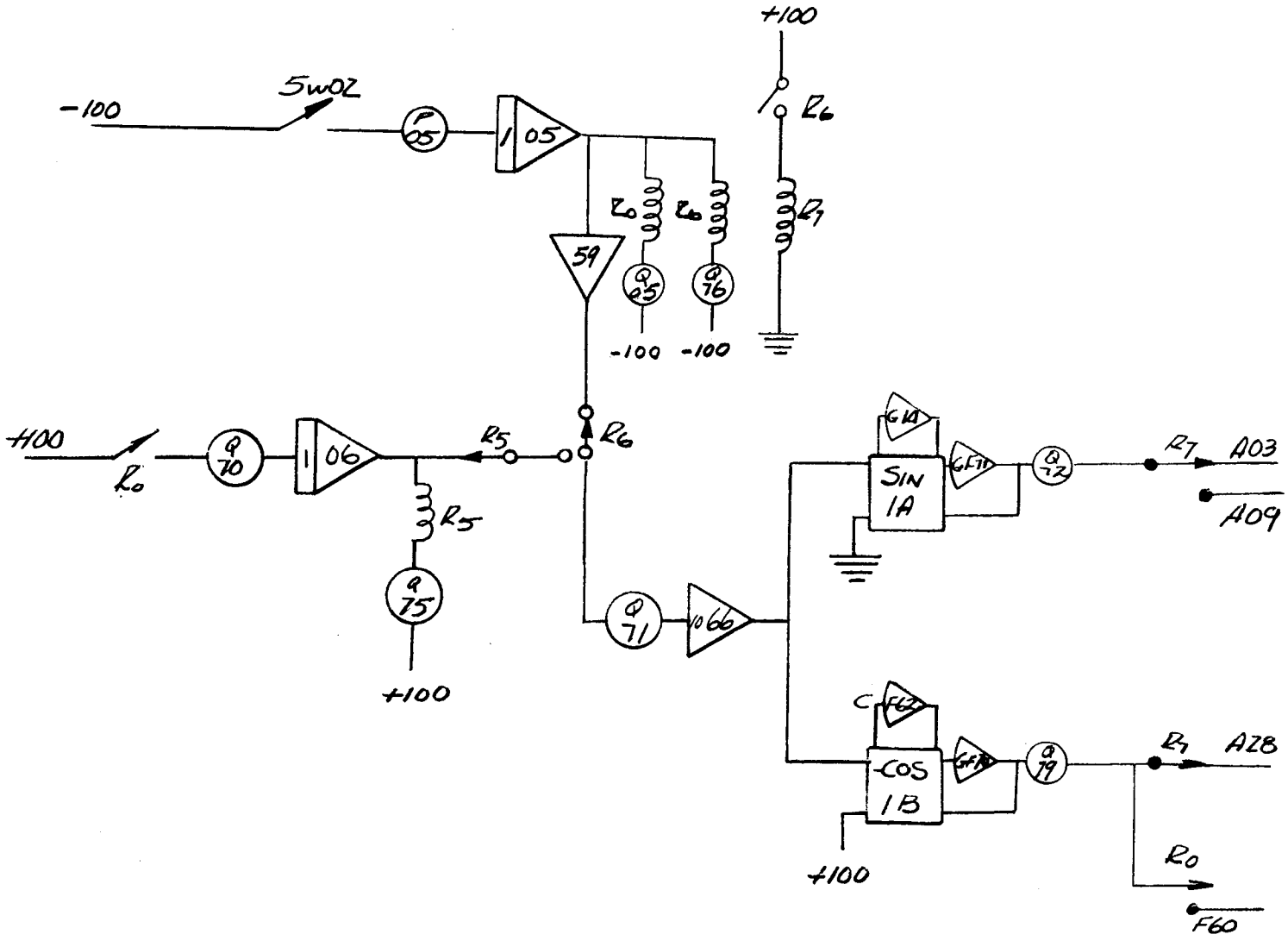

FIGURE B1F. ROLL PLANE - 4 WHEEL VEHICLE
(1 BODY CONFIGURATION)

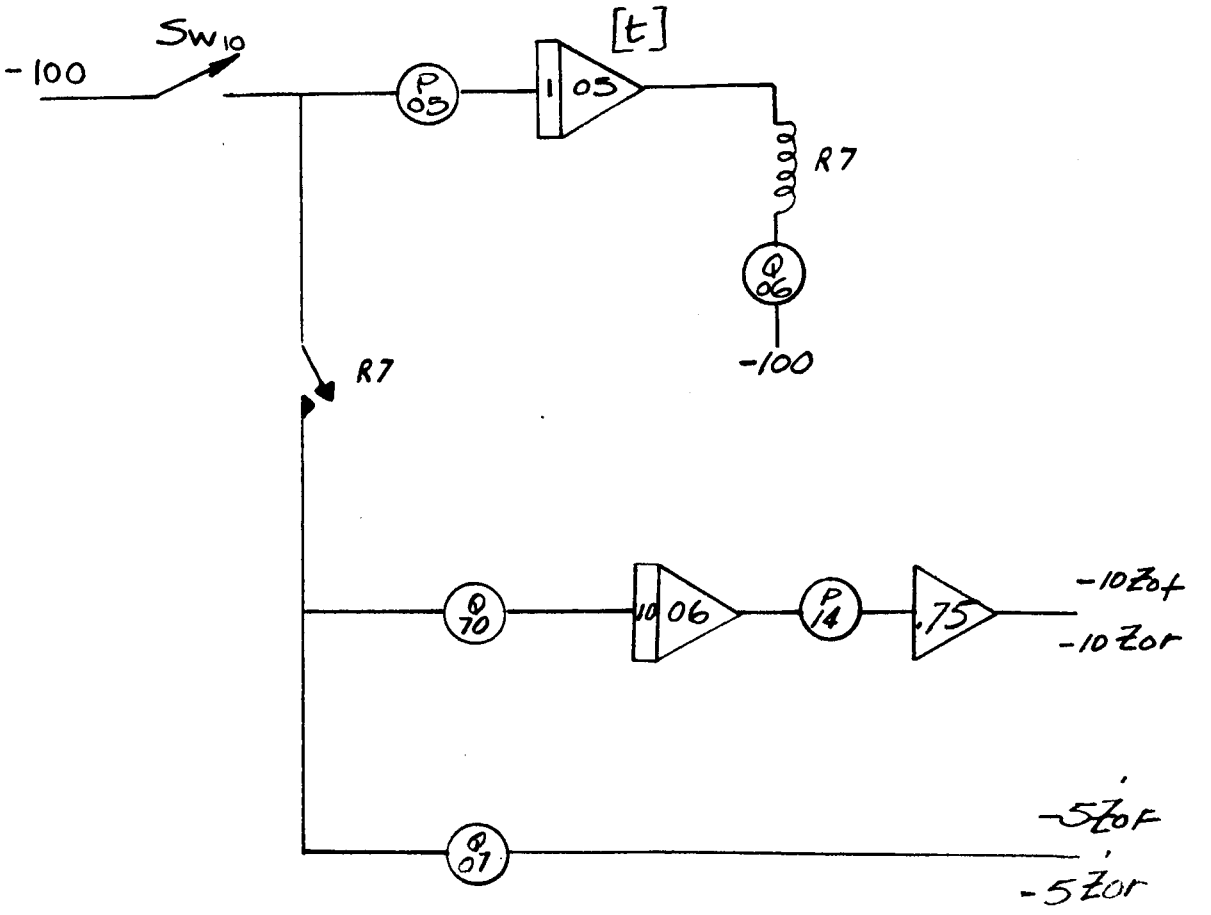

FIGURE B1G. ROLL PLANE - SINGLE BODY 4 WHEEL CONF.
(FORCING FUNCTION STEERING)

P00	$K_1/5M_1$	Q00	$2D_{11}/5m_{11}$	Q57	$X_1/10$
P01	$K_2/5M_1$	Q01	$2K_{11}/10m_{11}$	Q58	$X_2/10$
P02	$2D_2/5m_1$	Q05	$10[D_{13}(X_2+X_5)]/I_{ym}$	Q59	$X_2/10$
P03	$Y_1/5$	Q08	$10[D_3(X_2+X_5)]/I_{ym}$	Q60	$5K_1X_1/I_{ym}$
P04	$g/50$	Q09	$10X_1D_1/I_{ym}$	Q61	$5k_{11}X_1/I_{ym}$
P05	.10	Q10	K_3/M_3	Q62	$5k_3(X_2+X_5/I_{ym}$
P06	Y_1D_3/I_{xm}	Q11	$K_4/5M_3$	Q63	$D_{11}X_1/50$
P07	$10Y_2D_{12}/I_{xm}$	Q12	$2D_4/5M_3$	Q64	$5k_{13}(x_2+x_5)/I_{ym}$
P08	$2D_3/5m_3$	Q14	$g/50$	Q65	$X_5/5$
P10	$10Y_2D_{11}/I_{ym}$	Q15	$g/50$	Q66	$Y_2/10$
P11	$k_{12}/5m_{13}$	Q16	$K_4/5M_m$	Q67	I_c
P12	$2D_{12}/5m_{13}$	Q17	$2D_4/5M_m$	Q68	$X_5/10$
P13	$k_1/5$	Q18	$K_2/5M_m$	Q69	$X_2/10$
P14	$g/50$	Q19	$D_2/5m_m$		
P15	$K_{13}/5m_{13}$	Q20	$K_{12}/5M_m$		
P16	$K_{14}/5m_2$	Q21	$2D_{14}/5M_m$		
P17	$2D_{14}/5M_{13}$	Q22	$5Y_2K_{11}/I_{xm}$		
P19	$g/50$	Q24	$5Y_2K_{13}/I_{xm}$		
P20	$2D_{12}/5M_m$	Q26	$Y_1/5$		
P21	$K_{12}/5m_m$	Q27	$Y_1/5$		
P22	$5Y_1K_3/I_{ym}$	Q28	$X_2/5$		
P23	$5Y_1K_1/I_{ym}$	Q29	$2D_1/5m_1$		
P24	Forcing Function	Q50	$X_5/5$		
P25	$K_2/5$	Q51	$X_1/10$		
P26	$Y_2/5$	Q52	$Y_1/10$		
P27	$X_1/5$	Q53	$Y_1/10$		
P28	$2D_{13}/5m_{13}$	Q55	$Y_2/10$		
P29	$10Y_1D_1/I_{ym}$	Q56	IC		

FIGURE B1H. POT SETTINGS - 4 WHEEL VEHICLE
(ROLL PLANE ANALYSIS)

(See Text, page 6 for Diagram)

$M_1 = M_3 = M_{11} = M_{13} = 4.345$ slugs

$M_M = 185$ slugs, $I_{YM} = 8116$ slug-ft^2; $I_{XM} = 5075$ slug-ft^2

$K_1 = K_3 = K_{11} = K_{13} = 600$ #/ft

$D_1 = D_3 = D_{11} = D_{13} = 15$ #/ft/second

$K_4 = K_{14} = 7620$ #/rad $= 2075$ #/ft

$D_4 = D_{14} = 520$ #/ft/second

$K_2 = K_{12} = 725$ #/ft, $D_2 = D_{12} = 150$ #/ft/second

$X_1 = 7$ ft, $X_2 = 6.92$ ft, $X_5 = 3.67$ ft

$Y_1 = Y_2 = 5.75$ ft, $h = 5.83$ ft

$M_0 = 0$ For 0° slope

$= 170$ For 10° slope

$= 740$ For 20° slope

$= 1715$ For 30° slope

RAMP DATA:

	Wheel Angle	Time of Ramp	Max Torque of Ramp
4.18 Km/hr	6°	3 sec	149.5 #ft
	12°	4.12	281.5
	18°	5.25	399.0
	24°	6.35	506.0
8.36 Km/hr	6°	2.0	597.0
	12°	3.06	1125.0
	18°	4.11	1592.0
	24°	5.18	2022.0
16.72 Km/hr	6°	1.5	2385.0
	12°	2.53	4500.0
	18°	3.56	6370.0
	24°	4.6	8100.0

FIGURE B2. DATA AND CALCULATIONS - 4 WHEEL VEHICLE (ROLL PLANE ANALYSIS)

APPROXIMATE:

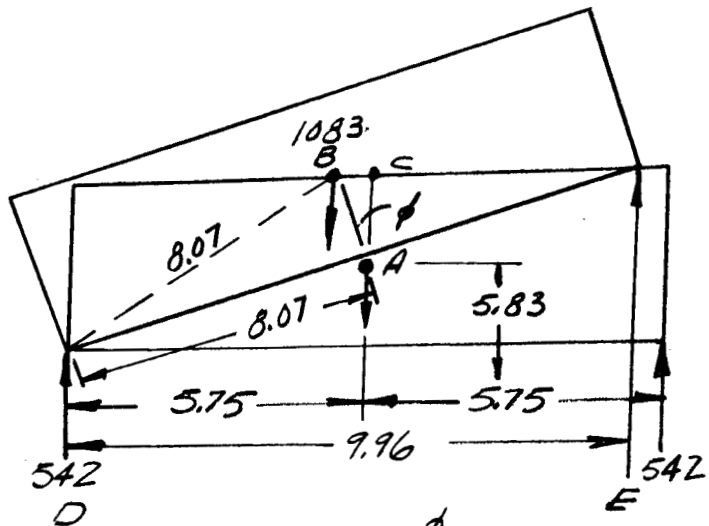

FOR A-B: $AB = 8.07 \times \frac{\phi}{57.3}$

B-C: $BC = AB \sin \phi$

FOR $\phi = 30°$: $AB = 4.23'$,
$BC = 2.12'$
$DE = .866 \times 11.5' = 9.96'$

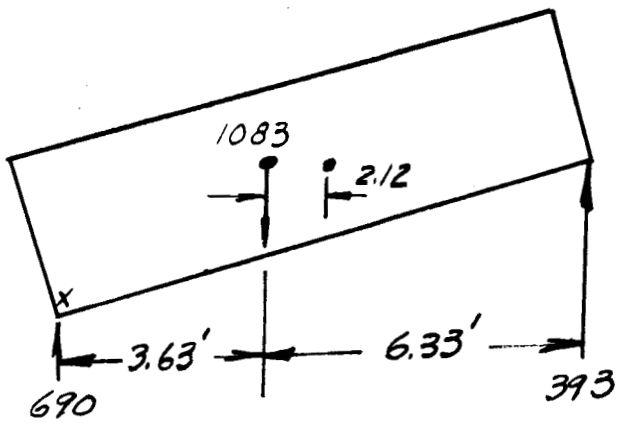

$5.75' - 2.12' = 3.63'$,
$9.96' - 3.63' = 6.33'$,

ABOUT X:

$1083 \times 3.63 - E \times 9.96 = 0$; $E = 393$

$D = 1083 - 393 = 690$

$M_o = (690 \times 5.75) - (393 \times 5.75) = 1715$

FIGURE B3. CALCULATIONS FOR PERFORMANCE ON A SLOPE - ROLL PLANE

SIMULATION OF THE 4 WHEEL VEHICLE ON A SLOPE ROLL PLANE ANALYSIS

The simulation of the vehicle on a slope (in the roll plane) was accomplished by using the computer diagram for the roll plane analysis and adding a constatly-applied torque in the roll angle equation. This torque was developed as shown in Figure B3 by shifting the forces on the right and left wheels. This simulation is not applicable when both right and left vehicle are off the lunar surface. However, as expected, this did not occur for any of the perturbations used in the roll plane studies. The pertrubations (forcing functions) were added to the simulation as in other studies, and should not be confused with the torque described above.

DEVELOPMENT OF THE FORCING FUNCTION FOR EXAMINING ACKERMAN STEERING---4 WHEEL VEHICLE

In developing the computer forcing function for examining Ackerman steering, two assumptions were made. First, the turning radius was defined as the radius of the circle described by the vehicle CG in a turn, and second, there is no skidding of the vehicle front wheels in the turn. The vehicle was assumed to maintain constant speed while in the turn. All these assumptions lead to the examination of a "worst case" condition with safety factors included in the computer simulation.

As indicated in Figure B4 and as a result of the above assumptions, the velocity of the vehicle CG and the velocity of the steering wheels are normal to the turning radius. Therefore turning radius of the vehicle are calculated for wheel angles of 6, 12, 18, and 24 degrees by using the vehicle width and length, as shown.

The next step calculates the time required for the vehicle to make a complete 90-degree turn using the vehicle speed (4.18, 8.36, and 16.72 Km/hr and each of the wheel angles.

Since the entire momentum of the vehicle (in the original direction of travel) changes during the execution of 90-degree turn, the force (acceleration times mass) toward the center of the turning circle is calculated. This forces times the CG height forms a couple (overturning moment) which is applied to the center of gravity.

The above couple (or torque) represents the maximum value of the overturn force on the vehicle when the vehicle has reached the position of full turning rate. Two time-delays are involved: the time for turning rate to become maximum and the time for the wheel angle (physical accomplishment time-delay) to reach the maximum. These are found by adding the rate to the given time-delay of 6^{o} per second. Normally Ackerman steering can be accomplished on the computer by a half-sine wave forcing function. However, as shown, the frequencies of the forcing functions for this simulation are so small that a ramp function (0 to maximum torque) was applied and held after maximum torque was reached.

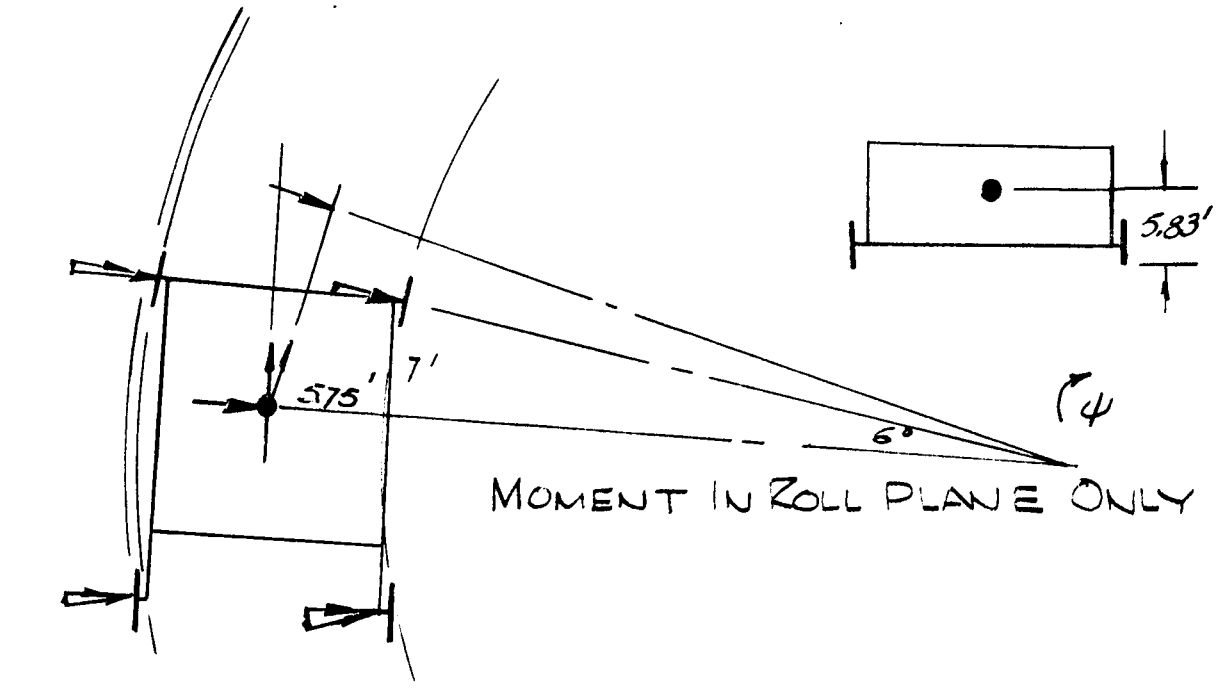

FIGURE B4. ROLL MOMENT - STEERING (4 WHEEL VEHICLE)

APPENDIX C
SIX WHEEL ARTICULATED VEHICLE - PITCH PLANE ANALYSIS

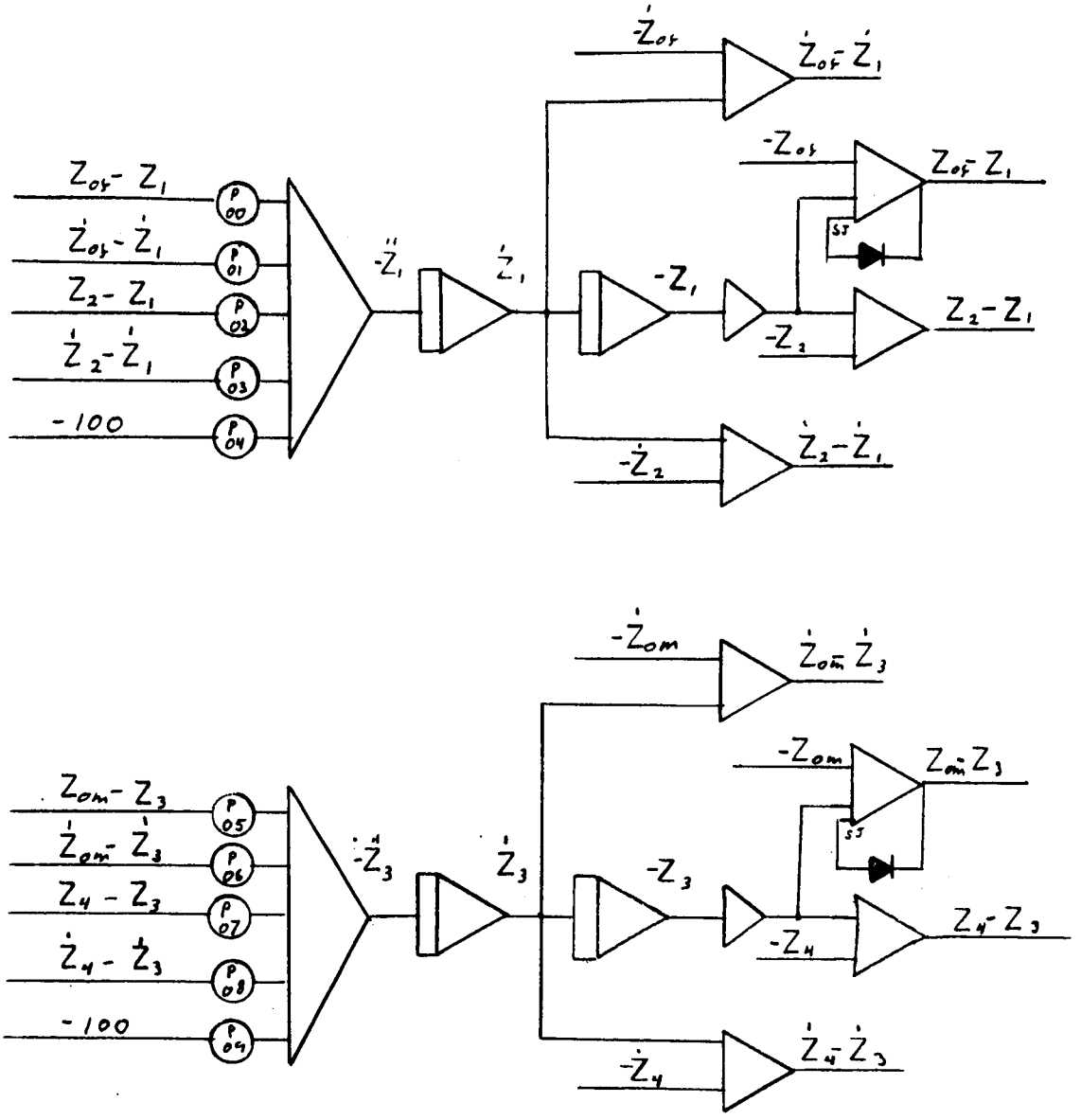

FIGURE C1A. 6 WHEEL ARTICULATED PITCH PLANE ANALYSIS

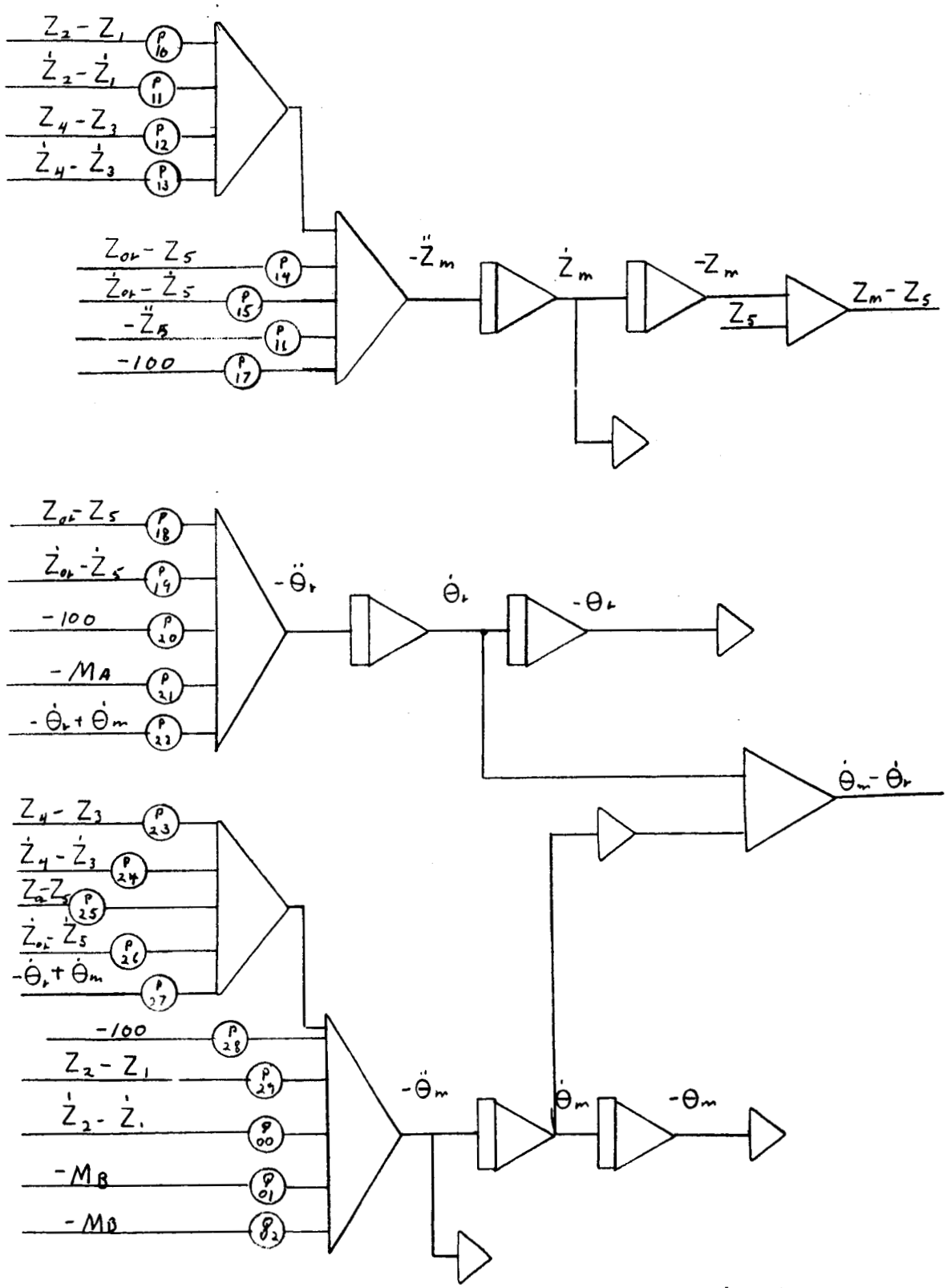

FIGURE C1B. 6 WHEEL ARTICULATED PITCH PLANE ANALYSIS

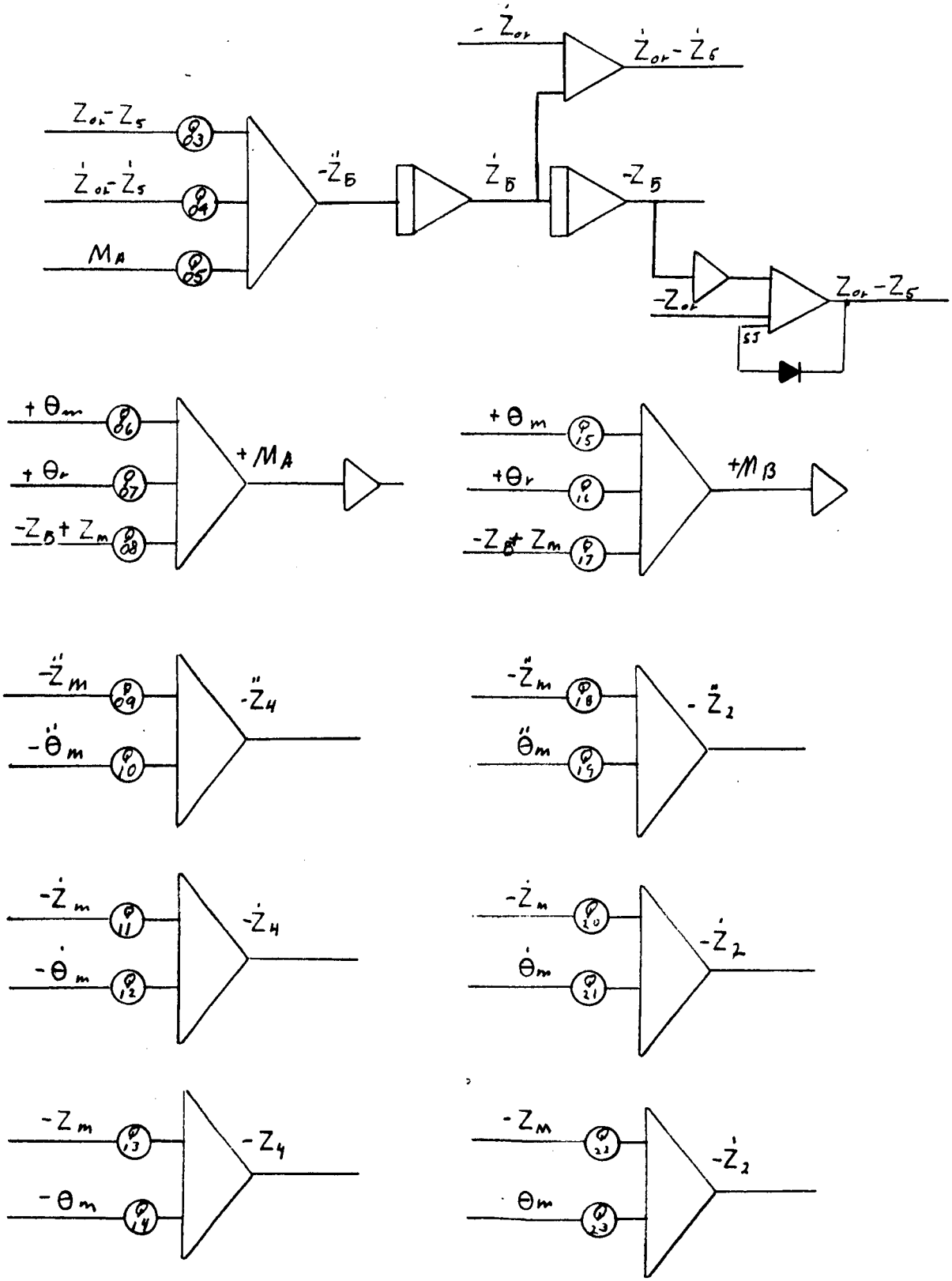

FIGURE C1C. 6 WHEEL ARTICULATED PITCH PLANE ANALYSIS

P00	K_1/m_1
P01	D_1/m_1
P02	K_2/m_1
P03	D_2/m_1
P04	$g/100$
P05	K_3/m_3
P06	D_3/m_3
P07	K_4/m_3
P08	D_4/m_3
P09	$g/100$
P10	K_2/m_m
P11	D_2/m_m
P12	K_4/m_m
P13	D_4/m_m
P14	K_5/m_m
P15	D_5/m_m
P16	$(m_t+m_5)/m_m$
P17	$g/100$
P18	$l_{t6}\ K_5/I_{yt}$
P19	$l_{t6}\ D_5/I_{yt}$
P20	$l_{t1}\ (m_t+m_5)\ g/I_{yt}$
P21	$1/I_{yt}$
P22	$D_7\ h_m/I_{yt}$
P23	$l_{m4}\ K_4/I_{ym}$
P24	$l_{m4}\ D_4/I_{ym}$
P25	$l_{m4}/K_5/I_{ym}$
P26	$l_{m4}/D_5/I_{ym}$
P27	$D_7 h_m/I_{ym}$
P28	$(m_5+m_t)\ g/100$
P29	$l_{m2}\ K_2/I_{ym}$

Q00	$l_{m2}\ D_2/I_{ym}$
Q01	$1/I_{ym}$
Q02	$l_{m2}/l_{m4} I_{ym}$
Q03	$K_5/(m_t+m_5)$
Q04	$D_5/(m_t+m_5)$
Q05	$1/(m_t+m_5)\ l_{t1}$
Q06	$2EI\ (l_c+l_{m4})/l_c^2$
Q07	$2EI\ l_{t1}/l_c^2$
Q08	$2EI/l_c^2$
Q09	1
Q10	l_{m4}
Q11	1
Q12	l_{m4}
Q13	1
Q14	l_{m4}
Q15	$2EI\ (l_c+l_{t1})/l_c^2$
Q16	$2EI\ l_{m4}/l_c^2$
Q17	$2EI/l_c^2$
Q18	1
Q19	l_{m2}
Q20	1
Q21	l_{m2}
Q22	1
Q23	l_{m2}

FIGURE C1D. 6 WHEEL ARTICULATED PITCH PLANE ANALYSIS

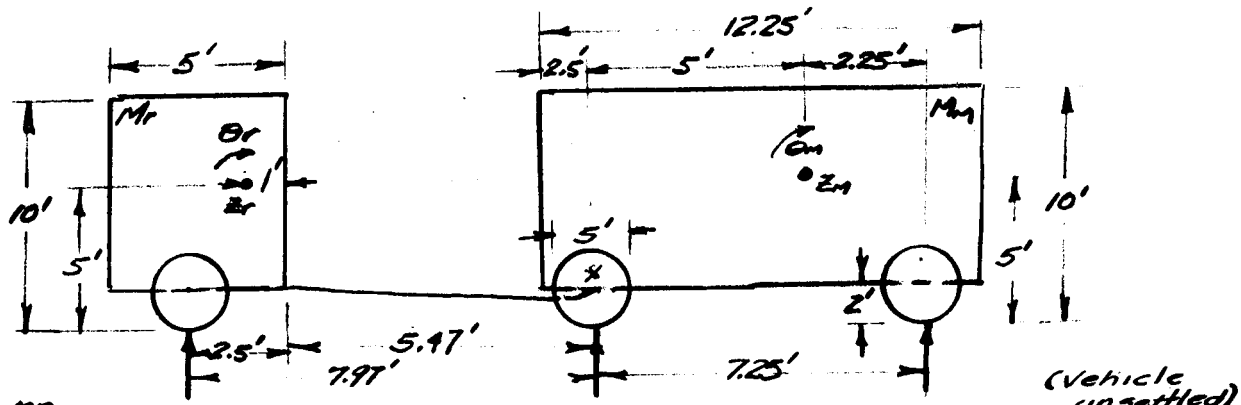

Given → 40% 28% 32%

TOTAL: 6400# = 2560 + 1792 + 2048

½ TOTAL: 3200# = 1280 + 896 + 1024

STATIC STABILITY: TAKE MOMENTS ABOUT X:

LET W_r BE THE WEIGHT OF THE TRAILER.

THEN, ↻ ↺ ↺ ↻

$$(1280)(7.97) - (W_r)(6.47) - (1024)(7.25) + (3200 - W_r)(5) = 0$$

$W_r = 1632$ $W_m = 1568$

Given → $M_W = 3.4$ Slugs

$M_r = 47.4$ Slugs $M_M = 42.0$ Slugs

DATA REFERRED TO MATHEMATICAL MODEL
(See Text Page 57)

$M_m = 42.0$ Slugs , $M_r = 47.4$ Slugs , $M_1 = M_3 = M_5 = 3.4$ Slugs

$I_{Ym} = 600$ Slug-ft² , $I_{Yr} = 312.5$ Slug-ft²

$h_m = h_r = 2.5$ ft , $EI = 39{,}000$ lb-ft², $D_7 = 1750$ lb/rad/sec

$D_1 = D_3 = D_5 = 0$, $D_2 = D_4 = D_6 = 1500$ lb/ft/sec

$K_1 = K_3 = K_5 = 801$ lb/ft , $K_2 = K_4 = 470$ lb/ft

$l_{r_1} = 1.0$ ft , $l_{r_6} = 2.5$ ft , $l_{m_2} = 2.25$ ft , $l_m = 5$ ft , $l_c = 5.47$ ft

FIGURE C2. BASIC DATA AND CALCULATIONS - 6 WHEEL ARTICULATED VEHICLE (PITCH PLANE ANALYSIS)

DEVELOPMENT OF THE MOMENT ON THE CONNECTING SPRING-BAR BETWEEN THE ELEMENTS OF THE 6-WHEEL ARTICULATED VEHICLE

Since the flexible coupling between the main module and the trailer of the 6 wheel articulated vehicle was found to function with higher bending modes than the first, it was necessary to develop a simple means of placing this function on the computer. Programming the higher order equations, normally used, proves to be impractical. Figures D3A and D3F show a simplified means of finding the coupling bar (spring) bending moment at the connection point of each module. As is shown, the formula for the end deflection of a cantilever beam and the moment on the end of the cantilever beam is used. The EI and the length of the coupling bar are given in the data.

The moments on the coupling bar are of interest in the computer simulation only at the bar-module contact point. The moments are derived, as shown on Figures C3A and D3B by equating the displacement between the contact points represented by two equations--the deflection equation and the equation formulated small angle theory. The moments thus derived are used, along with the bar shear forces at the contact points, in equations on pages and of the text. Further explanation of the combination of the moments and the shear forces is given in the text.

APPROXIMATE:

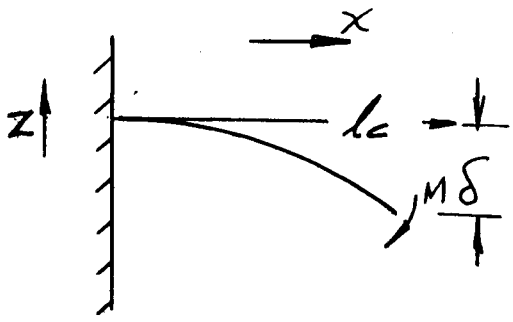

DEFLECTION: $\delta = \frac{Mk^2}{2EI}$

$$\delta = \frac{M_B l_c^2}{2EI} = l_c \theta_r + l_{n_i} \theta_r + l_{M_4} \theta_M - (z_r - z_M)$$

$$M_B = \frac{2EI}{l_c^2}\left[(l_c + l_{n_i})\theta_r + l_{M_4}\theta_M - (z_r - z_M)\right]$$

z_r, z_M, position, referenced to unsettled vehicle

FIGURE C3A. DEVELOPMENT OF MOMENT ON CONNECTING SPRING-BAR (6 WHEEL VEHICLE)

APPROXIMATE:

DEFLECTION: $\delta = \frac{Mk^2}{2EI}$

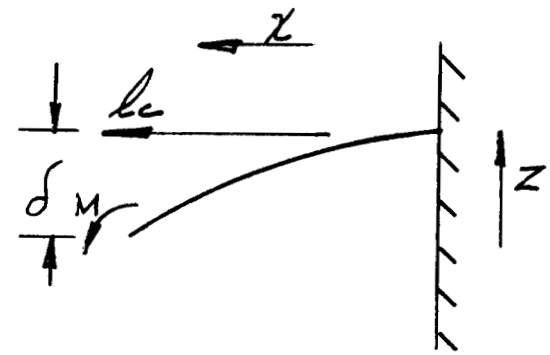

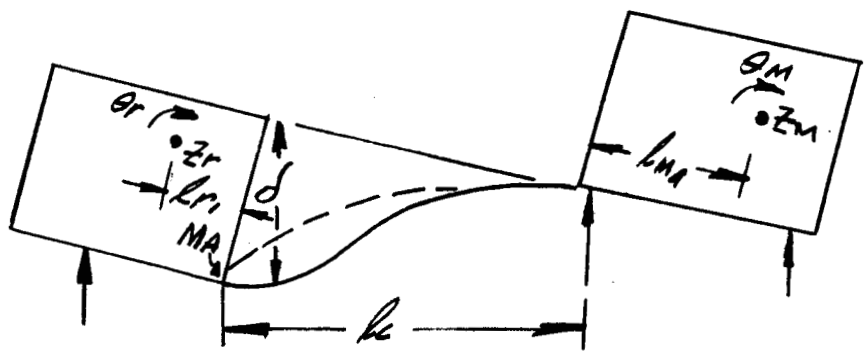

$$\delta = \frac{M_A l_c^2}{2EI} = l_c \theta_M + l_{M_4} \theta_M + l_{r_1} \theta_r - (z_r - z_M)$$

$$M_A = \frac{2EI}{l_c^2}\left[(l_c + l_{M_4})\theta_M + l_{r_1}\theta_r - (z_r - z_M)\right]$$

z_r, z_M, position, referenced to unsettled vehicle

FIGURE C3B. DEVELOPMENT OF MOMENT ON CONNECTING SPRING-BAR (6 WHEEL VEHICLE)

APPENDIX D
SIX WHEEL ARTICULATED VEHICLE
ROLL PLANE ANALYSIS

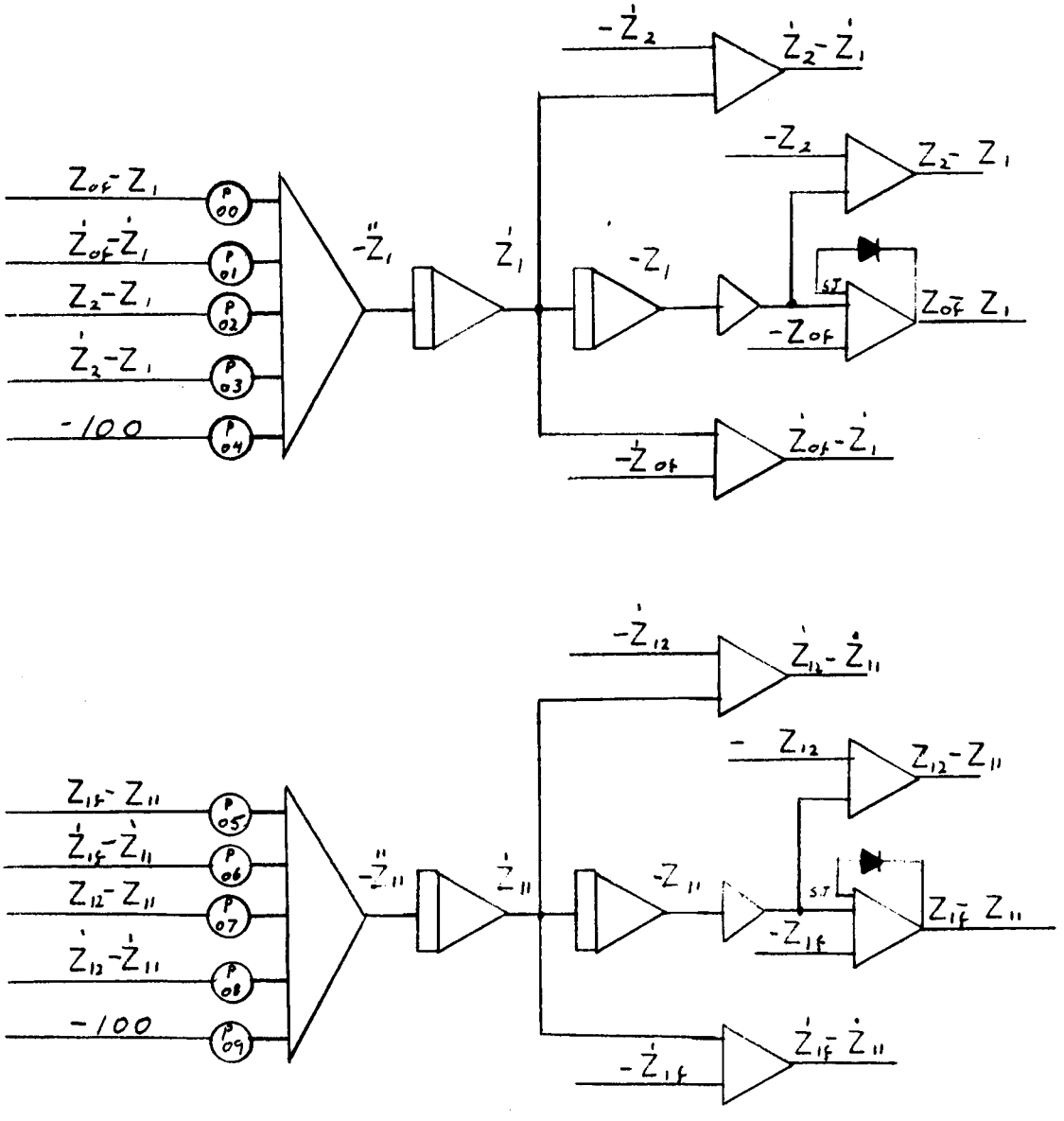

FIGURE D1A. 6 WHEEL ARTICULATED VEHICLE - ROLL PLANE ANALYSIS

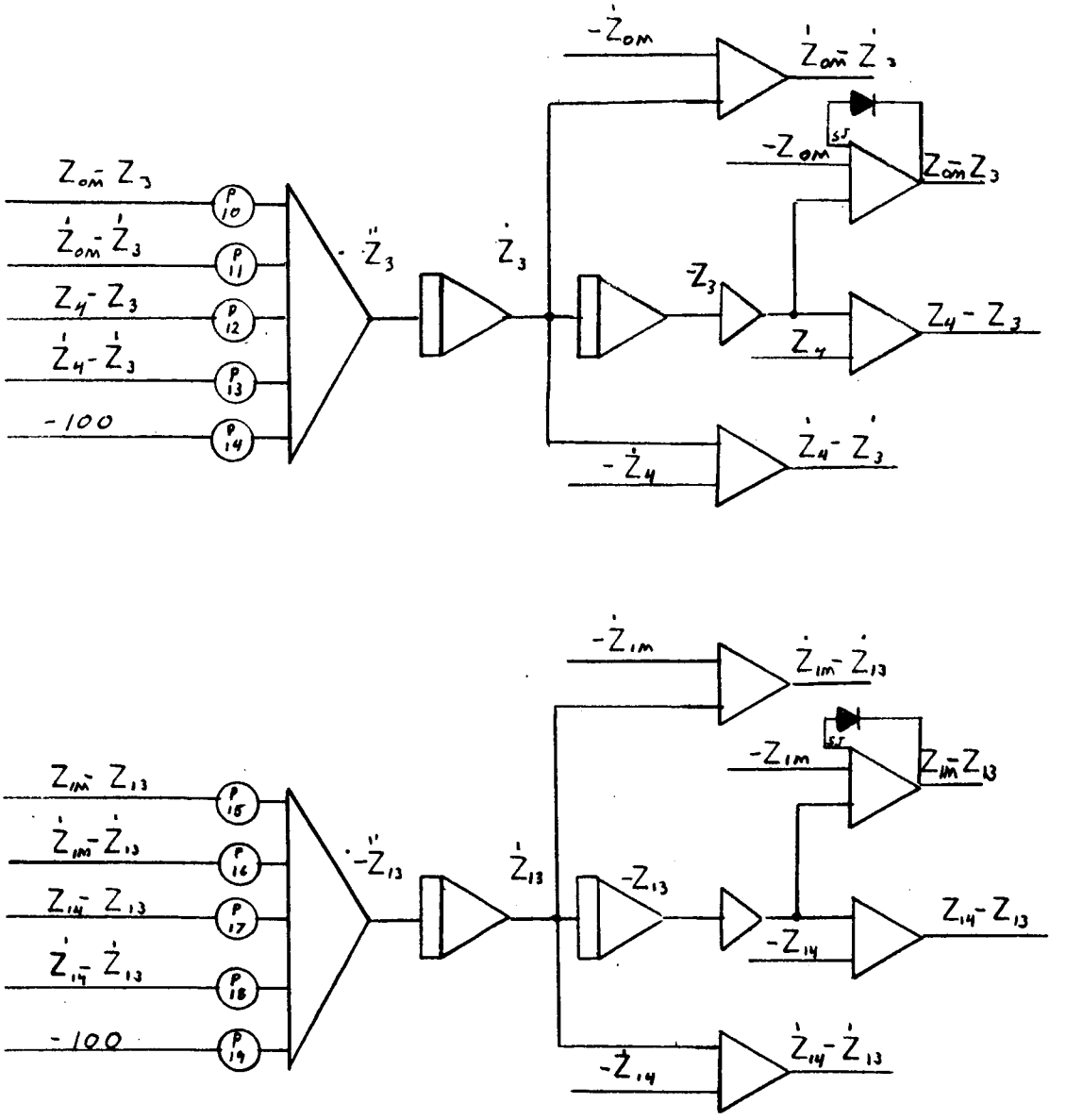

FIGURE D1B. 6 WHEEL ARTICULATED VEHICLE - ROLL PLANE ANALYSIS

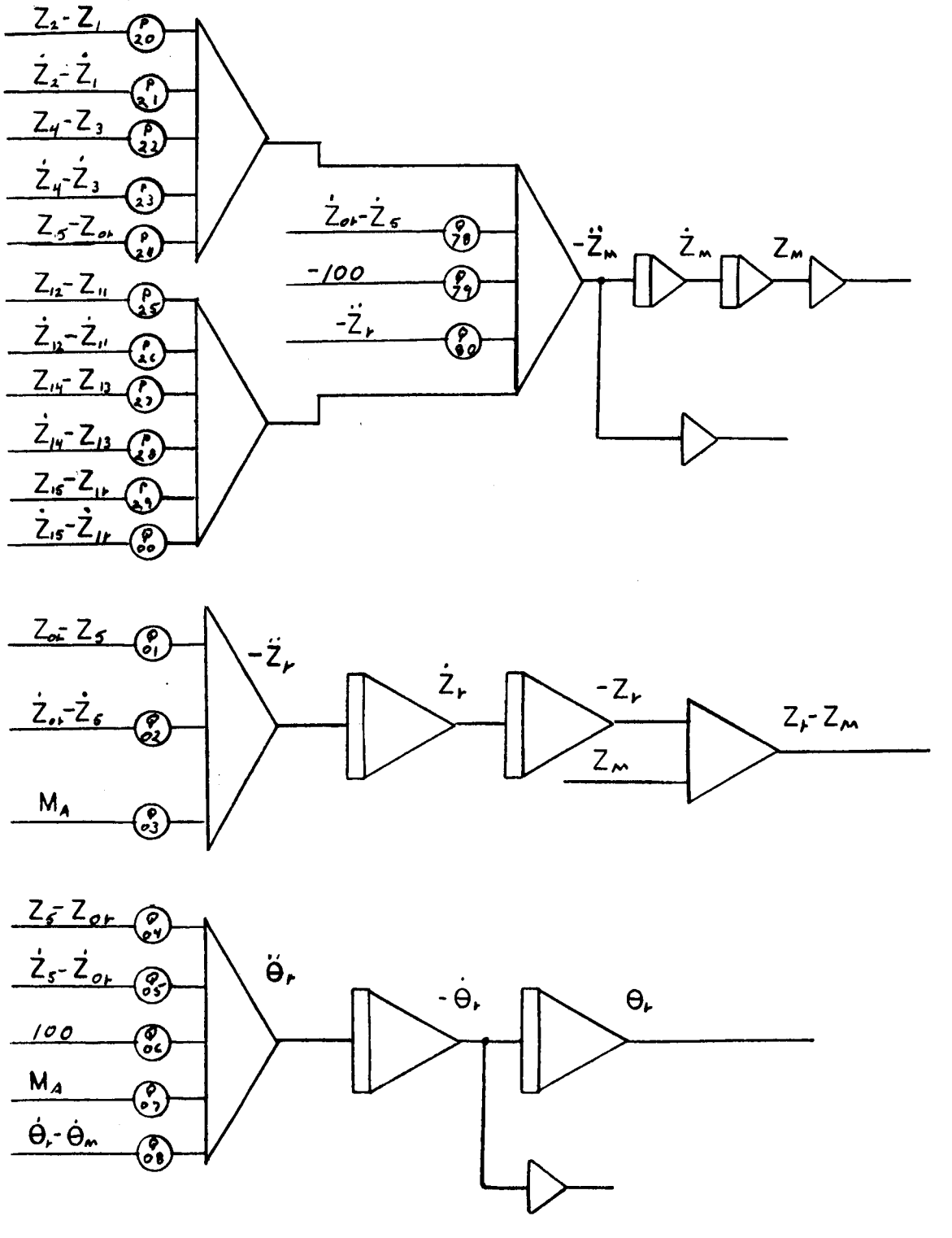

FIGURE D1C. 6 WHEEL ARTICULATED VEHICLE - ROLL PLANE ANALYSIS

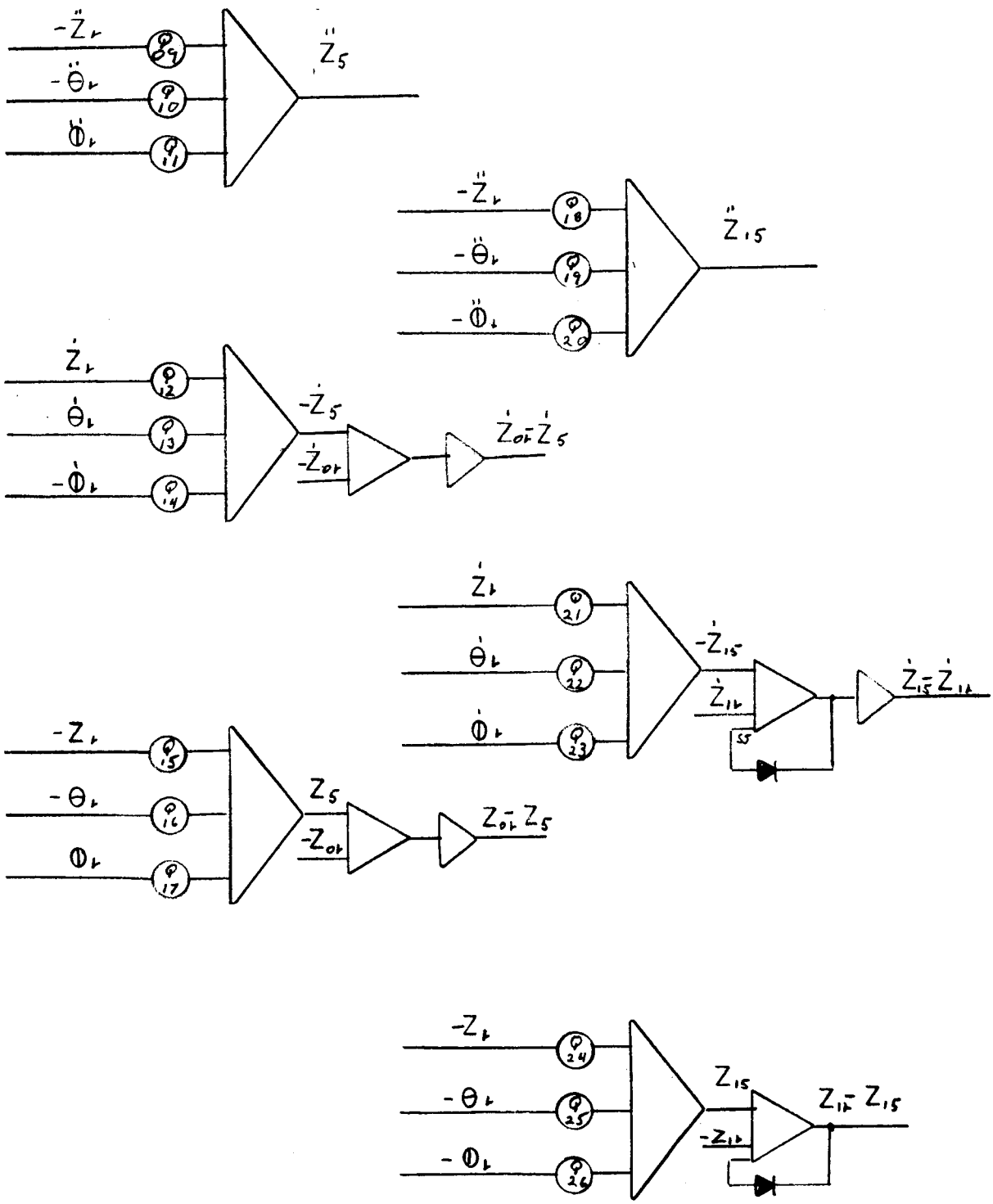

FIGURE D1D. 6 WHEEL ARTICULATED VEHICLE - ROLL PLANE ANALYSIS

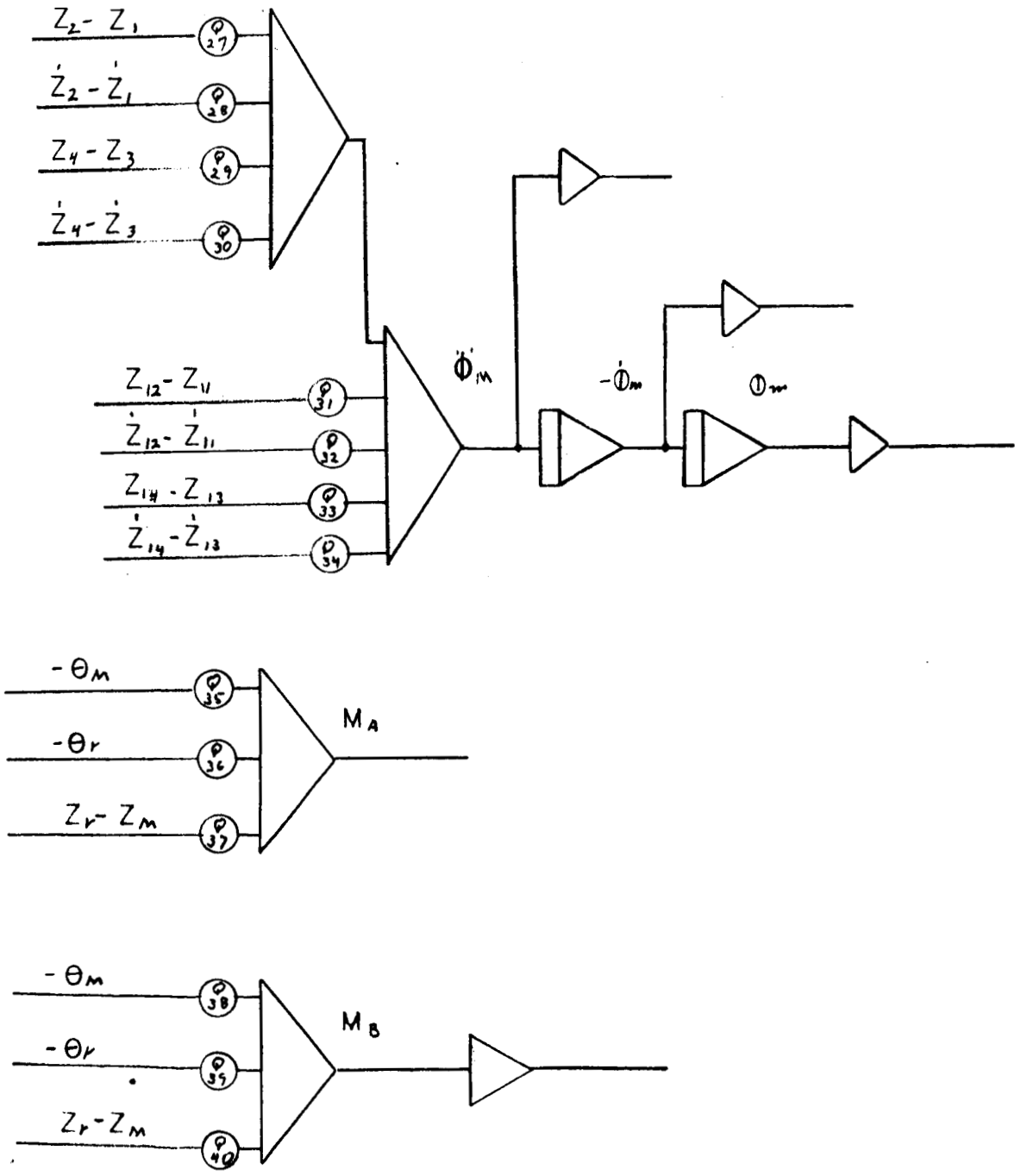

FIGURE D1E. 6 WHEEL ARTICULATED VEHICLE - ROLL PLANE ANALYSIS

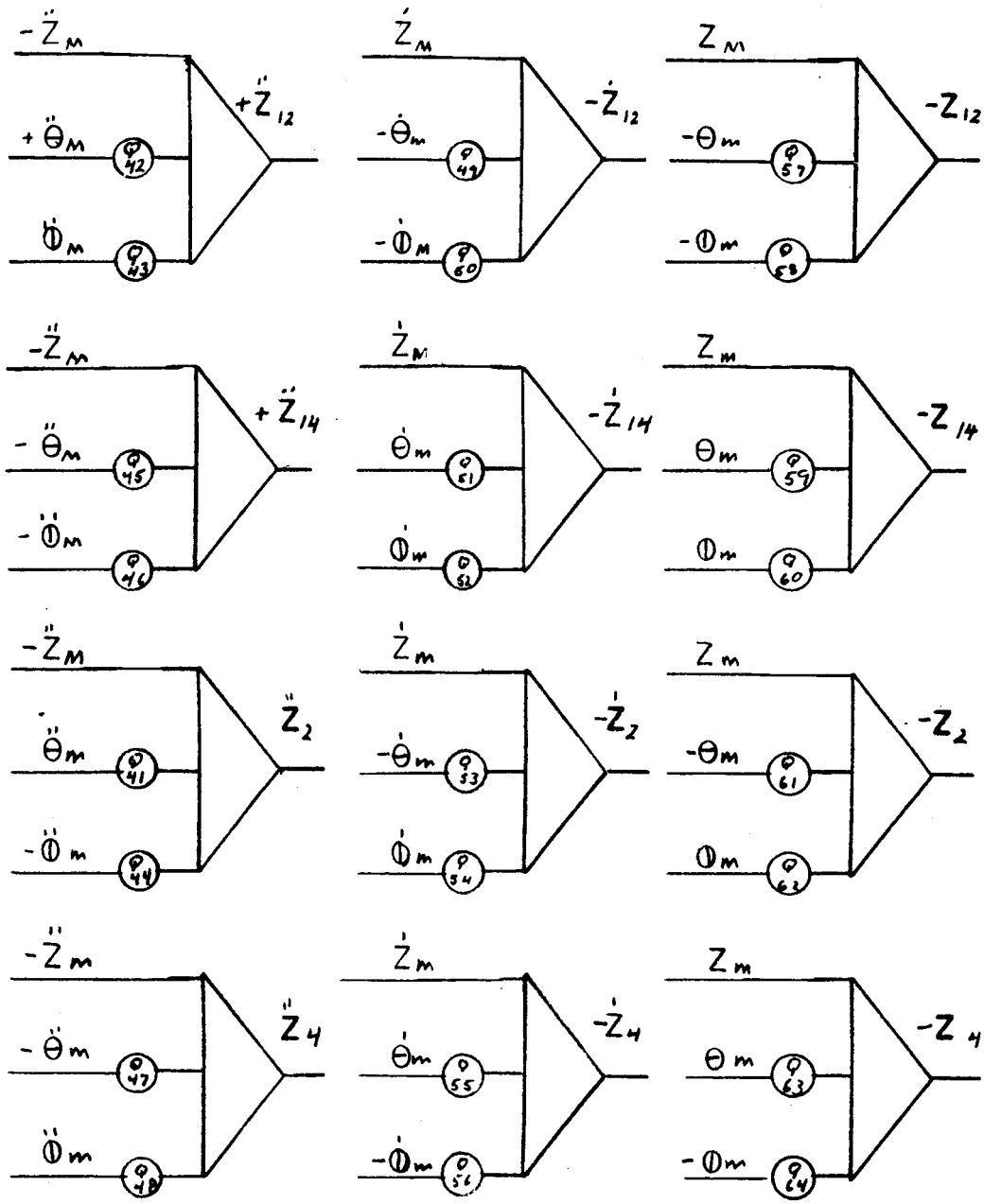

FIGURE D1F. 6 WHEEL ARTICULATED VEHICLE - ROLL PLANE ANALYSIS

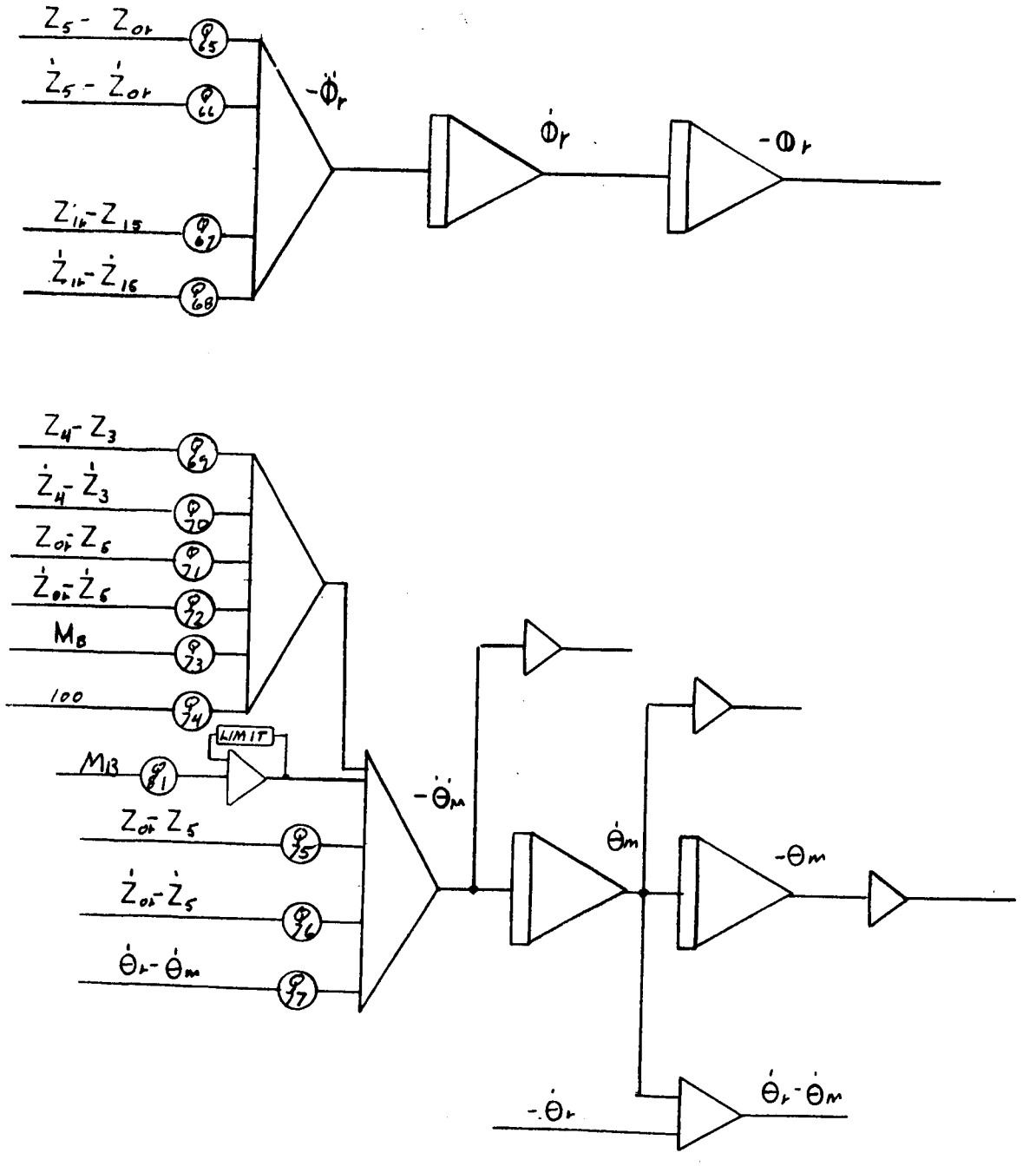

FIGURE D1G. 6 WHEEL ARTICULATED VEHICLE - ROLL PLANE ANALYSIS

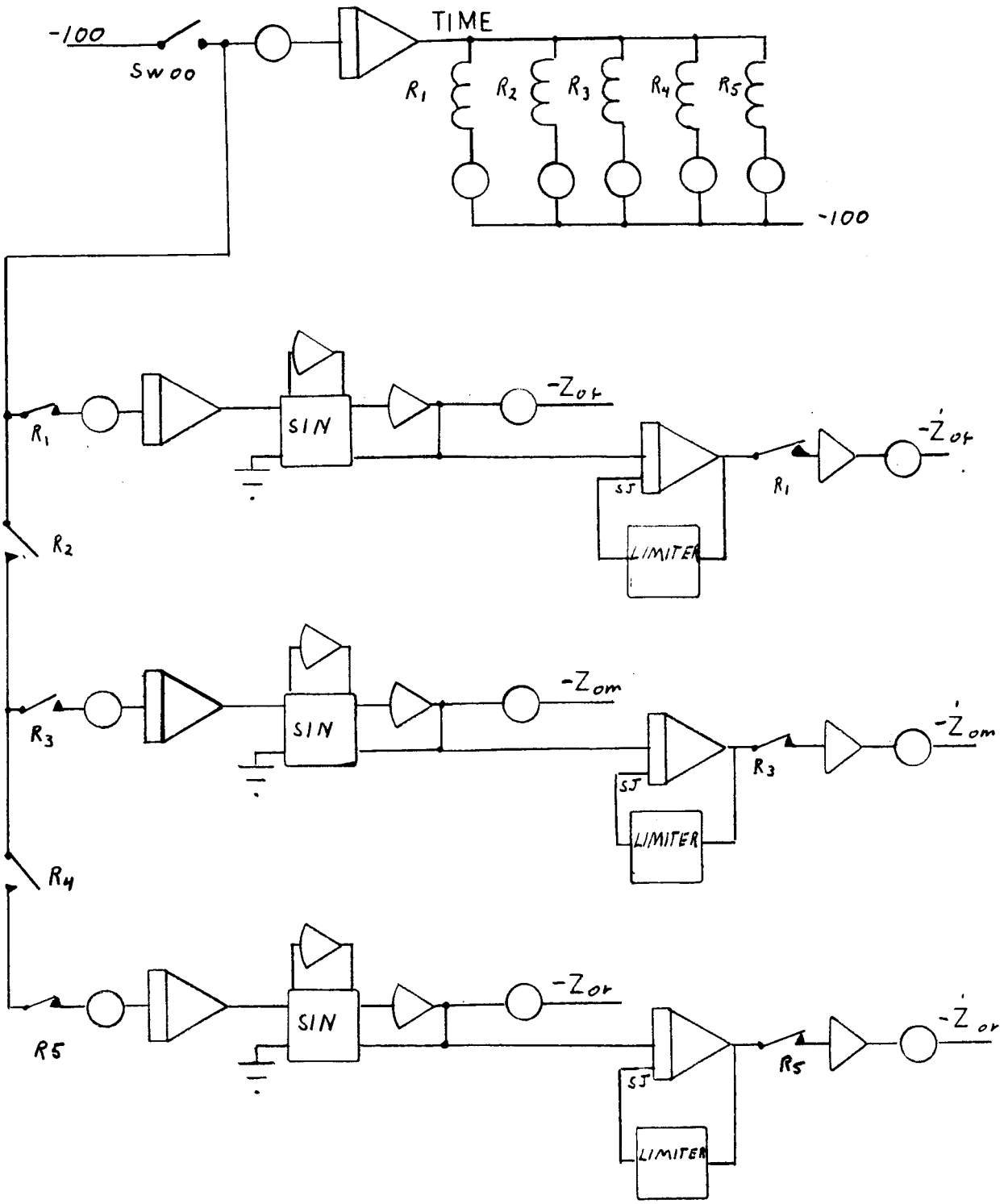

FIGURE D1H. FORCING FUNCTION (BUMPS) - ROLL PLANE ANALYSIS

P00	K_1/M_1	Q00	D_{15}/M_m	Q30	$D_4 \ell_{m1}/I_{ym}$
P01	D_1/M_1	Q01	$K_5/(M_t+M_5)$	Q31	$K_{12} \ell_{m1}/I_{ym}$
P02	K_2/M_1	Q02	$D_5/(M_t+M_5)$	Q32	$D_{12} \ell_{m1}/I_{ym}$
P03	D_1/M_1	Q03	$1/(M_t+M_5)\ell_{t1}$	Q33	$K_{14} \ell_{m1}/I_{ym}$
P04	$g \cdot 1/100$	Q04	$K_5 \ell_{t6}/I_{yt}$	Q34	$D_{14} \ell_{m1}/I_{ym}$
P05	K_{11}/M_{11}	Q05	$D_5 \ell_{t6}/I_{yt}$	Q35	$EI(\ell_c+\ell_{m4})/\ell_c^3$
P06	D_{11}/M_{11}	Q06	$g\left[\frac{\ell_{t1}(M_t+M_5)}{I_{yt}}\right]\cdot\frac{1}{100}$	Q36	$EI\,\ell_{t1}/\ell_c^3$
P07	K_{12}/M_{11}	Q07	$1/I_{yt}$	Q37	EI/ℓ_c^2
P08	D_{12}/M_{11}	Q08	$D_7 h_m/I_{yt}$	Q38	$EI(\ell_c+\ell_{t1})/\ell_c^2$
P09	$g \cdot \frac{1}{100}$	Q09	1	Q39	$EI\,\ell_{m4}/\ell_c^3$
P10	K_3/M_3	Q10	$(\ell_{t6}-\ell_{t1})$	Q40	EI/ℓ_c^3
P11	D_3/M_3	Q11	$\ell_{t5} \cdot 1/25$	Q41	ℓ_{m2}
P12	K_4/M_3	Q12	1	Q42	ℓ_{m2}
P13	D_4/M_3	Q13	$(\ell_{t6}-\ell_{t1})$	Q43	ℓ_{m1}
P14	$g \cdot \frac{1}{100}$	Q14	ℓ_{t5}	Q44	ℓ_{m1}
P15	K_{13}/M_{13}	Q15	1	Q45	ℓ_{m4}
P16	D_{13}/M_{13}	Q16	$(\ell_{t6}-\ell_{t1})$	Q46	ℓ_{m1}
P17	K_{14}/M_{13}	Q17	ℓ_{t5}	Q47	ℓ_{m4}
P18	D_{14}/M_{13}	Q18	1	Q48	ℓ_{m1}
P19	$g \cdot \frac{1}{100}$	Q19	$(\ell_{t6}-\ell_{t1})$	Q49	ℓ_{m2}
P20	K_2/M_m	Q20	ℓ_{t5}	Q50	ℓ_{m1}
P21	D_2/M_m	Q21	1	Q51	ℓ_{m4}
P22	K_4/M_m	Q22	$(\ell_{t6}-\ell_{t1})$	Q52	ℓ_{m1}
P23	D_4/M_m	Q23	ℓ_{t5}	Q53	ℓ_{m2}
P24	K_5/M_m	Q24	1	Q54	ℓ_{m1}
P25	K_{12}/M_m	Q25	$(\ell_{t6}-\ell_{t1})$	Q55	ℓ_{m2}
P26	D_{12}/M_m	Q26	ℓ_{t5}	Q56	ℓ_{m1}
P27	K_{14}/M_m	Q27	$K_2 \ell_{m1}/I_{ym}$	Q57	ℓ_{m4}
P28	D_{14}/M_m	Q28	$D_2 \ell_{m1}/I_{ym}$	Q58	ℓ_{m1}
P29	K_{15}/M_m	Q29	$K_4 \ell_{m1}/I_{ym}$	Q59	ℓ_{m4}

FIGURE D1I. POT SETTINGS - 6 WHEEL ARTICULATED LSV (ROLL PLANE ANALYSIS)

Q60	ℓ_{m_1}
Q61	ℓ_{m_2}
Q62	ℓ_{m_3}
Q63	ℓ_{m_4}
Q64	ℓ_{m_1}
Q65	$\ell_{t_5} k_5 / I_{x_1}$
Q66	$\ell_{t_5} D_5 / I_{x_2}$
Q67	$\ell_{t_5} K_{15} / I_{x_1}$
Q68	$\ell_{t_5} D_{15} / I_{x_2}$
Q69	$\ell_{m_4} K_4 / I_{ym}$
Q70	$\ell_{m_4} D_4 / I_{ym}$
Q71	$\ell_{m_4} K_5 / I_{ym}$
Q72	$\ell_{m_4} D_5 / I_{ym}$
Q73	$\ell_2 / I_{ym} \ell_{m_4}$
Q74	$(g/100)(M_5 + m_1)$
Q75	$\ell_{m_4} K_5 / I_{ym}$
Q76	$\ell_{m_4} D_5 / I_{ym}$
Q77	$h_m D_7 / I_{ym}$
Q78	D_5 / m_m
Q79	$[1 + (m_1 + m_5)/m_m] g \cdot 1/cc$
Q80	$(m_1 + m_5) / m_m$
Q81	$1/I_{ym}$

FIGURE D1J. POT SETTINGS - 6 WHEEL ARTICULATED LSV (ROLL PLANE ANALYSIS)

(See Text, page 57 for Diagram)

$M_1 = M_3 = M_5 = M_{11} = M_{13} = M_{15} = 3.4$ slugs

$M_M = 84$ slugs, $M_r = 94.8$ slugs

$h_m = 2.5\,ft = h_r$

$I_{YM} = 1200$ slug-ft^2, $I_{Yr} = 625$ slug-ft^2

$I_{XM} = 800$ slug-ft^2, $I_{Xr} = 920$ slug-ft^2

$D_1 = D_3 = D_5 = D_{11} = D_{13} = D_{15} = 0$

$D_2 = D_4 = D_{12} = D_{14} = 150$ lb/ft/sec, $D_7 = 175$ lb/rad/sec

$K_1 = K_3 = K_5 = K_{11} = K_{13} = K_{15} = 801$ lb/ft

$K_2 = K_4 = K_6 = K_{12} = K_{14} = K_{16} = 470$ lb/ft

$\ell_{M1} = 4.58\,ft$, $\ell_{M2} = 2.25\,ft$, $\ell_{M4} = 5.0\,ft$

$\ell_{r1} = 1.0\,ft$, $\ell_{r5} = 4.58\,ft$, $\ell_{r6} = 2.5\,ft$

$\ell_c = 5.47\,ft$, $EI = 39{,}000$ lb-ft^2

FIGURE D2. BASIC DATA AND CALCULATIONS - 6 WHEEL ARTICULATED VEHICLE (ROLL PLANE ANALYSIS)

DISTRIBUTION

INTERNAL

DIR
DEP-T
R-DIR
R-AERO-DIR
-S
-SP (23)
R-ASTR-DIR
-A (13)
R-P& VE-DIR
-A
-AB (15)
-AL (5)
R-RP-DIR
-J (5)
R-FP-DIR
R-FP (2)
R-QUAL-DIR
-J (3)
R-COMP-DIR
R-ME-DIR
-X
R-TEST-DIR
I-DIR
MS-IP
MS-IPL (8)

EXTERNAL

NASA Headquarters
MTF Col. T. Evans
MTF Maj. E. Andrews (2)
MTF Mr. D. Beattie
R-1 Dr. James B. Edson
MTF William Taylor

Kennedy Space Center
K-DF Mr. von Tiesenhausen

Scientific and Technical Information Facility
P.O. Box 5700
Bethesda, Maryland
Attn: NASA Representative (S-AK RKT) (2)

Manned Spacecraft Center
Houston, Texas
Mr. Gillespi, MTG
Miss M. A. Sullivan, RNR
John M. Eggleston
C. Corington, ET-23 (1)
William E. Stanley, ET (2)

Donald Ellston
Manned Lunar Exploration Investigation
Astrogeological Branch
USGS
Flagstaff, Arizona

Langley Research Center
Hampton, Virginia
Mr. R. S. Osborn